Palaeontologia Electronica
palaeo-electronica.org

Revision of the theropod dinosaur *Camarillasaurus cirugedae* from the Early Cretaceous (Barremian) of Teruel province, Spain

Oliver W.M. Rauhut, José Ignacio Canudo, and Diego Castanera

ABSTRACT

Camarillasaurus cirugedae is a medium- to large-sized theropod taxon based on fragmentary remains of a single specimen from the Barremian site of Fuente Arnar in Camarillas (Teruel, Spain). It was initially interpreted as a representative of Ceratosauria, making it a taxon "outside time and space". We revise the material that was originally assigned to *Camarillasaurus* as well as new fossil remains (surangular/articular, partial mid-caudal vertebra, femur, pedal ungual, partial tooth) from the type locality. The taxon can be diagnosed on the basis of a marked, rugose lateral tubercle on the surangular lateral to the mandibular glenoid, transversely concave dorsal prezygapophyseal articular surfaces, distally anteriorly flexed mid-caudal neural spines, and posteriorly extended distal caudal postzygapophyses that are connected to the neural spine by a bony web. Phylogenetic analysis identifies *Camarillasaurus* as a member of the Spinosauridae. Furthermore, it is morphologically different from the other named spinosaurid taxa from the Iberian Early Cretaceous *(Vallibonavenatrix, Iberospinus, Riojavenatrix)* demonstrating the high diversity of this group at that time. Phylogenetic analysis also indicates that *Iberospinus, Vallibonavenatrix,* and *Camarillasaurus* represent spinosaurines within the Spinosauridae, in contrast to the diverse contemporaneous baryonychines in England. Isolated spinosaurid remains, especially isolated teeth, are relatively abundant in the Hauterivian-Aptian of the Iberian Peninsula. Many of these remains, including the holotype of *Camarillasaurus*, have been found in continental facies such as alluvial plains, suggesting that these taxa may have had less aquatic affinities than has been proposed for the spinosaurs of the end of the Lower Cretaceous and the beginning of the Upper Cretaceous.

Oliver W.M. Rauhut. SNSB - Bayerische Staatssammlung für Paläontologie und Geologie, Richard-Wagner-Str. 10, 80333 Munich, Germany; Department für Umwelt- und Geowissenschaften, Ludwig-Maximilians-Universität München, Munich, Germany; and GeoBioCenter, Ludwig-Maximilians-Universität München, Munich, Germany (corresponding author). rauhut@snsb.de

Final citation: Rauhut, Oliver W.M., Canudo, José Ignacio, and Castanera, Diego. 2025. Revision of the theropod dinosaur *Camarillasaurus cirugedae* from the Early Cretaceous (Barremian) of Teruel province, Spain. Palaeontologia Electronica, 28(3):a40. https://doi.org/10.26879/1543
palaeo-electronica.org/content/2025/5627-revision-of-early-cretaceous-theropod-dinosaur

José Ignacio Canudo. Aragosaurus: Recursos geológicos y paleoambientes; IUCA, Facultad de Ciencias, Universidad de Zaragoza 50009, C/ Pedro Cerbuna 12, Zaragoza, Spain. jicanudo@unizar.es
Diego Castanera. Aragosaurus: Recursos geológicos y paleoambientes; IUCA, Facultad de Ciencias, Universidad de Zaragoza 50009, C/ Pedro Cerbuna 12, Zaragoza, Spain. dcasta@unizar.es

Keywords: Spinosauridae; Iberian Pensinsula; Palaeobiodiversity; Barremian; Maestrazgo Basin

Submission: 16 February 2025. Acceptance: 19 August 2025.

INTRODUCTION

Although theropod dinosaur remains from the Early Cretaceous of Europe were described as early as the middle of the nineteenth century (Owen, 1857), our knowledge of theropod faunas of this age is still very incomplete. Whereas most of the early discoveries were made in England and central Europe, the Iberian Peninsula has in the last few decades moved more into the spotlight in research on Early Cretaceous theropods from Europe, with several identified clades (see Alonso et al., 2017; Malafaia et al. 2020a; Isasmendi et al., 2024, 2025, and references therein). The first theropod taxon described from the Iberian Peninsula, *Suchosaurus girardi*, was also reported and named in the nineteenth century (Sauvage, 1897-98), though interpreted as a crocodile at the time. The species is based on very fragmentary material and is currently regarded as a probable spinosaurid *nomen dubium* (Mateus et al., 2011). Most of the Early Cretaceous theropod body fossils from this region reported in the following almost hundred years consisted of similar material, mostly isolated teeth and bones (e.g., Estes and Sanchiz, 1982; Canudo and Ruiz-Omeñaca, 2003; Sánchez-Hernández et al., 2007; Gasca et al., 2008, 2018; Alonso and Canudo, 2016; Alonso et al., 2017). More informative theropod material only came to light in the 1980s, from the exceptional conservation Lagerstätte of Las Hoyas in Cuenca Province, Castilla-La Mancha, Spain (Barremian), first in the form of avian theropods, but later also including the exceptionally well-preserved holotypes of the ornithomimosaur *Pelecanimimus polyodon*, the first valid non-avian theropod taxon to be published from the Early Cretaceous of the Iberian Peninsula (Pérez-Moreno et al., 1994; Cuesta et al., 2022), and the carcharodontosaur *Concavenator corcovatus* (Ortega et al., 2010; Cuesta et al., 2018a, 2018b, 2019).

Only a few further taxa of non-avian theropods have been described from the Early Cretaceous of the Iberian Peninsula since then. The first of these was published in 2014 under the name *Camarillasaurus cirugedae* by Sánchez-Hernández and Benton, based on very fragmentary remains from the Barremian of the Camarillas Formation in the province of Teruel, Aragón, Spain. This unit had yielded some sparse theropod remains previously, mainly isolated theropod teeth, including different spinosaurid morphotypes (e.g., Ruiz-Omeñaca et al., 2004; Sánchez-Hernández et al., 2007; Gasca et al., 2011; Cabrera-Argudo et al., 2024; Isasmendi et al., 2025, and references therein), while iguanodontian ornithopods represent the most abundant dinosaur record from this unit so far (Gasca et al., 2015; Verdú et al., 2015; 2020; García-Cobeña et al., 2024).

Camarillasaurus was originally interpreted as one of the earliest branching representatives of Ceratosauria, thus implying the existence of an early clade of ceratosaurs with a ghost lineage of some 40 Ma. However, it received comparatively little attention in the scientific literature until recently, probably due to the very fragmentary nature of the type specimen. More recently, a new spinosaurid species, *Vallibonavenatrix cani*, was named on the basis of fragmentary postcranial material from the Late Barremian of the Arcillas de Morella Formation in the province of Castellón, Valencia, Spain (Malafaia et al., 2020b); thus, this species is close geographically and chronologically to *Camarillasaurus*. In addition, another putative spinosaurid, *Protathlitis cinctorrensis*, was proposed on the basis of a maxilla and some caudal vertebrae from the Arcillas de Morella Formation (Santos-Cubedo et al., 2023), but this taxon is problematic (see below). Mateus and Estraviz-López (2022) described fragmentary remains from the Early Barremian Papo Seco Formation of Setúbal District, Portugal as a new species of spinosaurid, *Iberospinus natarioi*; this material had previously been referred to the spinosaurid *Baryonyx* (Mateus et al., 2011). Finally, new cranial and postcranial spinosaurid remains have been described from the latest Barremian – Early Aptian Enciso Group of La Rioja province, including the

new taxon *Riojavenatrix lacustris* (Isasmendi et al. 2023, 2024). Thus, spinosaurid theropods are the most common theropods identified in the Hauterivian-Aptian deposits of the Iberian Peninsula (Isasmendi et al., 2020, 2024, 2025; Malafaia et al., 2020a).

We revised the original material and visited the type locality of *Camarillasaurus* in 2017, followed by a renewed excavation of the site in 2018 (see below). This excavation resulted in the recognition of numerous misidentifications in the original description of that taxon and the recovery of new elements in the excavation, which led us to propose affinities of *Camarillasaurus* with spinosaurids and thus a considerable phylogenetic distance from ceratosaurs as initially proposed (Rauhut et al., 2019). Since then, *Camarillasaurus* has been considered as a possible spinosaurid (e.g., Malafaia et al., 2020a; Samathi et al., 2021) and recovered as a spinosaurid in subsequent analyses (e.g.: Samathi et al., 2021; Mateus and Estraviz-López, 2022; Sereno et al., 2022; Santos-Cubedo et al., 2023; Isasmendi et al., 2024). In this context, the aim of this paper is to undertake a complete redescription of the type material and the newly discovered elements of *Camarillasaurus*, as well as to more confidently establish its phylogenetic position.

Geological and Palaeontological Context

The *Camarillasaurus* type specimen was found in a site named Fuente Arnar, located approximately 3.5 km north-northwest of the village of Camarillas (Figure 1) in the Iberian Mountain Range (Teruel province, NE Spain). The coordinates of the site can be obtained from the palaeontological database accessible by consulting the General Office of Cultural Heritage of the Government of Aragon.

Geologically, Camarillas is located in the Maestrazgo basin. The end of the Jurassic saw a rifting process in the eastern part of the Iberian Peninsula that lasted until the latest Early Cretaceous (mid-Albian). A system of sedimentary basins was formed that developed independently, including the Maestrazgo Basin (Salas et al., 2001; Liesa et al., 2023). The latter was subdivided into seven sub-basins, with the area of Camarillas being located in the Galve sub-basin, at the western margin of the Maestrazgo Basin. The Upper Jurassic – Lower Cretaceous successions of the Galve sub-basin are mainly represented by shallow marine and coastal sediments during the Late Jurassic and terrestrial, transitional and shallow marine sediments during the Early Cretaceous (Aurell et al., 2016, 2019; Liesa et al., 2023).

The Fuente Arnar site is located in the siliciclastic Camarillas Formation, traditionally considered to be part of the continental Weald facies, and part of synrift sequence 2 (Aurell et al., 2016; Liesa et al., 2019, 2023). This unit overlies the El Castellar Formation and is overlain by the Artoles Formation, which together represent the Hauterivian-Barremian sequence 2a (see Liesa et al., 2023). The Camarillas Formation within the Galve sub-basin has extensive outcrops and thick successions of hundreds of metres, controlled by the synsedimentary extensional tectonics (Liesa et al., 2023; Soria et al., 2023 and references therein). The unit is mainly composed of siliciclastic sediments, mostly red clays with intercalations of red and white sandstones, and limestones and grey marls. It has traditionally been interpreted as having been deposited in fluvial environments of low sinuosity and broad floodplains, with coastal influence in the upper part of the formation interpreted as mixed-carbonate siliciclastic back-barrier system (Soria, 1997; Navarrete et al., 2013; 2014). Recent research (Soria et al. 2023) has shown that the fluvial origin of the deposits is restricted to the lower part of the succession and to the western areas of the sub-basin. Three stages, related to a tide-dominated estuary, a mixed-energy estuary, and a barrier island–tidal inlet suite have been identified. The age of the Camarillas Formation in the Galve sub-basin is Early Barremian to early Late Barremian, and it is constrained by its charophyte (included in the *Atopochara trivolvis triquetra* Zone; Martín-Closas, 1989; Canudo et al., 2012), ostracod (Schudack and Schudack, 2009), and palynomorph content (Villanueva-Amadoz et al., 2015; Barrón et al., 2025).

The original material of *Camarillasaurus* was mainly collected from the surface of the Fuente Arnar site, although some elements were also excavated from the sediments at the base of a low hill there (Cirugeda, pers. comm., 2017). During fieldwork in the area of Camarillas in 2017, we visited the site together with the original discoverer, Pedro Cirugeda, and found a partial caudal vertebra in situ that is compatible in size and morphology with the type material of *Camarillasaurus*. Thus, in 2018 we returned to carry out a systematic excavation of the site, digging into the side of the low hill where the original material was found. The excavation of the Fuente Arnar locality yielded only a few new elements, but these were found in situ and are generally well preserved. The bones were

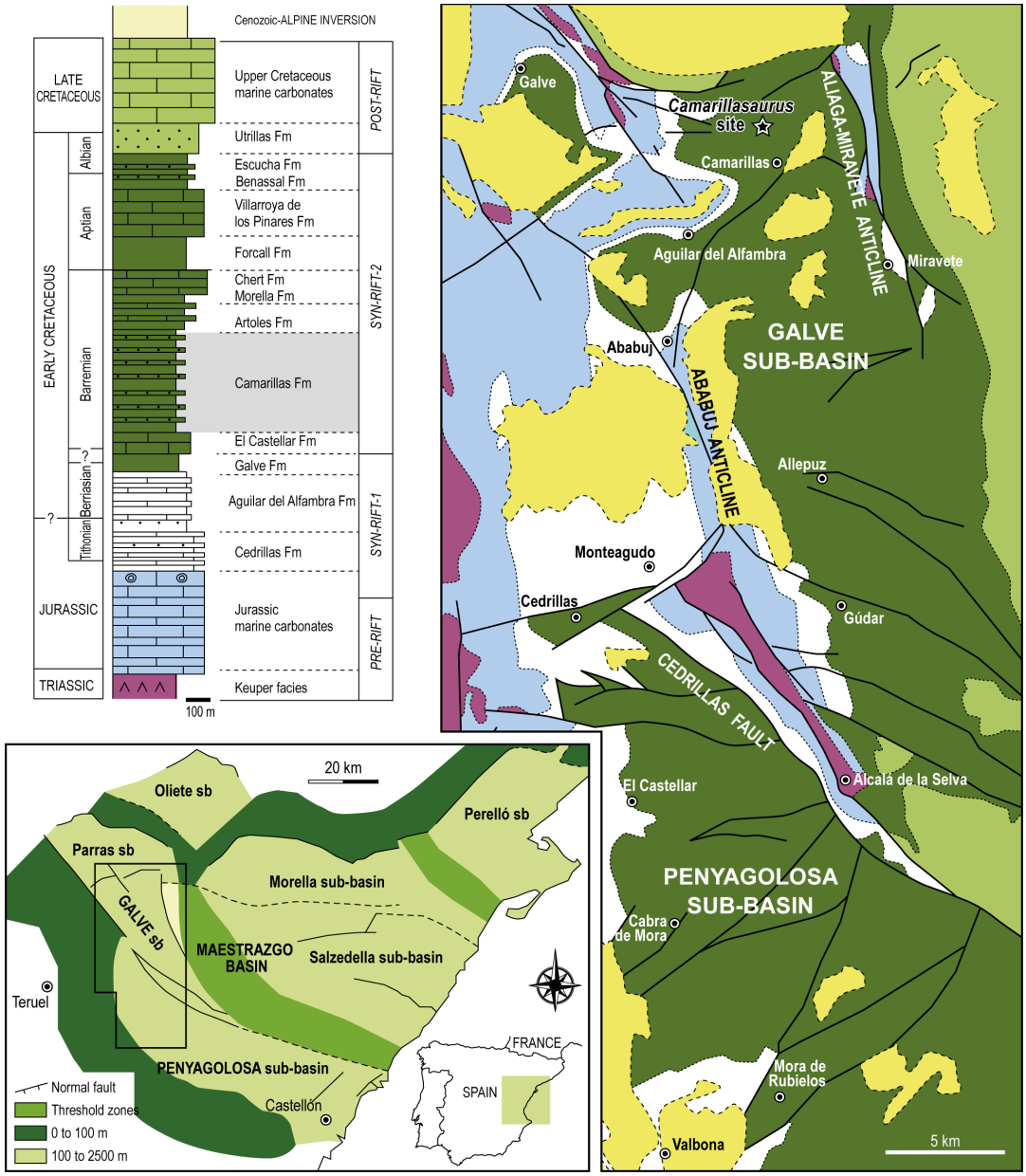

FIGURE 1. Geographic and geological setting and general stratigraphy of the Galve sub-basin in the Camarillas area (based on Aurell et al., 2016; Liesa et al., 2023), including the location of the Fuente Arnar site, type locality of *Camarillasaurus cirugedae*.

found disarticulated and dispersed in a grey mudstone level. The newly recovered material included the partial anterior mid-caudal vertebra found in 2017, and a complete right femur, a pedal ungual, and a cranial element, a partial right surangular, and fused articular found during the excavations in 2018. Apart from these theropod remains, which are consistent in size with the type specimen of *Camarillasaurus* and most probably belong to the same individual, all that was found was an isolated crocodylomorph tooth in a slightly higher level in the locality, as well as a partial turtle carapace in the same layer as the theropod remains. In addition, a recent visit to the site in 2024 by one of us (DC) has allowed the recovery of a partial tooth also collected from the surface; as the tooth clearly shows spinosaurid affinities (see below), we consider it likely that it also belongs to *Camarillasaurus*.

MATERIALS AND METHODS

The type material of *Camarillasaurus* described by Sánchez-Hernández and Benton (2014) is housed in the Museo Paleontológico de Galve José María Herrero (Teruel) and labelled MPG-KPC. The material excavated and found by us at the Fuente Arnar site is deposited in the Museo de Ciencias Naturales de la Universidad de Zaragoza and labelled MPZ (Canudo, 2018). Thus, the total known material considered to represent *Camarillasaurus* includes two partial teeth, a fused partial surangular and articular, several remains of dorsal, sacral and especially caudal vertebrae, scapular fragments, a possible fragment of an ilium, a femur, partial tibia, and a pedal ungual (Figure 2). A partial cervical vertebra originally referred to this taxon by Sánchez-Hernández and Benton (2014) is here removed from *Camarillasaurus* (see below).

In order to establish the phylogenetic affinities of *Camarillasaurus*, we included the taxon in the phylogenetic analysis of early branching tetanuran theropods of Schade et al. (2023). This matrix was chosen, as, during our study of the material, it became clear that *Camarillasaurus* is not a ceratosaur, but rather a megalosauroid tetanuran (Rauhut et al., 2019), and the matrix of Schade et al. (2023) is the newest iteration of the tetanuran theropod matrix originally published by Carrano et al. (2012) and was especially focused on the interrelationships of spinosaurids. Based on our own observations, nine characters (characters 154, 180, 228, 241, 242, 243, 256, 257, 374; the latter modified from Rauhut and Pol, 2019) were added (six of which postcranial characters, which were not the focus of the analysis of Schade et al., 2023) and two characters were modified (characters 153, 258). Furthermore, we also coded the recently described *Iberospinus* (Mateus and Estraviz-López, 2022) and *Riojavenatrix* (Isasmendi et al., 2024) into the matrix. Another recently described supposed spinosaurid taxon, *Protathlitis* (Santos-Cubedo et al. 2023), was not included, as the spinosaurid affinities of this taxon are questionable (see below). Thus, the finished phylogenetic matrix has a total of 79 operational taxonomic units (OTU) coded for 404 morphological characters (see Appendix 1 and Supplementary Data File).

The matrix was analysed in TNT version 1.6 (Goloboff and Morales, 2023), using an initial traditional search (with 1000 iterations), followed by TBR branch swapping. Prior to analysis, two OTUs, *Oxalaia* and the spinosaurid snout MNHN SAM 124, were removed, using safe taxonomic deletion criteria (Wilkinson, 1995), as all their codings were identical to the snout MSNM V4047 (Dal Sasso et al., 2005). We furthermore ran an additional analysis under the assumption that all spinosaurid material from the Kem Kem Group represents a single taxon, as argued by Smyth et al. (2020), for which the codings for the originally separately coded *Sigilmassasaurus* (Evers et al., 2015), FSAC-KK 11888 (Ibrahim et al., 2014, 2020) and the snout MSNM-V 4047 (Dal Sasso et al. 2005) were merged. Finally, all the analyses were repeated using implied weighting, with a weighting strength of 12 (see Goloboff et al., 2018).

We did not use traditional tests to recover support values, such as Bremer or bootstrap analyses, as the high number of extremely fragmentary taxa will inadvertently lead to extremely low support values for most clades. Instead, we looked at the number of steps needed to place *Camarillasaurus* in alternative positions within the tree in order to test the robustness of the results. For this, we constrained *Camarillasaurus* to different positions

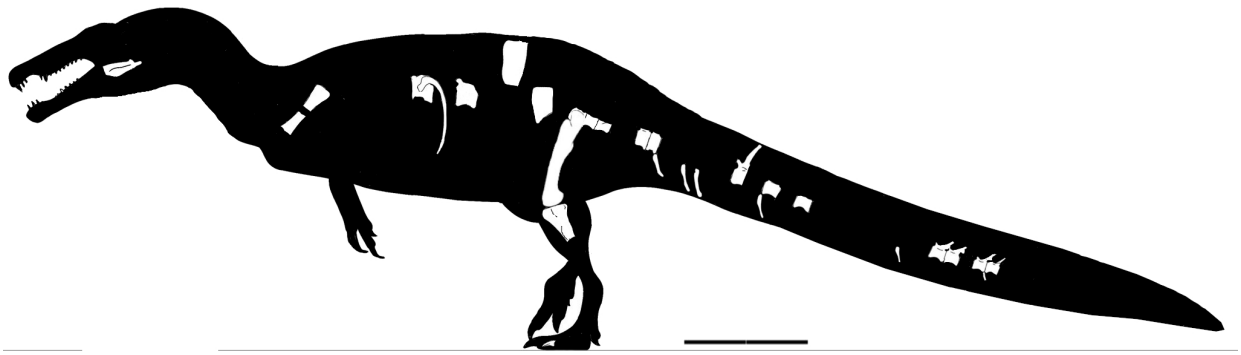

FIGURE 2. Reconstruction of *Camarillasaurus cirugedae* with preserved bones indicated. Note that some elements are from the right part of the skeleton (see text for details). Scale bar indicates 1 m.

within the phylogeny and ran equally weighted parsimony analyses in TNT, which were then compared to the results of the unconstrained equal weight analysis.

Institutional Abbreviations. BYU, Brigham Young University, Provo, USA; FSAC, Faculté des Sciences Aïn Chock, Casablanca, Morocco; MNHN, Muséum National d'Histoire Naturelle, Paris, France; MNN, Muséum National du Niger, Niamey, Niger; MPG, Museo Paleontológico de Galve José María Herrero, Galve, Spain; MPZ, Museo de Ciencias Naturales de la Universidad de Zaragoza, Spain; MSNM, Museo Civico di Storia Naturale, Milan, Italy; SMNS, Staatliches Museum für Naturkunde Stuttgart, Germany; SNSB-BSPG, Staatliche naturwissenschaftliche Sammlungen Bayerns, Bayerische Staatssammlung für Paläontologie und Geologie, Munich, Germany.

SYSTEMATIC PALAEONTOLOGY

THEROPODA Marsh, 1881
TETANURAE Gauthier, 1986
MEGALOSAUROIDEA (Fitzinger, 1843)
SPINOSAURIDAE Stromer, 1915
CAMARILLASAURUS Sánchez-Hernández and Benton, 2014

Type species. *Camarillasaurus cirugedae* Sánchez-Hernández and Benton, 2014

Diagnosis. As for type and only known species (see below).

Camarillasaurus cirugedae
Sánchez-Hernández and Benton, 2014

Holotype. Fragmentary postcranial skeleton, including two dorsal vertebral centra (MPG-KPC 9, 15, 18), two dorsal prezygapophyses (MPG-KPC 40, 42), three dorsal postzygapophyses (MPG-KPC 41, 61, 62), dorsal transverse process (MPG-KPC 14), dorsal or sacral neural spine (MPG-KPC 2), partial sacral vertebral centrum (MPG-KPC 16), two and a half articulated sacral vertebral centra (MPG-KPC 3, 4), two partial anterior caudal vertebrae (MPG-KPC 20, 21), partial anterior caudal neural arch (MPG-KPC 39), two mid-caudal vertebral centra (MPG-KPC 17, 27), four posterior caudal vertebrae (MPG-KPC 10-13), a posterior dorsal rib (MPG-KPC 7), several partial to complete chevrons (MPG-KPC 5, 44, 47, 60), fragments of left (MPG-KPC 30) and right (MPG-KPC 1) scapula, fragment of an (?)ilium (MPG-KPC 23), proximal end of right tibia (MPG-KPC 8), and numerous fragments of vertebrae, ribs and chevrons. Isasmendi et al. (2024) also mentioned a fragment of a fibula, but we have not seen that specimen in the collections in Galve.

Referred material. Tip of a tooth, originally described by Sánchez-Hernández and Benton (2014: figure 2); partial mid-caudal vertebral centrum (MPG-KPC 63); partial mid-caudal vertebra (MPZ2022/182a), discovered in situ by one of the authors (OR) during a visit to the type locality in 2017; partial right surangular and articular (MPZ 2022/182b), right femur (MPZ 2022/182c), and pedal ungual (MPZ 2022/182d), resulting from a systematic excavation of the type locality in 2018; partial tooth (MPZ 2022/182e), discovered in situ by one of the authors (DC) during a visit to the type locality in 2024. All of these materials almost certainly represent the same individual as the type specimen.

Remarks. An allegedly anterior cervical vertebral centrum (MPG-KPC 24) was tentatively referred to *Camarillasaurus* by Sánchez-Hernández and Benton (2014). The specimen could not be located in the collections of Museo Paleontológico de Galve José María Herrero. If this element represents a cervical vertebra, it is considerably too small to fit the rest of the material. The above authors estimate its original length to have been 28-30 mm, and, according to their figure, the anterior articular surface is c. 15 mm wide. Even though vertebral size increases from anterior cervicals towards the posterior dorsal series, this is incompatible with the width of the completely preserved posterior dorsal centrum, which is more than 100 mm wide. This incomplete vertebra is thus removed from the taxon here (see also Samathi et al., 2021).

Emended diagnosis. A mid- to large-sized member of the Spinosauridae defined by the following combination of characters: surangular with a notable rugose lateral tubercle at the posterior end of the lateral surangular ridge, lateral to the posterior half of the mandibular glenoid (a similar tubercle is found in *Irritator*, but is located above the surangular ridge and posterior to the glenoid; Schade et al., 2023); articular facets of prezygapophyses of dorsal vertebrae transversely concave; mid-caudal neural spines elongated, rod-like and slightly flexed anteriorly dorsally; posterior caudal vertebrae with posteriorly projecting postzygapophyses that are dorsally connected to the neural spine by a bony web.

Type locality and horizon. Fuente Arnar site, Camarillas Formation (Barremian) near the village of Camarillas (Teruel, Spain).

DESCRIPTION

Cranial Remains

Surangular/articular. The newly excavated material includes the posterior end of the right surangular (MPZ 2022/182b; Figure 3), which is completely fused with the articular, without any visible suture, as is the case in *Irritator* (SMNS 58022; Schade et al., 2023). Most of the anterior vertical lamina of the main body of the surangular is missing, but the posterior end of the laterodorsally-facing shelf for the attachment of the *m. adductor mandibulae externus superficialis*, the jaw articulation, and the retroarticular process are well preserved. The preserved portion of the posterior mandible has a total length of c. 215 mm.

The posterior end of the mandible is robust and considerably expanded medially in the region of the mandibular glenoid, reaching a maximal width of slightly more than 90 mm in the area of the jaw articulation. Of the portion of the surangular anterior to the glenoid, it is mainly the facet for the insertion of the *m. adductor mandibulae externus superficialis* that is preserved (Figure 3A). Unlike other theropods, such as *Allosaurus* (Madsen, 1976) and *Asfaltovenator* (Rauhut and Pol, 2019), where this facet is developed as a longitudinal depression on the mediolaterally widened dorsal surface of the surangular, delimited by a dorsal ridge medially and somewhat offset anteriorly from the mandibular glenoid, in MPZ 2022/182b it faces more laterally than dorsally and extends posteriorly to the anterior rim of the glenoid, extending onto the lateral surangular ridge in this area (Figure 3A). Its medial margin forms a broadly rounded dorsal surface posteriorly, then becomes triangular in outline, with a sharp dorsal margin a short distance anterior to the glenoid, and broadens towards the anterior break. Halfway between the glenoid margin and the anterior break, a shallow and narrow groove appears on the dorsal surface of this medial margin and gradually widens anteriorly towards the break (Figure 3D). Whereas the medial margin is generally thickened posteriorly, it becomes an inverted L-shape in cross-section towards the anterior break (Figure 3C), forming a medioventrally overhanging shelf over the medial side of the bony shelf that holds the facet for the adductor muscle on its dorsolateral side. This shelf is robust posteriorly, but becomes thinner anteriorly. Posteriorly the largely broken thin lamina of the main lateral body of the surangular extends ventrally from about the mid-width of this shelf, facing slightly ventrolaterally, and then extends anterolaterally, reaching the lateral side of the shelf some 60 mm anterior to the mandibular glenoid. The facet for the attachment of the *m. adductor mandibulae externus superficialis* on this dorsolaterally-facing shelf is developed as a mediolaterally very slightly concave depression that gradually widens anteriorly and then seems to become slightly narrower again towards the anterior break (Figure 3A). Whereas the facet is c. 25 mm wide posteriorly, it is c. 40 mm wide in the widest preserved part.

On the lateral surface of the posterior part of the surangular, the lateral surangular ridge is well developed and delimits the facet for the *adductor mandibulae* muscle posteroventrally, as mentioned above. It becomes less conspicuous anteriorly and disappears at approximately the point where the thin lamina of the main surangular body reaches the lateral surface of the dorsolaterally-facing shelf. Posteriorly, a large, well-marked, oval lateral tubercle is present as a continuation of the lateral ridge, lateral to the posterior half of the glenoid facet (Figure 3A, B, D). The lateral surface of this tubercle is slightly rugose. A similar tubercle is present in *Irritator* (Schade et al., 2023) but has not been described for any other theropod. From the anterodorsal end of this tubercle, a marked, step-like ridge extends anteriorly and then curves medially (Figure 3A), thus marking the anterolateral edge of the glenoid facet and the posterior end of the facet for the insertion of the *m. adductor mandibulae externus superficialis*. From the posterodorsal margin of the tubercle, a massive projection extends dorsally, thus forming the posterior margin of the glenoid facet (Figure 3). This projection becomes anteroposteriorly thinner dorsally in lateral view, with a slightly concave anterior and a convex posterior margin. In posterior view, the expansion is trapezoidal in outline, extends over the lateral half of the glenoid facet, and has its apex approximately in the posterior extension of the medial margin of the posterolateral shelf anterior to the glenoid. Laterally, two small surangular foramina are present below the lateral surangular ridge: a smaller, more anteriorly-facing foramen some 30 mm anterior to the anterior rim of the glenoid facet, located directly below the ridge, and a slit-like, slightly larger, laterally-facing foramen located directly below the anterior margin of the facet slightly more ventrally (Figure 3A).

At the anterior margin of the glenoid, the medial side of the surangular flares medially, forming the anterior wall of the glenoid area, which is mediolaterally concave in dorsal view. In anterior view, this wall is triangular in outline, tapering dor-

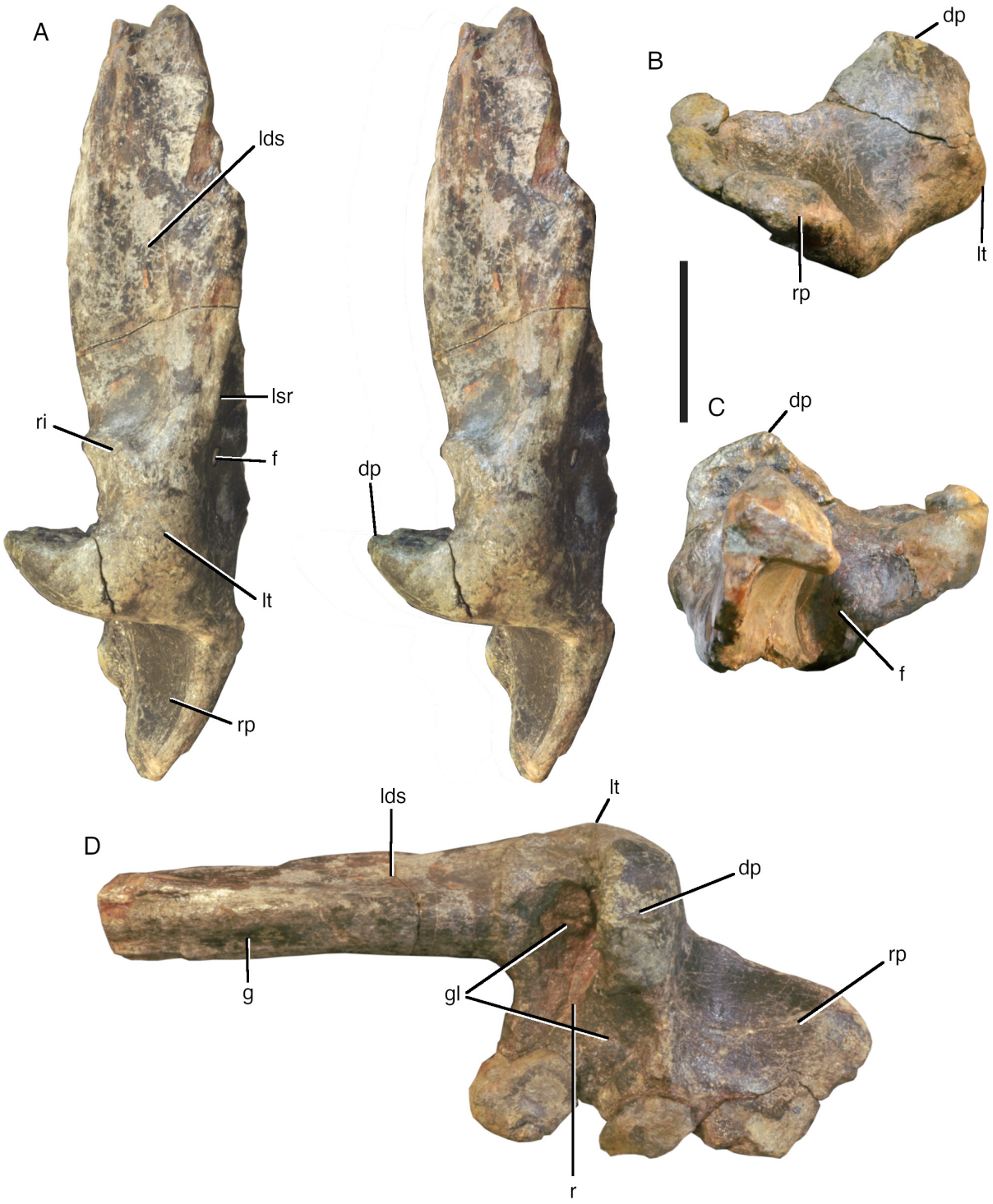

FIGURE 3. Fused right surangular/articular of *Camarillasaurus cirugedae*, MPZ 2022/182b. A, lateral view (stereophotograph); B, posterior view; C, anterior view; D, dorsal view. Abbreviations: dp, dorsal process; f, foramen; g, groove; gl, concave facets of the mandibular glenoid; lds, laterodorsally facing shelf for the attachment of the *m. adductor mandibulae externus superficialis*; lsr, lateral surangular ridge; lt, lateral tubercle; r, ridge separating the mandibular glenoid cotyles; ri, ridge bordering the glenoid anterolaterally; rp, retroarticular process. Scale bar is 5 cm.

somedially (Figure 3C), indicating that the articulation with the prearticular was ventromedially inclined, although the bone seems to be damaged in this area. The wall is dorsoventrally slightly concave and shows an oval foramen in its lateroventral part, which enters the bone in a lateroposterior direction.

In dorsal view, the glenoid facet is subdivided into a lateral and a medial part by an oblique ridge that extends anteromedially from the anteromedial edge of the dorsal projection that borders the lateral part of the facet posteriorly (Figure 3D). The lateral part of the facet, anterolateral to this ridge and anterior to the dorsal projection, is considerably narrower anteroposteriorly (c. 27 mm maximally) than wide mediolaterally (maximally c. 60 mm). It is roughly rectangular anterior to the dorsal projection, but tapers anteromedially anterior to the ridge that separates it from the medial facet. It is generally slightly concave both anteroposteriorly and mediolaterally, but flexes sharply downwards on the lateral side, resulting in a marked mediolateral convexity anterior to the lateral margin of the dorsal projection. The medial glenoid facet extends further posteriorly than the lateral facet, with its lateral side extending onto the medial margin of the dorsal projection. Due to the anterior expansion of the medial margin of the glenoid facet, it also extends further anteriorly on its medial side than the lateral facet. It is roughly triangular in outline, becoming narrower posterolaterally, and gently concave anteroposteriorly. Its medial margin is damaged, but its maximal anteroposterior extension (c. 54 mm) was more than its mediolateral width (c. 45 mm).

The retroarticular process shows an unusual morphology for theropods, only mirrored by that seen in *Irritator* (Schade et al., 2023). It is well developed, somewhat inset medially from the lateral side of the posterior mandible (Figure 3D), and approximately 60 mm long. The process is broad (c. 65 mm at its base, medial side slightly damaged) and notably flat, with a maximal dorsoventral thickness of 17 mm. Its lateral margin is notably offset ventrally from the glenoid articulation, but in posterior view, the process is dorsomedially inclined, so the medial edge is approximately level with the glenoid facet at its base (Figure 3B). In dorsal view, the process is roughly tongue-shaped, with an apparently squared, but slightly damaged posteromedial edge. In contrast to most theropods, where the attachment area for the *m. depressor mandibulae* is developed as a groove (e.g., Rauhut and Pol, 2021), the dorsal surface of the process is mediolaterally notably convex, with only a slight mediolateral concavity towards the posterior end of its medial half. The ventral side seems to be mainly flat, becoming mediolaterally convex towards its medial and lateral margins, but is generally poorly preserved. A facet for the attachment of the angular cannot be identified, indicating that this bone did not contribute to the ventral margin of the retroarticular process, as is the case in some theropods.

Teeth. An isolated tooth tip (MPG-KPC 43; Figure 4A-C), found on the surface of the field next to the site, was referred to *Camarillasaurus* by Sánchez-Hernández and Benton (2014). The element is rather small, with a lenticular, almost rounded cross-section and strongly worn mesial and distal edges, so the presence of marginal denticles cannot be established. The enamel shows slight ornamentation close to the distal carina in the form of anastomosing grooves and ridges. Although the tooth is consistent with representing the tip of a spinosaurid tooth, a crocodylomorph identification cannot be ruled out completely in the light of the preservation.

The partial tooth (MPZ 2022/182e) recently found at the type locality clearly represents a spinosaurid tooth (Figure 4D-F). Preserved is the basal part of the crown, missing the tip and the root. Although it cannot be ruled out completely that the tip described by Sánchez-Hernández and Benton (2014) comes from the same tooth, as it would fit in size as the tip of the same element, the preserved parts do not seem to fit together directly, and the morphology is not entirely compatible. The base of the tooth has an oval cross-section, with a ratio between mesiodistal length (14.44 mm) and labiolingual width (12.15 mm) of c. 1.2. A small labial protuberance is present at the mid-length of the crown in basal view (Figure 4H). The crown is moderately recurved, with the mesial margin being gently convex, and the distal margin slightly concave in lingual or labial view. In mesial or distal view, the crown is straight. There is a poorly developed, sharp-keeled, and unserrated distal carina, but a mesial carina is absent in at least the preserved part (Figure 4F, G). Approximately eight well-developed flutings are present on the presumed lingual side, while the presumed labial side shows six to seven poorly developed flutes. Two weakly pronounced flutes are present on the mesial side. The enamel shows a finely anastomosed enamel texture (sensu Hendrickx et al., 2015).

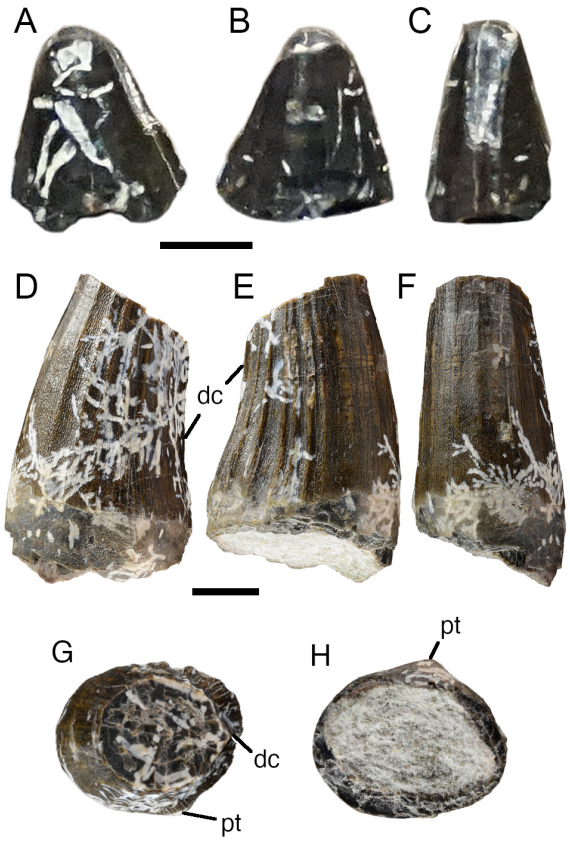

FIGURE 4. Teeth referred to *Camarillasaurus cirugedae*. A-C, MPG-KPC 43, tooth tip in ?labial (A), ?lingual (B) and ?distal views. D-F, MPZ 2022/182e, partial tooth in labial (D), lingual (E), mesial (F), apical (G) and basal (H) views. Abbreviations: dc, distal carina; pt, protuberance. Scale bars are 5 mm.

Vertebral Column

The vertebral column of *Camarillasaurus* is represented by two posterior dorsal vertebral centra, several fragments of dorsal neural arches, parts of four sacral vertebrae, anterior, middle, and distal caudal vertebrae, an almost complete posterior dorsal rib, several chevrons, and numerous fragments of vertebrae, neural arches, and ribs. For vertebral measurements see Table 1.

Dorsal vertebrae. An isolated prezygapophysis (MPG-KPC 40, Figure 5A, B) is the only remaining element of the anterior part of the dorsal vertebral column, as judged by the presence of a hypantrum facet and its placement on a separate pedicle, as cervical vertebrae usually lack hypantra and middle and posterior dorsal prezygapophyses tend to be placed directly anteroventral to the neural spine on the base of the neural arch. The prezygapophysis was thus projected forward from the neural arch and is supported ventrally by a stout, anteriorly broadly convex centroprezygapophyseal lamina. The articular surface of the prezygapophysis is slightly longer than wide and widens anteriorly. It is inclined medially at an angle of at least 45° and is notably concave transversely, with an especially raised lateral edge (Figure 5B). On the medial side, a flat, anteroposteriorly elongated, triangular articular facet of the hypantrum is present.

The best-preserved presacral vertebra (MPG-KPC 9, Figure 5C-E) was identified as a probable posterior cervical vertebra by Sánchez-Hernández and Benton (2014), but the position of the small parapophyses high on the neural arch indicates

TABLE 1. Measurements of vertebrae of *Camarillasaurus cirugedae* (in cm). Abbreviations: Ant, anterior; Post, posterior. [a]Element is damaged, minimum estimate.

Specimen	Length	Ant. height	Ant. width	Post. height	Post. width
MPG-KPC 9	9.5	9	11.1	9.4	11.2
MPG-KPC 18		9.8	8[a]		
MPG-KPC 19		11.1	7.7[a]		
MPG-KPC 16				8.7	7.6
MPG-KPC 21		10	7.4[a]		
MPG-KPC 20		10.2	6.3[a]		
MPZ2022/182a		6.8	6.3		
MPG-KPC 11	8.7	5.3	5.4	5.5	4.8
MPG-KPC 10	8.4	5	4.9	5.5	4.7
MPG-KPC 12	8	4.6	4.5	5.1	3.9[a]
MPG-KPC 13	7.8	5	4.6	5.7	4.8

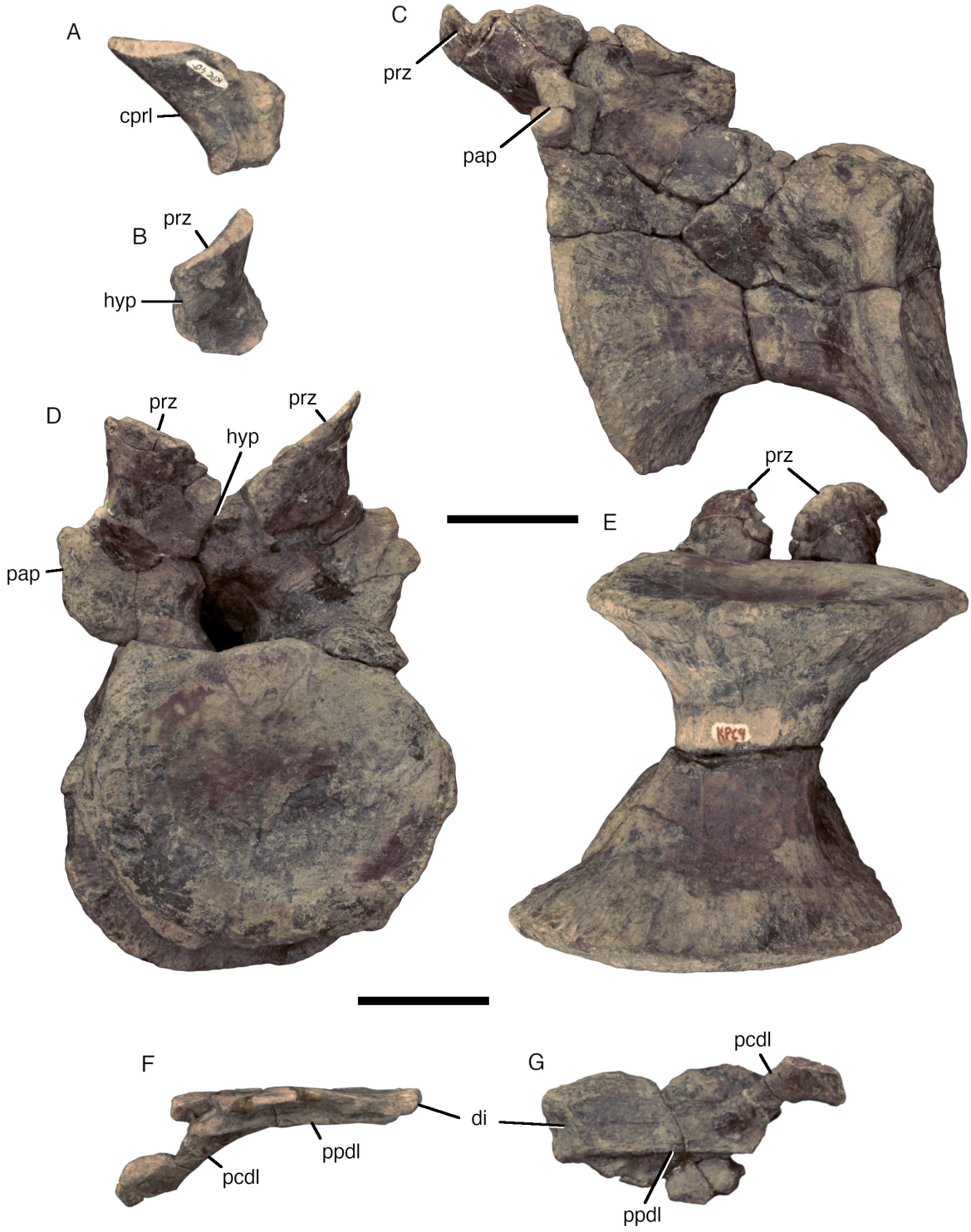

FIGURE 5. Remains of dorsal vertebrae of *Camarillasaurus cirugedae*. A, B, isolated anterior dorsal left prezygapophysis (MPG-KPC 40) in lateral (A) and anterior (B) views. C-E, posterior dorsal vertebral centrum and partial neural arch (MPG-KPC 9) in left lateral (C), anterior (D) and ventral (E) views. F, G, isolated left transverse process (MPG-KPC 14) in anterior (F) and ventral (G) views. Abbreviations: cprl, centroprezygapophyseal lamina; di, diapophysis; hyp, hypantrum; pap, parapophysis; pcdl, posterior centrodiapophyseal lamina; ppdl, paradiapophyseal lamina; prz, prezygapophysis. Scale bars are 5 cm.

that this is a posterior dorsal vertebra. Preserved are the centrum and the anterior part of the neural arch, including the prezygapophyses, but the transverse processes, postzygapophyses, and neural spine are missing. The vertebra is slightly deformed, giving the centrum a parallelogram-like outline in lateral view.

The vertebral centrum of MPG-KPC 9 is stout and approximately as high as long (Table 1), with the articular facets being oval in outline and slightly wider than high. The articulations are slightly amphicoelous, with the posterior articular surface being more notably concave than the anterior. The centrum is strongly constricted in the midline and has large, but shallow, oval pleurocentral depressions in the dorsal part of the sides. Contra Sánchez-Hernández and Benton (2014) and Malafaia et al. (2020a, b), these depressions are not subdivided, but continuous. Below these depressions, the centrum widens mediolaterally, and the ventral side is broad and flattened, as in *Baryonyx* (Charig and Milner, 1997) and *Vallibonavenatrix* (Malafaia et al., 2020b).

The anterior end of the neural arch, as measured from the dorsal rim of the centrum to the dorsal margin of the prezygapophyses, is only slightly lower than the height of the centrum. The neural canal is narrow ventrally and slightly incised into the dorsal surface of the centrum, but widens dorsally. The parapophyses are located entirely on the neural arch, slightly above halfway up the neural arch on a lateral expansion of the stout centroparapophyseal lamina (Figure 5C, D). The articular facets of the parapophyses are high oval to kidney-shaped in outline and small, being c. 20 mm high dorsoventrally and 13 mm wide anteroposteriorly. They are slightly concave both anteroposteriorly and dorsoventrally. Dorsally, the anterodorsal edge of the parapophysis connects to the ventrolateral surface of the prezygapophysis via a stout but short prezygoparapophyseal lamina. In anterior view, the centroparapophyseal and prezygoparapophyseal laminae form a broad bony wall lateral to the neural canal, which is slightly concave dorsoventrally at the level of the parapophyses. A slight swelling and ridge are present at the posterodorsal edge of the parapophysis, but a true paradiapophyseal lamina seems to be absent.

The prezygapophyses are large and steeply angled dorsomedially, at approximately 30-40° towards the horizontal (Figure 5D), unlike the usually small and subhorizontal posterior dorsal prezygapophyses in most theropods. They are almost round in outline, with a diameter of c. 40 mm, and slightly concave transversely; the same morphology is also seen in an isolated posterior dorsal prezygapophysis (MPG-KPC 42), indicating that this concavity is real and not an artifact of deformation. The hypantrum is well developed, but dorsoventrally low. It is narrow dorsally between the medial edges of the prezygapophyses (c. 5 mm), but rapidly widens ventrally to a maximal width of 15 mm.

Two further vertebral remains, MPG-KPC 15 and MPG-KPC 18, described as an anterior caudal and a sacral vertebra, respectively, by Sánchez-Hernández and Benton (2014), represent the anterior and posterior halves of the same posterior dorsal vertebral centrum. The centrum is less well preserved than MPG-KPC 9, but shows the same characteristics, being only slightly less robust, indicating that it might represent a more anterior position. Furthermore, a very shallow, poorly defined longitudinal sulcus seems to be present on the ventral side. A further vertebral fragment, MPG-KPC 19, might represent another posterior dorsal vertebral centrum, but the element is so poorly preserved that it cannot be ruled out that it represents an anterior caudal, as identified by Sánchez-Hernández and Benton (2014).

An isolated left dorsal transverse process (MPG-KPC 14; Figure 5F, G) provides additional information on the structure of the dorsal neural arches. This element was described and figured as “a fragment of the lateral side of a centrum with postzygapophysis” of a posterior cervical or anterior dorsal vertebra under the erroneous number MPG-KPC 51 by Sánchez-Hernández and Benton (2014: p. 586 and figure 5E). The element is a plate-like transverse process, which is incomplete proximally. The process was apparently posterolaterally directed and slightly tapers distally, with the posterior edge flexing anteriorly towards the distally placed diapophysis in its distalmost part (Figure 5G). Thus, whereas the anteroposterior width is c. 50 mm proximally, the distal end is only 25 mm wide. Proximally, the dorsal part of a stout, but relatively short posterior centrodiapophyseal lamina is present (the “postzygapophysis” of Sánchez-Hernández and Benton, 2014). This extends to approximately two fifths of the length of the process, is located slightly posterior to the proximal mid-width of the process, and is steeply inclined posteroventrally. The anterior centrodiapophyseal or paradiapophyseal lamina is obviously poorly developed proximally, but extends over the entire length of the process up to the anterior edge of the diapophysis as a notable, slightly anteroventrally overhanging ridge (Figure 5F, G). The articular sur-

face of the diapophysis is lateroventrally inclined. It is rectangular to subtriangular in outline, with a rounded, slightly elevated dorsal margin. This transverse process probably belongs to a middle or posterior dorsal vertebra, but nothing can be said about its exact position within the dorsal vertebral column.

Several isolated dorsal postzygapophyses (MPG-KPC 41,61,62) are obliquely oval in outline, were obviously steeply lateroventrally inclined, corresponding to the inclination of the dorsal prezygapophyses, and preserve the ventral bases of well-developed, stout spinopostzygapophyseal laminae, indicating that a well-developed spinopostzygapophyseal fossa was present between the postzygapophyses.

An isolated posterior dorsal or sacral neural spine, MPG-KPC 2 (Figure 6C, D), was identified as a sternal plate by Sánchez-Hernández and Benton (2014: figure 10B; labelled MPG-KPC 1 in the figure caption). The spine is an anteroposteriorly wide and high bone plate, similar to the spines of *Ichthyovenator* (Allain et al., 2012), *Baryonyx* (Charig and Milner, 1997: figure 27A), and *Vallibonavenatrix* (Malafaia et al., 2020b). As in these taxa, the spine expands anteroposteriorly dorsally, with a slightly convex posterior edge and an apparently straight to very slightly concave anterior margin. Whereas the anterior and posterior margins of the spine are sharp-edged, it slightly expands transversely towards its dorsal margin, more so posteriorly than anteriorly. As in *Vallibonavenatrix* (Malafaia et al., 2020b), shallow, but notable dorsoventral grooves and ridges are present on the lateral side towards the dorsal end. The posterodorsal edge of the spine is taphonomically bent laterally. A spinodiapophyseal lamina, as is present in *Vallibonavenatrix* (“lateral process” in Malafaia et al., 2020b), does not seem to be present, although it cannot be completely ruled out that a small lamina might have been present in the unpreserved base of the spine, as this lamina is restricted to the basal parts in the latter taxon. The total height of the spine, as preserved, is 23 cm; its dorsal anteroposterior width is c. 12 cm.

Several fragments that were figured as possible tips of dorsal neural spines by Sánchez-Hernández and Benton (2014: figure 4B) are distal ends of dorsal (e.g., MPG-KPC 33) and caudal (e.g., MPG-KPC 32) transverse processes.

Sacral vertebrae. Sánchez-Hernández and Benton (2014) suggested that the sacrum of *Camarillasaurus* consisted of six vertebrae, although they only listed the remains of five vertebral centra, one of which, MPG-KPC 18, is half of a posterior dorsal centrum, as outlined above. Thus, the remains of only four sacral vertebral centra are preserved, two of which are only represented by half of the centrum (and it cannot be completely ruled out that they represent the same vertebra, although the halves do not fit together). MPG-KPC 3 and 4 represent the remains of two and a half fused sacral centra, preserved in two parts, which do, however, fit together (Figure 6A, B). We interpret these centra as the primordial sacra one and two and a caudosacral, the latter representing the element identified as sacral two by Sánchez-Hernández and Benton (2014). The remaining probable sacral, MPG-KPC 16, is only represented by a poorly preserved half of a centrum, the position of which cannot be identified with any certainty.

As noted above, the three articulated sacrals seem to be S1 and S2 and CS1, given that the first and second centra are completely fused, with the border between the vertebrae being marked only as a slight swelling. The sacrals form a straight line, not an arch, contra Sánchez-Hernández and Benton (2014). The third vertebra is fused to the second, but the swelling is considerably more marked and comparable to the height of the anterior caudal vertebrae MPG-KPC 20 and 21 (see below). The sacral vertebrae are strongly waisted, elongated, and rounded ventrally, with the second vertebra (S2) being slightly broader than the first (S1) and CS1 slightly more flattened. A ventral keel is not present, contra Sánchez-Hernández and Benton (2014). Sacral 1 and the caudosacral vertebra have the broken bases of large transverse processes preserved anterodorsally on the centrum. The anterior articular surface of S1 is flattened and was not fused to the dorsosacral centrum, indicating immaturity (contra Sánchez-Hernández and Benton, 2014). The articular surface is slightly heart-shaped, being pointed ventrally. Although there seems to be a small foramen just below the posterior end of the transverse process on the left side, no sign of such a foramen can be found on the right side. Only the CS1 seems to have a small pleurocentral depression, but pneumatic recesses or foramina are absent.

Centrum MPG-KPC 16 is a very poorly preserved centrum of a strongly waisted vertebra (Figure 6E, F). This element probably represents a sacral vertebra, based on the constriction of the centrum, which is more pronounced than in the dorsal vertebrae, and the fact that the size of the articular surface coincides with the other sacrals. Ventrally, the centrum is narrowly rounded; the

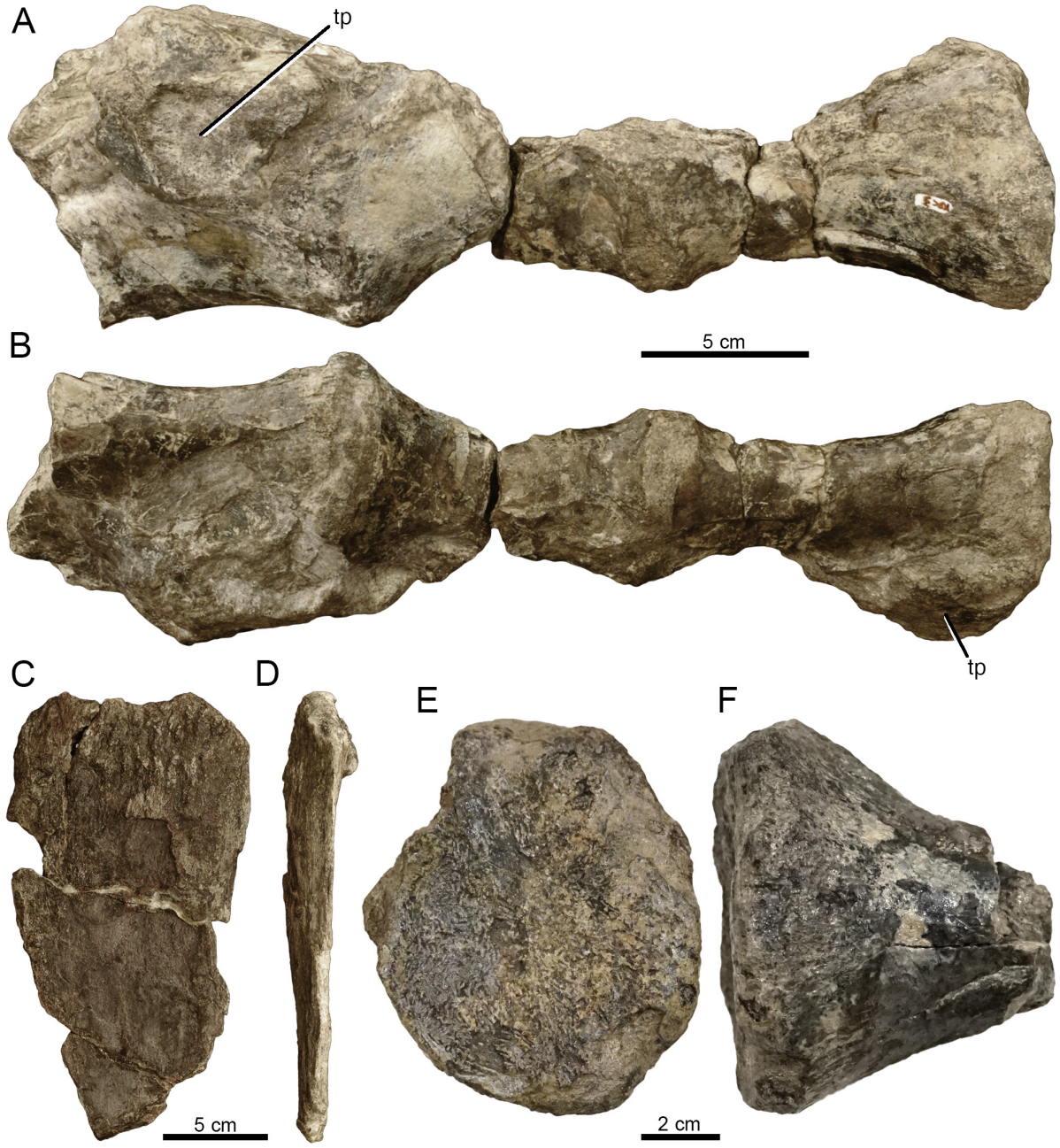

FIGURE 6. Sacral vertebrae and possible posterior dorsal or sacral neural spine of *Camarillasaurus cirugedae*. A, B, probable partial primordial sacral centra one and two and a caudal sacral vertebral centrum (MPG-KPC 3 and 4) in left lateral (A) and ventral (B) views. Anterior is to the left. C, D, posterior dorsal or sacral neural spine (MPG-KPC 2) in left lateral (C) and anterior (D) view. E, F, half sacral centrum (MPG-KPC 16) in anterior (E) and ventral (F) view. Abbreviation: tp, broken basis of the transverse process. Scale bars are 5 cm (A-D) and 2 cm (E, F).

ventral keel indicated by Sánchez-Hernández and Benton (2014: figure 6C1) represents a slight displacement at a break in the centrum.

Caudal vertebrae. Anterior caudal vertebrae are represented by two partial centra (MPG-KPC 20, 21) and a partial neural arch (MPG-KPC 39). The most complete element, MPG-KPC 21 (identified as a mid-dorsal vertebra by Sánchez-Hernández and Benton, 2014), represents one of the anteriormost caudal vertebrae (Figure 7A, B). The centrum is incomplete posteriorly, but enough of the posterior end is preserved to establish its length. In gen-

FIGURE 7. Anterior to mid-caudal vertebrae of *Camarillasaurus cirugedae*. A, B, partial anterior vertebral centrum MPG-KPC 21 in left lateral (A) and anterior (B) views. C, partial anterior caudal neural arch MPG-KPC 39 in left lateral view. D, E, partial anterior caudal centrum MPG-KPC 20 in ventral (D) and left lateral (E) view. F, G, partial mid-caudal vertebra MPZ 2022/182a in anterior (F) and left lateral (G; including the neural spine that belongs to this vertebra) view. Abbreviations: cf, chevron facets; poz, postzygapophysis; spdr, spinodiapophyseal ridge; tp, transverse process; vg, ventral groove. Scale bars are 5 cm.

eral, this vertebra is comparable in size to the posterior dorsals, but the anterior articular surface is higher than wide, unlike the condition in the dorsal vertebrae. The centrum is amphicoelous, with the anterior articular surface being very deeply concave, similar to the condition in *Spinosaurus* (Stromer, 1915), *Ichthyovenator* (Allain et al., 2012), and a spinosaurid caudal from the Kem Kem beds, probably belonging to *Sigilmassasaurus* (SNSB-BSPG 2008 I 67; Lex, 2016). The ventral side of the centrum is less wide than in the dorsal vertebrae, but also flattened, with a weakly developed longitudinal midline sulcus. As the posterior end of the ventral side is not preserved, it cannot be said whether chevron facets were present in this vertebra. Large, but very shallow pleurocentral depressions are present on the lateral side of the centrum. Only small parts of the neural arch are preserved, including the broken attachment of the left transverse process. The neural canal is similar to that seen in the dorsal vertebrae, being narrow and slightly incised into the centrum ventrally and widening dorsally. The base of the transverse process is entirely located over the posterior half of the centrum. It is oval in outline, anteroposteriorly short (35 mm), and robust. No lateral laminae extending from or towards the transverse process are present; only the anterior centrodiapophyseal lamina is indicated by a very weak ridge on the anteroventral margin of the process. Together with the dorsal edge of the transverse process, this ridge defines a distally narrowing, triangular, flat area on the anterior side of the process. Although only the base is preserved, it can be said with some certainty that the transverse process was directed strongly posterolaterally, but only slightly, if at all, dorsally.

A posterior half of another anterior caudal vertebral centrum, MPG-KPC 20 (identified as a dorsal centrum by Sánchez-Hernández and Benton, 2014), largely conforms to the element described above (Figure 7D, E). Here, the pleurocentral depressions are only very weakly developed, and well-developed chevron facets are present on the ventral side of the posterior end of the centrum. In ventral view, these chevron facets continue anteriorly in two notable, rounded ridges that define a well-developed midline sulcus, at least in the posterior half of the centrum.

The element MPG-KPC 39 is a poorly preserved partial anterior caudal or anterior mid-caudal neural arch (Figure 7C). This bone was identified as a dorsal neural arch by Sánchez-Hernández and Benton (2014), but such an identification can be ruled out due to the lack of lateral laminae and the development and placement of the postzygapophyses. The neural arch is anteroposteriorly short and preserves the base of an anteroposteriorly short, but rather broad neural spine. The postzygapophyses (identified as prezygapophyses by Sánchez-Hernández and Benton, 2014) are located below the posterior base of the neural spine, as is usual in theropod caudal vertebrae. A notable spinopostzygapophyseal fossa is present, with a ridge-like postspinal lamina in the midline. The “fossae” identified by Sánchez-Hernández and Benton (2014) on the lateral side of the neural arch are very slight depressions, most of which might well be diagenetic rather than representing true anatomical features.

An anterior mid-caudal vertebra, MPG-KPC 17, is only represented by the centrum, which is relatively short, strongly waisted, and higher than wide. As in the anterior caudal vertebra, the anterior articular surface is more notably concave than the posterior surface. The ventral surface is flat anteriorly, but has a slight ventral sulcus posteriorly towards the well-developed, widely separated chevron facets.

The newly recovered element, MPZ 2022/182a is a mid-caudal vertebra (Figure 7F, G). The vertebra is represented by the anterior half of the centrum, the right transverse process and the neural spine, which were all found in situ, but detached, with weathered portions separating them. However, given the association of the remains, there can be no doubt that all of these bones represent the same element. The vertebral centrum has a slightly concave anterior articular facet. The facet is slightly higher (68 mm) than wide (63 mm) and has a straight to slightly concave dorsal margin and well-rounded lateral and ventral margins, becoming slightly wider ventrally. There is no clearly defined haemapophysis facet on the anterior end of the centrum, but the ventral side of the articular end is slightly flexed ventrally. The centrum is strongly constricted between the articular ends, its minimal width (27 mm) being less than half the maximal width of the anterior articular surface. A notable pleurocentral depression is present on the right side of the centrum, similar to the condition in megalosaurines (Rauhut et al., 2016), but not on the left side. Ventrally, the centrum gradually narrows to a narrow ventral side that has a weak midline ridge in the preserved anterior part.

The neural arch is low, and the neural canal small, with an anterior diameter of 8 mm. No lateral laminae are present. The centroprezygapophyseal

FIGURE 8. Distal caudal vertebrae of *Camarillasaurus cirugedae*. A-E, vertebra MPG-KPC 11 in left lateral (A), anterior (B), posterior (C), dorsal (D), and ventral (E) view. F-J, vertebra MPG-KPC 10 in left lateral (F), anterior (G), posterior (H), dorsal (I), and ventral (J) view. K-O, vertebra MPG-KPC 12 in left lateral (K), anterior (L), posterior (M), dorsal (N), and ventral (O) view. P-T, vertebra MPG-KPC 13 in left lateral (P), anterior (Q), posterior (R), dorsal (S), and ventral (T) view. Abbreviations: bw, bony web; cf, chevron facets; ns, neural spine; poz, postzygapophysis; psr, prespinal ridge, tp, transverse process. Scale bars are 2 cm.

laminae form a broad anterior wall lateral to the neural canal, unlike the funnel-shaped entrance to the neural canal in some carcharodontosaurids (Rauhut, 2011). The broken prezygapophyses were located on stout, anterodorsally directed stalks. Weakly developed spinoprezygapophyseal laminae are present some way posterior to the prezygapophyses on the roof of the neural arch.

A large part of the right transverse process is preserved, but detached from the neural arch. The process is anteroposteriorly slender and was obviously directed posterolaterally. Its dorsal surface is very slightly concave anteroposteriorly in its proximal part and slightly flexes ventrally distally. The ventral surface is strongly convex anteroposteriorly, without any indication of distinct lateral laminae. The distal end of the process seems to be not or only very slightly expanded anteroposteriorly, unlike the condition in *Allosaurus* (Madsen, 1976) and many other early branching tetanurans. It is rounded in dorsal or ventral view.

Like the transverse process, the neural spine is detached from the rest of the vertebra, but complete and well preserved (Figure 7G). The spine is elongated, being c. 200 mm high above the neural canal and considerably inclined posteriorly, with the distal tip flexing slightly anteriorly. It is rod-like, its minimal anteroposterior width being 23 mm some 130 mm above the neural canal, from where it expands slightly and gradually to a width of 30.5 mm at the distal tip. Weakly developed spinodiapophyseal ridges are present on the lateral side of the neural spine, which extend over most of the height of the spine, but are most notable in the area just above the postzygapophyses. The postzygapophyses are steeply angled and located at the ventral end of the posterior margin of the neural spine. They are connected to the lateral edges of the proximal part of the spine by weakly developed spinopostzygapophyseal laminae. Between these laminae, and extending almost all the way up to the distal end, a ridge-like postspinal lamina is present. Anteriorly, neither a prespinal lamina nor spinoprezygapophyseal laminae are preserved, underlining the poor development of the latter, as seen on the neural arch.

Four distal caudal vertebrae are present in the original type material, MPG-KPC 10-13 (Figure 8). The element MPG-KPC 11 (Figure 8A-E) is the most anterior of these vertebrae, as demonstrated by the presence of the broken base of a small transverse process (Figure 8A), which is absent in the other elements. The vertebral centra are considerably elongated compared to the anterior and mid-caudal vertebrae, and the articular facets are approximately as high as wide. The articular facets are rounded subrectangular in outline, and the posterior facet is slightly more deeply concave than the anterior facet. In lateral view, the ventral side is considerably concave anteroposteriorly. The ante-

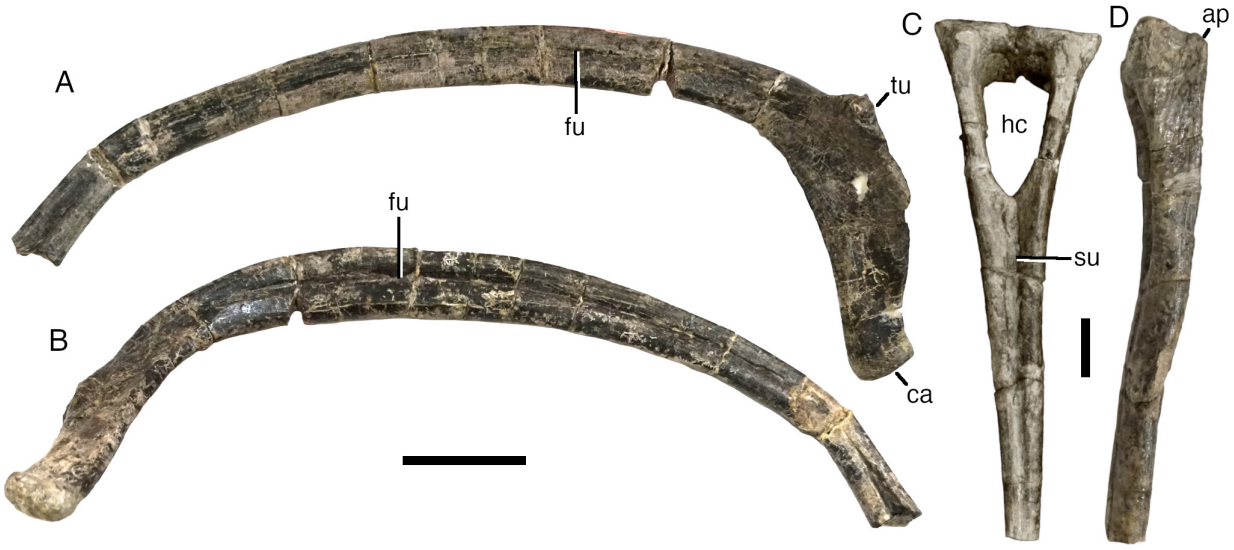

FIGURE 9. Ribs and chevrons of *Camarillasaurus cirugedae*. A, B, posterior dorsal rib of the left side, MPG-KPC 7, in posterior (A) and anterior (B) view. C, D, anterior chevron, MPG-KPC 5, in anterior (C) and right lateral (D) view. Abbreviations: ap, anterior process; ca, capitulum; fu, furrow; hc, haemal canal; su, sulcus; tu, tuberculum. Scale bars are 5 cm (A, B) and 2 cm (C, D).

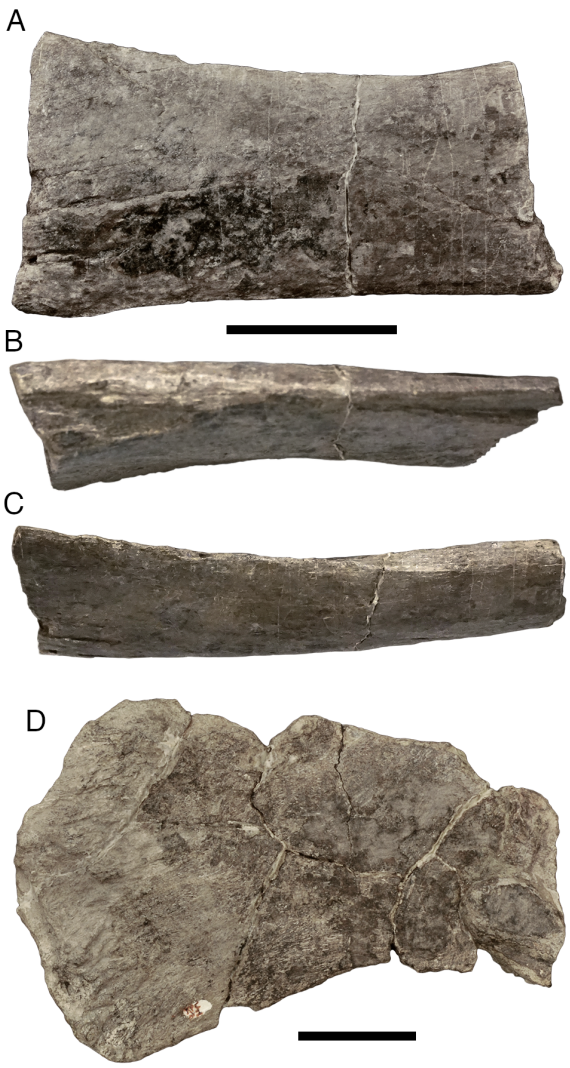

FIGURE 10. Pectoral girdle elements of *Camarillasaurus cirugedae*. A-C, mid-shaft section of left scapula, MPG-KPC 30, in lateral (A), ventral (B), and dorsal (C) view. D, distal end of right scapula, MPG-KPC 1, in lateral view. Scale bars are 5 cm.

rior ventral margin of the articular facet is flexed ventrally to form a small chevron facet, and posteriorly, well-developed chevron facets are present, but there is only a slight hint of a ventral sulcus; otherwise, the ventral side is flat to slightly convex transversely. Large, but shallow pleurocentral depressions are present on the lateral sides. The broken bases of the small transverse processes are located at the dorsal rim of the centrum, just posterior to its mid-length. They are plate-like and c. 20 mm wide anteroposteriorly. The neural arch is low, and the neural canal narrow and high oval in outline. The neural spine is posteriorly located on the neural arch. It is rod-like and inclined posterodorsally; its tip is broken off, so nothing can be said about its original height. The prezygapophyses were set on notable stalks, but are broken off. A weakly developed ridge extends anteriorly from the neural spine between the prezygapophyseal stalks, but an anterior spur in front of the neural spine, as is present in some theropods, is absent. The postzygapophyses are small, high oval in outline and extend from the base of the neural spine posteriorly, overhanging the centrum for their entire length. They are connected to the spine by a stout web of bone.

The other three distal caudal vertebrae preserved are generally very similar to this vertebra, but differ mainly in the absence of a transverse process (Figure 8F-T). The vertebra with the most complete neural spine, MPG-KPC 13, shows that the prespinal ridge extends dorsally to the break of the tip, well dorsal to the level of the postzygapophyses (Figure 8P, Q). The postzygapophyses extend a long way posteriorly from the base of the neural spines and also show a robust web connecting them to the latter.

Ribs. Several rib fragments are present, but only one more complete element, MPG-KPC 7, representing a posterior dorsal rib of the left side (Figure 9A, B). The tuberculum and capitulum are widely separated, with the capitulum sitting on a long and slender shaft, whereas the tuberculum is located directly dorsally on the proximal rib shaft. The rib shaft is strongly curved, as is usual for posterior dorsal ribs, and has a well-developed longitudinal furrow both anteriorly and posteriorly, resulting in an 8-shaped cross-section. The rib shaft gradually tapers distally, further supporting the interpretation of this element as a lumbar rib.

Chevrons. One complete chevron and remains of several further chevrons are present. The complete chevron (MPG-KPC 5; figured by Sánchez-Hernández and Benton 2014: figure 8B) is remarkably straight throughout its preserved length (Figure 9C, D), probably indicating that it is an anterior chevron. The haemal canal is large and inverted bell-shaped. It is dorsally bridged by a stout bony rod that is triangular in lateral view, the proximal articular facet being subdivided into an anteroproximally and a posteroproximally-facing facet by a straight transverse ridge. A well-developed anterior process is present on either side of the chevron shaft, marked as a notable step below the proximal articular facet in lateral view. As noted by Sánchez-Hernández and Benton (2014), there is a triangular depression below the haemal canal on the anterior surface of the bone, which distally leads into a

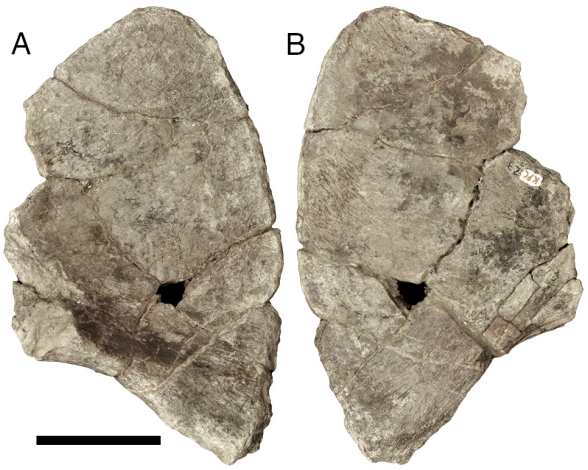

FIGURE 11. Possible anterior end of the preacetabular blade of the left ilium, MPG-KPC 23, in medial (A) and lateral (B) view. Scale bar is 5 cm.

marked median longitudinal sulcus. A similar depression and a short sulcus are also present on the posterior surface, but distally the sulcus is replaced by a sharp median ridge.

Appendicular Skeleton

Scapula. The scapula is represented by two bone fragments: MPG-KPC 30, representing a section of the mid-shaft of the left element (described as part of the right scapulocoracoid by Sánchez-Hernández and Benton, 2014); and MPG-KPC 1, the distal end of the right scapula (identified as a left sternal plate by Sánchez-Hernández and Benton, 2014; labelled MPG-KPC 2 in the figure captions of figure 10A in that paper).

The proximal mid-shaft of the left scapula MPG-KPC 30 is relatively robust, becoming more flattened distally (Figure 10A-C). The bone is slightly longitudinally curved and has a gently dorsoventrally convex lateral surface. The dorsal margin is robust distally and becomes more sharp-edged proximally, rising slightly dorsally towards the missing acromion process. In contrast, the ventral margin is thin distally and becomes more robust proximally. On the medial side, the bone is flat distally, but bulges medially in its ventral part towards the unpreserved scapular glenoid. The fragment preserves the part with the minimal shaft height in its distal section, as the shaft very slightly expands again towards the distal break. Thus, the minimal height of the shaft is located in its distal half, as in *Baryonyx* (Charig and Milner, 1997) and abelisaurids (Burch and Carrano, 2012; Filippi et al., 2018), whereas it is located close to the proximal expansion of the acromion process in most other non-coelurosaurian theropods (e.g., Madsen, 1976; Currie and Zhao, 1993; Marsh and Rowe, 2020).

The distal end of the right scapula, MPG-KPC 1, is plate-like and very slightly flexed medially (Figure 10D). Compared to the dorsoventral width of the shaft at the proximal break (which seems roughly to coincide or slightly overlap with the distal end of the fragment MPG-KPC 30), the distal end shows a considerable, fan-shaped expansion to approximately 160-180% of the minimal shaft width (the dorsal margin of the expansion is somewhat incomplete). Although the distal end expands both dorsally and ventrally, the expansion is considerably more marked ventrally. Whereas the dorsal margin is rather broad, the ventral margin is thin, in agreement with the morphology seen in MPG-KPC 30. The distal end is very slightly thickened mediolaterally and has a rugose texture, marking the attachment of a cartilagenous suprascapula.

(?)Ilium. A bone fragment identified as the right coracoid by Sánchez-Hernández and Benton (2014), MPG-KPC 23, is difficult to interpret (Figure 11). Although the shape as preserved is reminiscent of theropod coracoids, only parts of the anterior and ventral margins seem to be original; all the other margins are broken, and the element lacks characteristic features of theropod coracoids, such as a strongly convex exterior and concave interior surface, a marked thickening towards the glenoid region, or a coracoid foramen (the opening identified as such by Sánchez-Hernández and Benton, 2014, would be in a very unusual position, is located at the intersection of two glued breaks, and has broken, angular margins). As preserved, the bone is mainly flat and rather thin, with an only very slightly convex lateral surface. The anterior margin is gently convex and meets the more or less straight ventral margin at an acute angle of 60-65°. The ventral margin is slightly thickened and becomes more notably thickened towards the posterior break, where the margin also becomes slightly concave in lateral view. This fragment might represent the ventral part of the preacetabular process of the left ilium. The shape of the anterior margin and the angle between the anterior and ventral margins closely correspond to what is seen in other early branching tetanurans (e.g., Madsen, 1976; Currie and Zhao, 1993; Currie and Chen, 2001; Xu et al., 2006), and the concavity in the ventral margin towards the break might mark the transition towards the pubic peduncle. The thickening above that concavity would thus correspond to the anterior end of the medial shelf and the attach-

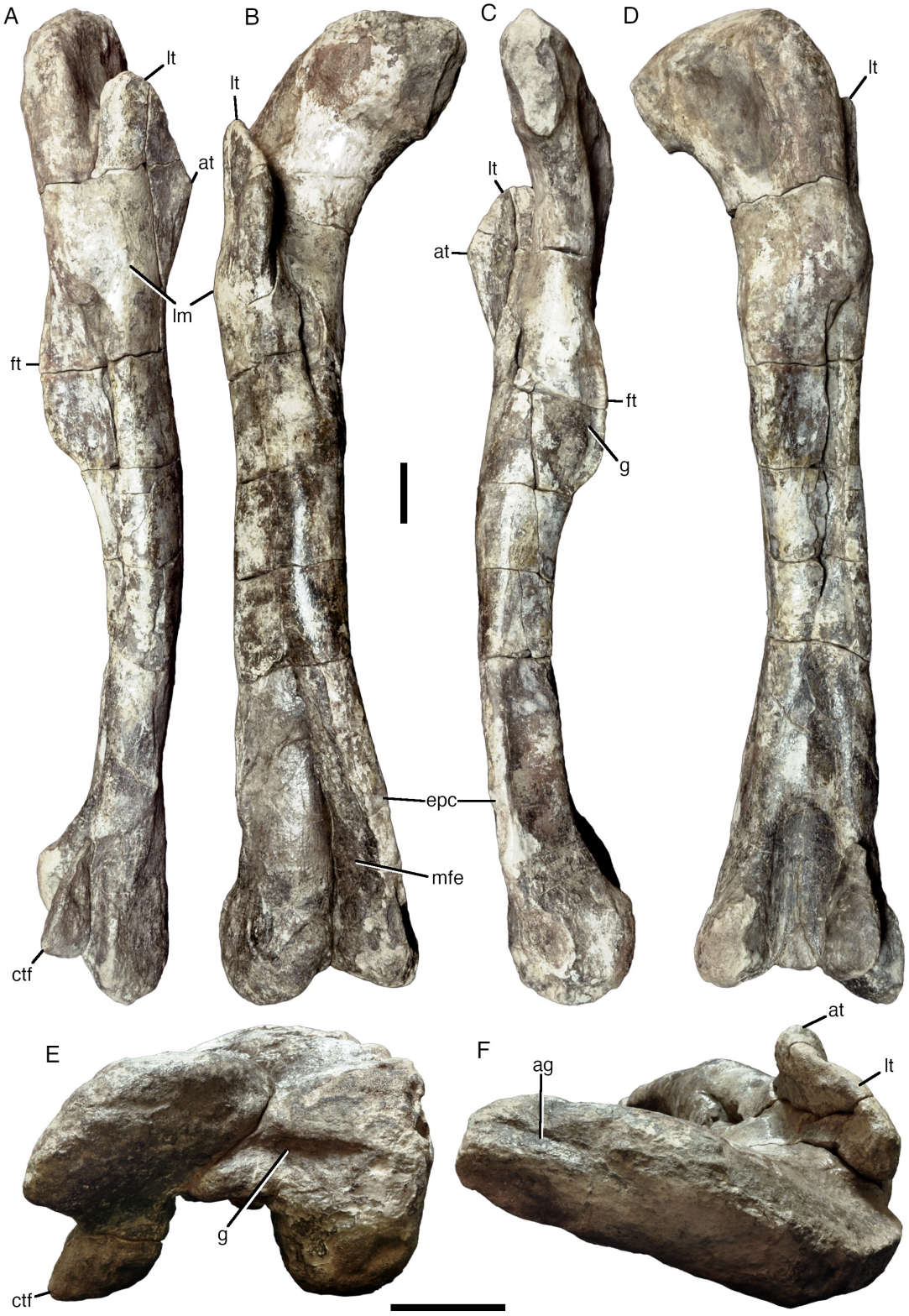

FIGURE 12. Right femur of *Camarillasaurus cirugedae*, MPZ 2022/182c, in lateral (A), anterior (B), medial (C), posterior (D), distal (E), and proximal (F) view. Abbreviations: ag, articular groove; at, accessory trochanter; ctf, *crista tibiofibularis*; epc, epicondylar crest; ft, fourth trochanter; g, groove; lm, lateral mound; lt, lesser trochanter; mfe, *m. femorotibialis externus*. Scale bars are 5 cm.

ment of the second sacral rib (see Madsen, 1976). However, the angle between the anterior and ventral margins is closer to 90° in the megalosauroids *Megalosaurus* (Benson, 2010) and *Ichthyovenator* (Allain et al., 2012), and the anterior part of the ventral hook of the ilium in early branching tetanurans does not usually have a thickened ventral margin, so this identification should be regarded as tentative.

Femur. The right femur MPZ 2022/182c resulting from the excavation in 2018 is complete and well preserved, although it has undergone some anteroposterior compression (Figure 12). It is a slender bone with a complete length of 830 mm and a minimal transverse width of 91 mm. The shaft is only very slightly flexed in lateral or medial view and is straight in anterior view (Figure 12A-D).

The femoral head is anteroposteriorly slender, which might be exaggerated by compression, and mainly medially and slightly anteriorly directed, at an angle of between 20° and 40°, similar to the condition in *Riojavenatrix* (Isasmendi et al., 2024). The proximal surface of the head flexes gradually into the narrow greater trochanter laterally. On the proximal surface of the head, a narrow, but well-developed articular groove (Carrano et al., 2002, 2012; Benson, 2010) extends transversely over the medialmost part of the head (Figure 12F). This groove is more or less directed in the direction of the transverse long axis of the head, not strongly obliquely angled anteromedially, as in *Riojavenatrix* (Isasmendi et al., 2024) The oblique ligament groove on the posterior side of the head (Rauhut, 2003) is only poorly developed, which might, however, reflect the fact that the posteriorly flexed lip on the medialmost part of the femoral head is largely missing, as the medialmost portion of the head is not preserved. In consequence, it also cannot be said whether the medialmost part of the head flexed distally to form a small hook, as is the case in a spinosaurid femur from the Morella Formation of Castellón (Malafaia et al., 2018), and *Riojavenatrix* (Isasmendi et al., 2024).

The anterior (lesser) trochanter is wing-like, slightly anteromedially inclined, and separated from the shaft by a broad, U-shaped incision. The trochanter reaches slightly more proximally than the ventral rim of the femoral head and is anteroposteriorly broad. At about its mid-height, a small, triangular, notably transversely thickened accessory trochanter is present. A small, elongated oval, roughened facet, presumably for a muscle insertion, extends distally from the apex of the accessory trochanter on its lateral side. A trochanteric shelf is absent, but a broad, anterolaterally positioned lateral mound is present at the base of the lesser trochanter (Figure 12A, B). Proximal to this mound, the femoral shaft is slightly inclined medially, as in many non-coelurosaurian theropods.

Distal to the lesser trochanter, the shaft is slender. The fourth trochanter is well developed and extends distally for some 13 cm from the level of the trochanteric mound on the posteromedial surface of the femoral shaft. The fourth trochanter is low and semioval in medial view, and slightly curved proximomedially in posterior view. On the medial side, the trochanter is flanked by a curved, narrow, and well-defined longitudinal groove (Figure 12C). This groove is obviously a natural feature and not due to deformation or erosion, as it is also present in a spinosaurid femur described from Castellon (Malafaia et al., 2018). At the level of the distal end of the fourth trochanter, the femoral shaft is approximately as wide transversely as anteroposteriorly, with a strongly convex anterior and more flattened posterior outline. Distally, the shaft becomes gradually more flattened anteroposteriorly.

The distal end is expanded transversely to a maximal width of c. 17 cm. Anteriorly, a broad, but shallow depression for the *m. femorotibialis externus* is present on the medial side (Figure 12B), but its lateral border is poorly defined due to compression of the bone in this area. In contrast, the attachment of this muscle is marked only by a small rugose patch in *Riojavenatrix* (Isasmendi et al., 2024). The epicondylar crest on the anteromedial edge of the distal femur is developed as a stout, but low, medially directed ridge (Figure 12B, C); its distal end is damaged. Anteriorly, a well-developed extensor groove is present. On the posterior side of the distal femur, the distal condyles are widely separated by a pronounced distal depression. The tibial condyle is only slightly wider (c. 60 mm) than the posterior groove between the condyles (c. 50 mm) and well-rounded anteroposteriorly distally. In contrast to other spinosaurids (see Isasmendi et al., 2024) it is strictly posteriorly, and not posteromedially directed in distal view. The crista tibiofibularis is narrower than the tibial condyle (c. 40 mm), triangular in outline in distal view, and slightly inclined laterally, although this might be due to compression. Its medial side faces posteromedially and is flattened to slightly convex. The crista is offset from the lateral side of the distal shaft by a flat, semioval shelf, and from the main articular surface of the distal end of the femur by a groove that extends from below the condyle medially across the distal

FIGURE 13. Proximal end of right tibia of *Camarillasaurus cirugedae*, MPG-KPC 8, in lateral (A), medial (B), anterior (C), posterior (D), and proximal (E) view. Abbreviations: cc, cnemial crest; fc, fibular condyle; fcr, fibular crest. Scale bar is 5 cm.

articular surface (Figure 12E), as in megalosaurids (Benson, 2010). Whereas the lateral part of the distal articular surface of the femur forms a slightly oblique, well-rounded surface, the distal surface of the *crista tibiofibularis* is almost flat. Thus, the tibial condyle extends slightly further distally than the fibular condyle, whereas the fibular condyle reaches slightly further proximally than the tibial condyle; both condyles fade rather gradually into the femoral shaft proximally. A marked depression with a rounded proximal end separates the two condyles on the posterior side (Figure 12D).

The flat distal surface of the *crista tibiofibularis* is offset from the rounded anterior side of the distal surface of the lateral side of the femur by a shallow groove, which extends medially across the distal surface of the femur and fades medially into the lateral side of the rounded tibial condyle (Figure 12E). Posterior to the groove, a low, robust convexity expands slightly distally in the space between the two femoral condyles.

Tibia. The proximal end of the right tibia, MPG-KPC 8, is preserved (Figure 13). The proximal tibia is notably narrow mediolaterally, although this seems to be at least partially exaggerated by compression. A well-developed cnemial crest is present and is triangular in lateral or medial view, arising gradually from the shaft. The maximal anteroposterior expansion of the crest, as measured anterior to the anterior end of the fibular condyle, is about 117% of the anteroposterior width of the tibial shaft at the distal break at the level of the lateral fibular crest (and might originally have been slightly more, as the anterior margin is somewhat eroded). This is comparable to some other early branching tetanurans, such as *Suchomimus* (c. 117%; MNN GAD 500), *Sinraptor* (c. 117%; Currie and Zhao, 1993), *Allosaurus* (c. 117%; Madsen, 1976), and *Tyrannosaurus* (c. 115%; Brochu, 2003), but is considerably more than in *Dilophosaurus* (c. 69-75%; Marsh and Rowe, 2020), *Piatnitzkysaurus* (100%; Bonaparte, 1986), *Megalosaurus* (c. 91%; Benson, 2010), and *Torvosaurus* (c. 74%; BYU VP 2016; see Britt, 1991), and less than in ceratosaurs such as *Ceratosaurus* (c. 130%; Madsen and Welles, 2000), *Majungasaurus* (c. 155%; Carrano, 2007), or *Pycnonemosaurus* (c. 177%; Kellner and Campos, 2002). In contrast to many early branching tetanurans, the cnemial crest does not seem to be anteroproximally expanded, although this might be due to damage to the proximal surface of its anterior end, as indicated by a slight proximal bulge in the base of the crest (Figure 13A, B). The proximal end is also somewhat posteriorly expanded, with the medial condyle forming a small, lobe-shaped posterior expansion in lateral view.

In proximal view, the proximal articular surface of the tibia is remarkably narrow mediolaterally (Figure 13E), being approximately 2.5 times as long anteroposteriorly as its maximal mediolateral width. The cnemial crest is elongated rectangular in proximal outline, whereas the posterior end tapers, and the medial side of the tibia is gently convex. The proximal articular surface is notably convex over the fibular condyle, but becomes con-

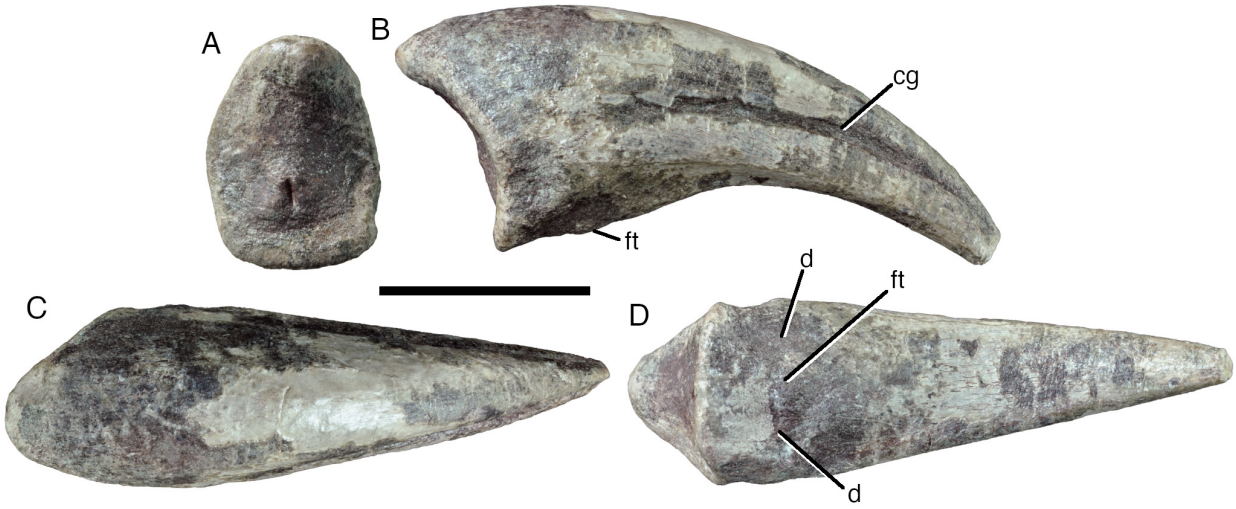

FIGURE 14. Left pedal ungual four of *Camarillasaurus cirugedae*, MPZ 2022/182d, in proximal (A), right lateral (B), dorsal (C) and ventral (D) view. Abbreviations: cg, claw groove; d, depression; ft, flexor tubercle. Scale bar is 5 cm.

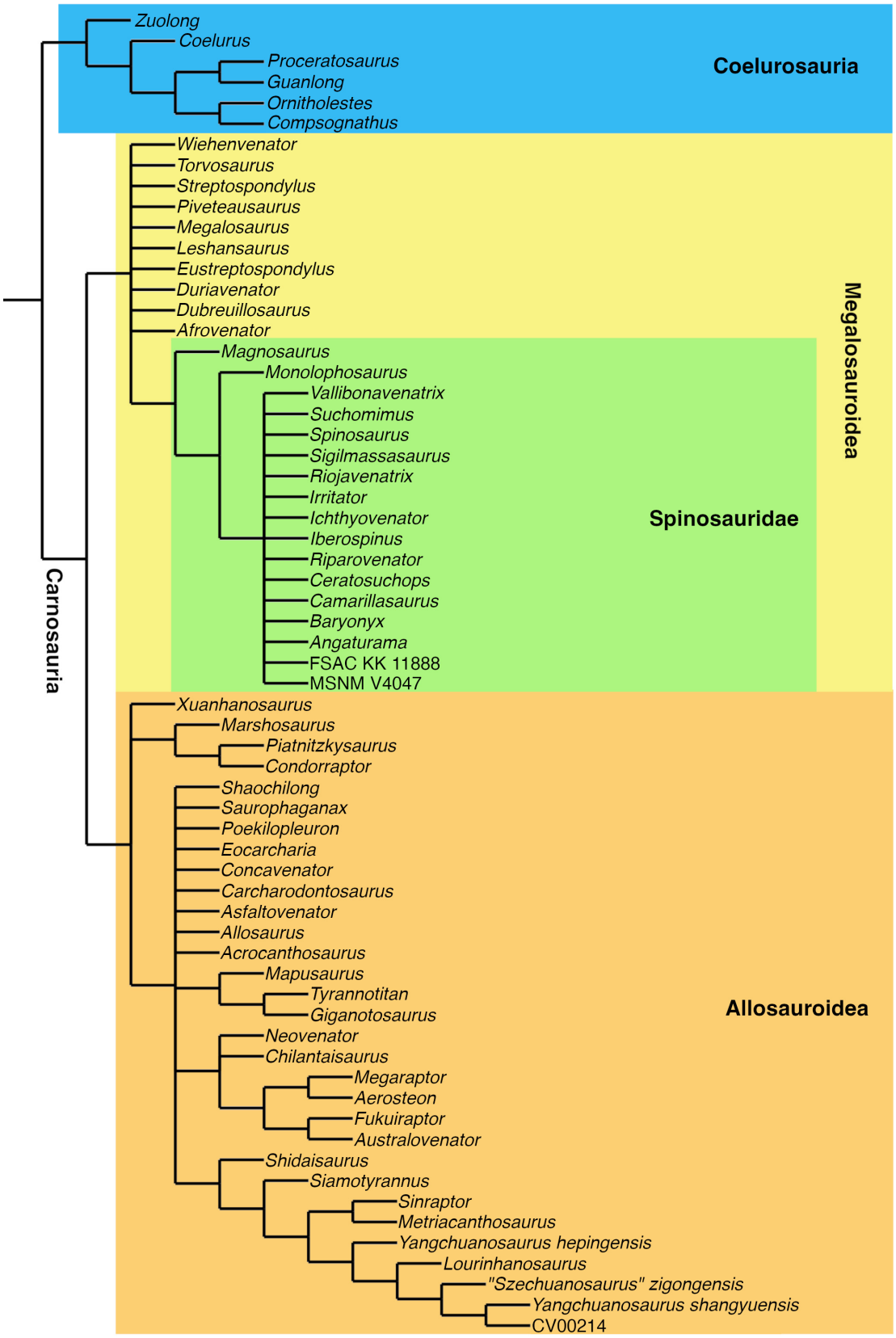

FIGURE 15. Phylogenetic hypothesis of tetanuran interrelationships, strict consensus tree resulting from a phylogenetic analysis using equal weights. See text for details of phylogenetic analysis.

cave between the fibular condyle and the cnemial crest. There is no clearly defined lateral ridge at the anterior end of the cnemial crest, as is present in many theropods, although this might again be at least partially due to damage in this area. The fibular condyle is moderately developed, rounded in its main, posterior part, and it has a small lateral bulge anteriorly. This bulge is aligned with the lateral fibular crest of the tibial shaft, but clearly separated from it, and developed as a triangular tubercle at the proximal end in lateral view. The fibular condyle is offset anteriorly from the posterior end of the medial part of the tibia, but there is no marked incision between the medial and fibular condyles, as is usually present in theropods (Rauhut, 2003). Likewise, the fibular condyle rather gradually fades into the cnemial crest anteriorly, as in early branching theropods (Rauhut, 2003), many ceratosaurs (e.g., Bonaparte et al., 1990; Carrano, 2007; Rauhut and Carrano, 2016; Grillo and Delcourt, 2017), and the spinosaurids *Suchomimus* (MNN GAD 500) and *Riojavenatrix* (Isasmendi et al., 2024), whereas the two structures are separated by a pronounced *incisura tibialis* in most tetanurans (Rauhut, 2003).

The fibular crest is located at about the level of the distal end of the cnemial crest and is clearly offset from the proximal end, in contrast to non-tetanuran theropods, where the crest extends distally from the proximal end (Rauhut, 2003), and some early branching tetanurans, in which a low ridge is present as a proximal extension of the crest (Benson, 2010). Most of the crest is broken away, but its base is anteroposteriorly broadened and suboval in outline (Figure 13A, C), as in *Megalosaurus* and a few other early branching tetanurans (Benson, 2010). As noted by Sánchez-Hernández and Benton (2014), there is a large, elongate oval foramen on the posterolateral side of the base of the crest, just below its mid-length. A longitudinal depression is present anteriorly between the fibular crest and the tibial shaft, but the narrow incision between these two structures distally, which was used as a diagnostic character by Sánchez-Hernández and Benton (2014), is quite certainly an artefact of preservation, due to the lateral compression of the bone. A shallow, triangular depression is present on the posterior half of the medial side of the bone towards its proximal end. The cross-section of the shaft at the distal break is almost round.

Ungual. The only pedal ungual, MPZ 2022/182d, probably comes from the fourth digit of the left foot, judging by its size, curvature, and the slight asymmetry of the articular surface (Figure 14). The element is 145 mm long as measured over the dorsal surface and 112 mm long over the ventral surface, lacking its distalmost tip (an estimated 5-6 mm), and it is 54 mm high and 42 mm wide proximally. The ungual is only weakly curved and ventrally flattened, being slightly wider below the well-developed, single claw groove than above (Figure 14B, C). However, the flattening is not as pronounced as in unguals referred to spinosaurine spinosaurids from the Southern Hemisphere (e.g., Stromer, 1934; Novas et al., 2005; Ibrahim et al., 2014), and, unlike these, the ungual is higher dorsoventrally than broad mediolaterally. The claw groove does not reach the proximal end of the ungual, but is separated from it by some 52 mm. The flexor tubercle on the proximal part of the ventral side is weakly developed and flanked proximally by two small, oval depressions (Figure 14B, D). The proximal articular surface is weakly ginglymoidal, although the ridge separating the articular facets is only developed as a weak median mound (Figure 14A). The articular facets are slightly asymmetrical, the probably lateral facet being slightly wider and with a more rounded lateral margin than the medial facet.

PHYLOGENETIC ANALYSIS

The phylogenetic analysis found more than 100,000 most parsimonious trees with a length of 1572 steps. The strict consensus of these trees shows a reasonably good resolution (Figure 15; Supplementary Figure 1), and finds a monophyletic Carnosauria, which is subdivided into Megalosauroidea and Allosauroidea, as in Schade et al. (2023). Within these two subclades of Carnosauria, large polytomies are present. In Allosauroidea, the analysis found the piatnitzkysaurids (comprising *Marshosaurus, Piatnitzkysaurus* and *Condorraptor*) as the earliest branching clade, as in Rauhut and Pol (2019). Above this clade, the analysis recovered a large polytomy of metriacanthosaurids, allosaurids and carcharodontosaurians, with only the Metriacanthosauridae, the Neovenatoridae, and the Giganotosaurini *(Tyrannotitan, Giganotosaurus* and *Mapusaurus)* being found as monophyletic clades. Reduced consensus methods (Pol and Escapa, 2009) identified *Saurophaganax* and *Poekilopleuron* as problematic taxa within Allosauroidea. The *a posteriori* removal of these taxa resulted in a much improved resolution (Supplementary Figure 2) that found the usually recovered monophyletic clades within Allosauroidea, the Metriacanthosauridae and the Allosauria, with the latter being divided into Allosauridae (genus *Allosaurus* only) and Carcharodontosauria, with

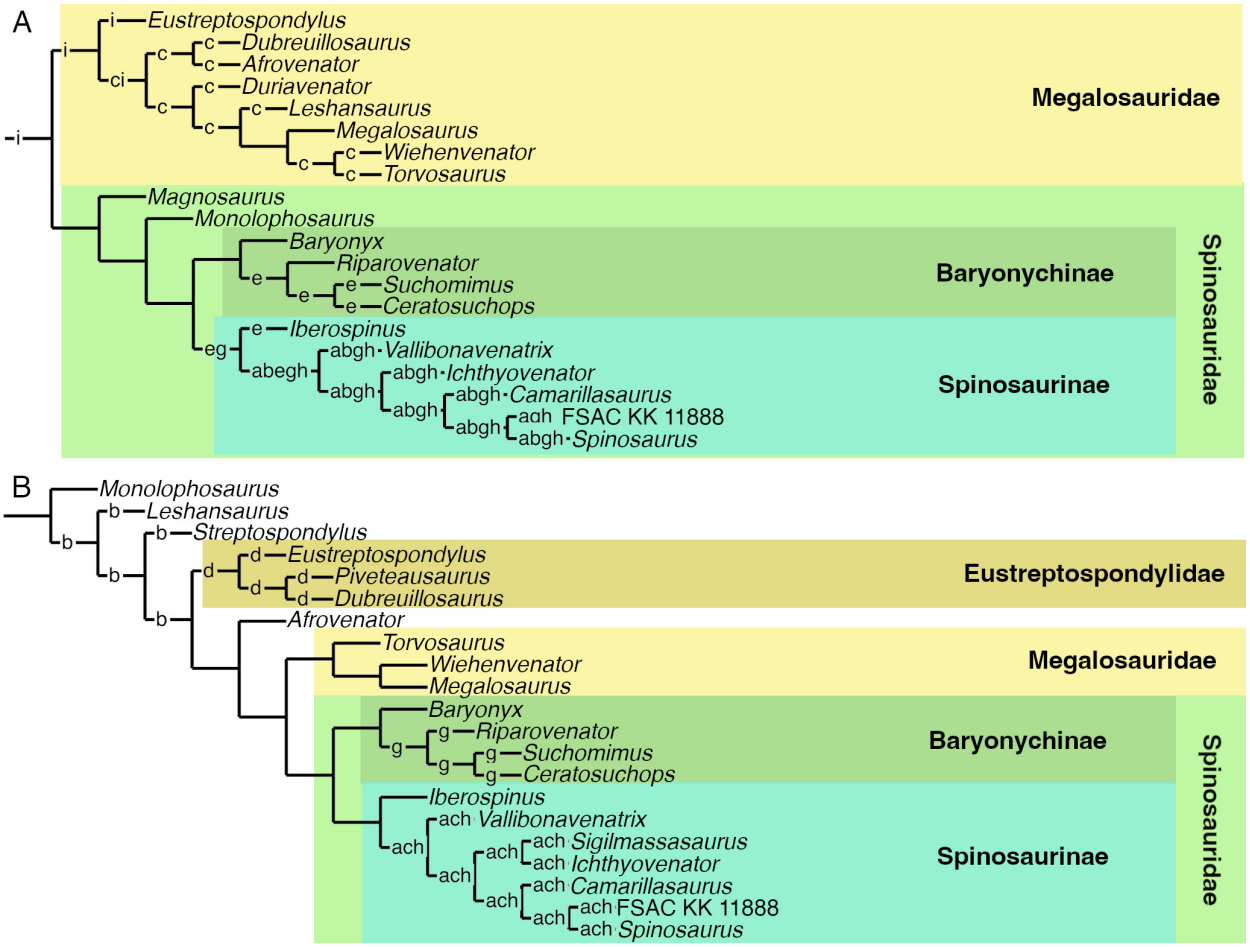

FIGURE 16. Phylogenetic hypotheses of megalosauroid interrelationships. A, reduced consensus tree resulting from a phylogenetic analysis using equal weights. The different positions of taxa excluded by reduced consensus methods are marked by lowercase letters on the branches: a, *Angaturama*; b, *Irritator*; c, *Piveteausaurus*; e, *Riojavenatrix*; g, *Sigilmassasaurus*; h, MSNM V4047; i, *Streptospondylus*. B, reduced consensus tree resulting from a phylogenetic analysis using implied weights (k=12). The different positions of taxa excluded by reduced consensus methods are marked by lowercase letters on the branches: a, *Angaturama*; b, *Duriavenator*; c, *Irritator*; d, *Magnosaurus*; g, *Riojavenatrix*; h, MSNM V4047. See text for details of phylogenetic analysis.

Neovenatoridae and Carcharodontosauridae. Interestingly, the problematic *Lourinhanosaurus,* which has been found in various positions within early branching tetanurans over the years (see e.g., Carrano et al., 2012; Rauhut et al. 2016; Malafaia et al., 2020b) is here recovered as a metriacanthosaurid, and the poorly known Middle Jurassic French theropod *Poekilopleuron* (Allain and Chure, 2002), usually considered to be a megalosauroid (e.g., Carrano et al., 2012) is found to be an allosauroid, with some trees finding this taxon in an early branching position within Carcharodontosauridae.

Within Megalosauroidea, the strict consensus tree finds a large basal polytomy that includes most of the taxa usually recovered as megalosaurids (Figure 15). However, within this polytomy, a monophyletic Spinosauridae is found. This clade includes the poorly known *Magnosaurus* as the earliest branching member, followed by *Monolophosaurus*, which was found in a similar position in the equally weighted parsimony analysis of Schade et al. (2023). Given that the phylogenetic definition of Spinosauridae as currently employed (all theropods that are more closely related to *Spinosaurus aegyptiacus* than to either *Megalosaurus bucklandii* or *Allosaurus fragilis*; Rauhut and Pol 2019) is stem-based, these taxa would have to be regarded as a member of the Spinosauridae under this topology. The remaining spinosaurids, including *Camarillasaurus*, are placed in a large polytomy.

Reduced consensus methods found the poorly known *Streptospondylus* and *Piveteausaurus* as problematic taxa in the basal polytomy within megalosauroids (Figure 16A). After removal of these taxa, all remaining taxa at this node form a monophyletic Megalosauridae that includes *Eustreptospondylus* as the earliest branching taxon, followed by Afrovenatorinae *(Afrovenator* and *Dubreuillosaurus)* and Megalosaurinae *(Duriavenator, Leshansaurus, Megalosaurus, Wiehenvenator,* and *Torvosaurus).*

Within Spinosauridae, five operational taxonomic units were found to be problematic and create the polytomy in this clade (Figure 16A). *Riojavenatrix* can be placed in several different positions within Baryonychinae and early branching Spinosaurinae, whereas the other four OTUs are responsible for the polytomy within Spinosaurinae. Three of these – *Irritator, Angaturama,* and the snout described by Dal Sasso et al. (2005) – represent taxa known only from cranial remains. As the remaining spinosaurines are mainly or even entirely known from postcranial remains, these taxa cannot currently be placed more precisely within Spinosaurinae with any certainty. The other taxon removed is *Sigilmassasaurus*, which is only known from vertebral remains. After removal of all these taxa, monophyletic Baryonychinae and Spinosaurinae are recovered. As it is to be expected that future analyses and future discoveries recover spinosaurids that are outside this Baryonichinae-Spinosaurinae split, as it is the case in our analysis, and to facilitate communication about spinosaurid interrelationships, we here propose the name Spinosauria for the clade including these two subclades, with a node-based definition as the clade including *Baryonyx walkeri* and *Spinosaurus aegyptiacus* and all descendants of their most recent common ancestor. Baryonychinae include the genera *Baryonyx, Riparovenator, Suchomimus,* and *Ceratosuchops* in a pectinate arrangement. Within Spinosaurinae, also a pectincate arrangement is found, with *Iberospinus* representing the earliest branching taxon, followed by *Vallibonavenatrix* and *Ichthyovenator*. *Camarillasaurus* is found as sister taxon to a clade consisting of *Spinosaurus* and FSAC-KK 11888 at the top of this pectinate arrangement. Following the assumption that all spinosaurid remains from the Kem Kem beds represent a single spinosaurid taxon (Smyth et al., 2020) does not change the result – the Kem Kem spinosaurid is found as sister taxon of *Spinosaurus*, with *Camarillasaurus* representing the immediate outgroup.

The implied weighting analyses did not change anything in the interrelationships of Spinosauria, although the strict consensus of the most parsimonious trees found already a Baryonychinae-Spinosaurinae dichotomy (Supplementary Figure 3), with *Baryonyx* found as the earliest branching baryonychine, followed by a polytomy of the remaining taxa, which include *Riojavenatrix*. Within Spinosaurines, *Iberospinus* was again recovered as the earliest branching taxon, followed by a polytomy of the remaining spinosaurines, which include *Camarillasaurus*. The interrelationships of spinosaurines in the reduced consensus tree (Supplementary Figure 4) conform to the reduced consensus tree of the unweighted analysis (Figure 16B). Interesting changes were found in the outgroup to this Baryonychinae-Spinosaurinae clade within Megalosauroidea, as in Schade et al. (2023). Thus, under implied weights, the Chinese *Monolophosaurus* is found as the earliest branching megalosauroid, followed by a paraphyletic array of megalosaurids, with the Chinese *Leshansaurus* as the earliest branching taxon after *Monolophosaurus*, followed by *Streptospondylus*, a clade including the European *Eustreptospondylus*, *Piveteausaurus*, and *Dubreuillosaurus*, the African *Afrovenator*, and finally the megalosaurines *(Megalosaurus, Wiehenvenator,* and *Torvosaurus)* as the sister taxon to Spinosauridae, which, under this topology, is a senior synonym of Spinosauria (Figure 16B).

Character evolution in Megalosauroidea on the way to spinosaurids, and within this clade, was evaluated using the character trace option of Mesquite on the reduced consensus tree of the unweighted parsimony analysis, with *Irritator* and the spinosaurine snout MSNM V4047 placed in an uncertain position within higher spinosaurines, to better understand skull evolution in this clade. The position of *Camarillasaurus* within Spinosauridae is supported by numerous characters, although many of these are found as ambiguous apomorphies at different nodes under ACCTRAN and DELTRAN, owing to the very fragmentary nature of many spinosaurids known. Thus, under the current topology, spinosaurid monophyly is supported by a single unambiguous synapomorphy, a ventrally bulging anterior end of the dentary. However, several characters present in *Camarillasaurus* represent ambiguous synapomorphies either at the node of Spinosauridae, or the node of Spinosauria, as they are currently unknown in *Magnosaurus* and *Monolophosaurus*. These include the rectangular outline of the articular surfaces of distal caudal ver-

tebrae (character 256), rod-like mid-caudal neural spines that are as wide or wider transversely than they are anteroposteriorly (character 258), and a fibular flange on the tibia that is clearly offset from the proximal end of the tibia (character 378; also present in Allosauria and coelurosaurs). Furthermore, *Camarillasaurus* shares two unambiguous synapomorphies with other Spinosauria, very broad and ventrally flattened posterior dorsal vertebrae (character 236; this character is also present in megalosaurines, and interpreted as a synapomorphy of megalosaurines + spinosaurids in the weighted analysis), and funnel-shaped, gradually dorsally expanding posterior dorsal or sacral neural spines (character 242; see Charig and Milner 1997: figure 27A; Allain et al. 2012: figures 1, 2; Malafaia et al. 2020b: figure 5A, B). The placement of the Iberian taxon in Spinosaurinae is based on two unambiguous synapomorphies, the absence of L-shaped neural spines in the anterior to mid-caudal vertebrae (character 251), and a postzygapophyses in the distal caudal vertebrae that projects posteriorly from the base of the neural spine (character 257). Within Spinosaurinae, *Camarillasaurus* shares with *Vallibonavenatrix* and all spinosaurines more derived than *Iberospinus* the steep inclination of the middle and posterior dorsal prezygapophyses (character 241), with *Ichthyovenator* and all spinosaurines more derived than *Vallibonavenatrix* the presence of a spinodiapophyseal ridge or lamina in the mid-caudal vertebrae (character 254), and with *Spinosaurus* and FSAC-KK11888 the absence of an accessory centrodiapophyseal lamina (character 229; a reversal to the non-spinosaurian condition). Furthermore, there are a number of characters that are shared by *Camarillasaurus* and some other member of Spinosauria and are absent in non-spinosaurian or non-spinosaurid taxa, but that cannot be evaluated in other spinosaurs. Many of these concern the surangular and articular, which are otherwise only known from *Irritator* within spinosaurs (Schade et al. 2023). These characters include the presence of a depressed shelf on the dorsal surface of the surangular anterior to the mandibular glenoid (character 168; also present in allosauroids and some other theropods, but absent in *Monolophosaurus* and *Megalosaurus* within megalosauroids), the laterodorsal orientation of this shelf (character 169), the presence of two posterior surangular foramina (character 170; also present in *Sinraptor* and some coelurosaurs), the complete fusion of the surangular and articular (character 171), an elongate retroarticular process of the mandible (as long as or longer than the mandibular glenoid; character 175), a mediolaterally convex attachment area for the *m. depressor mandibulae* (character 178), a retroarticular process that is strongly offset ventrally from the glenoid (character 179), and the presence of a very high semioval dorsal process posterior to the medial cotyle of the mandibular glenoid (character 180).

Testing for alternative positions for *Camarillasaurus* consistently resulted in considerably longer trees. Placing this taxon as sister taxon to Spinosauria requires only three additional steps, but a placement one node further out is 12 steps longer, and placing *Camarillasaurus* in Megalosauridae even requires 14 additional steps. Finally, a position of *Camarillasaurus* within ceratosaurs, as advocated by Sánchez-Hernández and Benton (2014) is at least 20 steps longer than the most parsimonious trees. Given that only 67 of the total of 404 characters could be coded for this taxon, the placement of *Camarillasaurus* in Spinosauridae and even in Spinosauria seems to be well supported.

DISCUSSION

Affinities of *Camarillasaurus* and Other Iberian Spinosaurids

As mentioned above, in the original description, Sánchez-Hernández and Benton (2014) identified *Camarillasaurus* as an early branching ceratosaurian. As detailed in the description, though, their initial assessment was based mainly on erroneous interpretations of elements and their morphology (such as the identification of six sacral vertebrae), and their phylogenetic analysis, which recovered it as an early branching ceratosaurian, was strongly biased in favour of this result, as it included only three non-ceratosaurian outgroup taxa. The originally proposed affinities of *Camarillasaurus* as an early branching ceratosaurian were supported in the phylogenetic analyses of Tortosa et al. (2014) and Filippi et al. (2016), but, again, both used phylogenetic matrices that were centred on ceratosaurians and only included a very limited array of non-ceratosaurian outgroup taxa. Thus, they cannot really be seen as a robust test for the ceratosaurian affinities of *Camarillasaurus* in the context of theropods in general. The ceratosaurian affinities for this taxon were also accepted by Dal Sasso et al. (2018), although the taxon was not included in the phylogenetic analysis of that paper, which had a considerably wider taxon sampling. Rauhut et al. (2019) proposed the type of *Camaril-*

lasaurus as a megalosauroid and probably spinosaurid theropod, a view that was recently supported by a comparison with the newly described spinosaurid *Vallibonavenatrix* (Malafaia et al., 2020a, b) and with the distal caudal vertebrae of an indeterminate spinosaurid from Thailand (Samathi et al., 2021). More recently, *Camarillasaurus* was included in the phylogenetic analyses of Sereno et al. (2022; see also Santos-Cubedo et al., 2023, who used the same matrix), which found this taxon to be the earliest branching spinosaurid included in their sample. However, these results were based on the original description of *Camarillasaurus* of Sánchez Hernández and Benton (2014), with the corrections by Samathi et al. (2021), and did not take into account the new identifications and the new data presented here. Finally, Isasmendi et al. (2024) found *Camarillasaurus* as a spinosaurine based on a phylogenetic analysis using a modified version of the matrix of Rauhut and Pol (2021).

Our analysis also indicates that *Camarillasaurus* is a member of the Spinosaurinae, and even a rather derived member of that clade, being the sister taxon to the gigantic North African spinosaurines. Given the scarcity of material, and thus the high amount of missing scorings in the matrix (85%), the placement of *Camarillasaurus* as a spinosaurid seems to be rather well supported. Although synapomorphies of Spinosauridae or subclades thereof are distributed in all parts of the preserved skeleton, the many shared characters in the surangular and articular of *Camarillasaurus* and *Irritator* are striking. This further highlights the highly specialized cranial anatomy of spinosaurids, and is in accordance with the findings of Schade et al. (2023) that spinosaurs showed high rates of cranial morphological evolution over a long geological time. Unfortunately, more mandibular material of spinosaurids is needed to establish where within spinosaurid phylogeny the numerous changes shared by *Camarillasaurus* and *Irritator* happened; currently it cannot be said if all of these characters might represent synapomorphies of the Spinosauria, or if they might further support the placement of the Iberian taxon within Spinosaurinae.

Apart from finding a spinosaurine position for *Camarillasaurus*, our analysis also confirmed the spinosaurine affinities of *Vallibonavenatrix* (as originally found by Malafaia et al., 2020b) and indicates an early branching position within this clade also for another Iberian Early Cretaceous spinosaurid, *Iberospinus*. The latter taxon was considered to be a probable baryonychine by Mateus and Estraviz-López (2022), although their phylogenetic analysis found it in a polytomy with spinosaurines and baryonychines (note that their figure 31B, which seems to show *Iberospinus* as sister taxon of *Baryonyx* + *Suchomimus*, represents an agreement subtree, in which all other spinosaurids were pruned). Their assessment was based on the presence of "small denticles in teeth and longer than tall dorsal vertebrae" (Mateus and Estraviz-López 2022: p. 40). However, both of these characters are problematic. The presence of marginal denticles represents a theropodan symplesiomorphy. Thus, their presence in teeth of *Iberospinus* only indicates that this taxon does not belong to the spinosaurine subclade that includes *Spinosaurus* and *Irritator* (and *Camarillasaurus*, based on the referred partial teeth from the type locality), which show the apomorphic condition of lacking denticles altogether, but cannot be used to refer this taxon to the Baryonychinae. As for the relative length of the dorsal vertebrae, this is highly variable, both between taxa, but often also within a single vertebral column. In *Baryonyx*, for example, only the anterior dorsal vertebrae have centra that are longer than high, whereas the posterior dorsal centra are about as high as long (Charig and Milner 1997: table 1; note that some of the supposed anterior dorsals of *Baryonyx* were interpreted as cervical vertebrae by Evers et al. 2015). In general, elongate anterior to middle dorsal vertebral centra seem to be common in spinosaurids, and especially *Spinosaurus* has anterior to middle dorsal centra that are considerably longer than high, more so than in *Baryonyx* (Stromer 1915). Thus, the considerably elongate centrum described by Mateus and Estraviz-López (2022) probably represents an anterior to mid-dorsal centrum and might even be a further argument for spinosaurine affinities of this taxon.

The recently described *Riojavenatrix* from the uppermost Barremian to Lower Aptian Enciso Group of La Rioja, Spain, was interpreted as one of the youngest baryonychines in the fossil record (Isasmendi et al., 2024) and is one of the latest Iberian and European spinosaurid taxa. *Riojavenatrix* presents morphological characters that allow it to be clearly differentiated from *Camarillasaurus*, notably in the femur and the proximal tibia (Isasmendi et al., 2024). Mainly due to our still very poor knowledge of spinosaurine hindlimbs, *Riojavenatrix* could not be placed within one of the two subclades of the Spinosauria in our equal weights analysis, but the implied weights analysis supported the baryonychine position argued for by Isasmendi et al. (2024). More data on spinosaurine

hindlimbs, or on the non-hindlimb osteology of *Riojavenatrix* are needed to place this taxon with more certainty.

Furthermore, Santos-Cubedo et al. (2023) described a maxilla and five caudal vertebrae from the Upper Barremian Arcillas de Morella Formation of Castellón as a new taxon of spinosaurid, *Protathlitis cinctorrensis*. The material comes from the Ana site, a multitaxon bone bed in shallow marine sediments of this formation that has yielded remains of osteichthyes, crocodylomorphs, and ornithopod, sauropod, and theropod dinosaurs (Suñer et al., 2008; Gasulla et al., 2011). Despite the material coming from a multi-taxon bone bed, no information about possible association of the holotypic remains were provided by the authors. Based on the description and figures in the original publication, we have serious doubts about the spinosaurid affinities of this material. The maxilla shows a number of characters that are incompatible with a spinosaurid identification. The maxilla of *Protathlitis* becomes mediolaterally wider or is at least as wide posteriorly as anteriorly (Santos-Cubedo et al. 2023: figures 3C, D), whereas this bone tapers posteriorly in all non-avian theropods (e.g., Madsen, 1976; Currie and Zhao, 1994; Schade et al., 2023). The same is true for the height of the bone posterior to the ascending process: this is as high as or even higher than the anterior part, whereas this portion is usually lower than the anterior process in theropods that have an anterior process, including spinosaurids (e.g., Sereno et al. 1998; Dal Sasso et al. 2005; Schade et al. 2023). Other significant differences concern the shape and placement of the ascending process. In *Protathlitis*, it is placed above the approximate midlength of the maxilla, whereas it is anteriorly placed in most theropods, and in the posterior third in all spinosaurids for which more or less complete maxillae are known (Sereno et al., 1998; Dal Sasso et al., 2005; Schade et al. 2023). Furthermore, in dorsal view (Santos-Cubedo et al. 2023: figure 3C), the ascending process seems restricted to the lateral side of the bone, whereas it generally occupies the entire width of the maxilla in non-avian theropods. Likewise, the dorsal surface of both the anterior process and the jugal process are mediolaterally widened and bulbous, being dorsally convex transversely, in contrast to the usually narrow and longitudinally grooved dorsal surface of the jugal process in other theropods (see e.g., Evers et al., 2020). In summary, the maxilla of *Protathlitis* deviates considerably from the morphology seen in theropods generally and from spinosaurids in particular, making a spinosaurid identification of that bone unlikely.

As for the caudal vertebrae that are part of the type material of *Protathlitis*, these elements are compatible with caudal vertebrae known from other theropods, but cannot be shown to represent spinosaurid elements with any certainty. These vertebrae lack several characters that are common in spinosaurids and might represent synapomorphies of Spinosauria or subclades thereof. Thus, in *Spinosaurus* and the closely related form from Morocco, the anterior caudal vertebrae are rectangular in outline (Stromer, 1915; Ibrahim et al., 2020), and although this is not the case in some other spinosaurids (e.g., Allain et al., 2012; Malafaia et al., 2020b), at least from the mid-caudal section on, all spinosaurids seem to have more rectangular articular facets (e.g., Barker et al., 2021; Mateus and Estraviz-López, 2022). In contrast, all preserved caudal vertebrae of *Protathlitis* have oval articular facets. Another character shared by spinosaurids are anteroposteriorly short, rod-like neural spines from at least the mid-caudals onwards. Again, this does not seem to be the case in *Protathlitis*; although the spine is not preserved in the posteriormost vertebra present, its attachment is narrow and anteroposteriorly elongate (Santos-Cubedo et al., 2023: figure 6). Thus, although it cannot be excluded that the vertebrae from the Ana site represent some earlier branching spinosaurid, they are best regarded as indeterminate theropod at the moment. In summary, we regard *Protathlitis* as a probably chimeric *nomen dubium*, the spinosaurid affinities of which are highly questionable.

Spinosaurids in Iberian Palaeocommunities

Spinosaurid remains are abundant throughout the Barremian of the Iberian Peninsula, especially in the form of isolated teeth (e.g., Canudo et al., 2008; Alonso and Canudo, 2016; Alonso et al., 2017; Cabrera-Argudo et al., 2024; Isasmendi et al., 2025). The fossil record of spinosaurid theropods from the Lower Cretaceous of the Iberian Peninsula has recently been summarized (Malafaia et al., 2020a), although several new specimens have been described since (Isasmendi et al. 2022, 2024, 2025; Mateus and Estraviz-López 2022). The characteristic derived morphology of spinosaurian teeth makes them easily recognizable, even though they are fragmentary remains. The teeth show ornamentation comprising longitudinal flutes and mesial and distal denticles that are small in size and may even be missing. In the Ibe-

rian Peninsula, spinosaurid teeth have been found in sites deposited in fluvial environments, in association with a sauropod carcass such as the *Europatitan* of the upper Barremian – lower Aptian of Burgos (Alonso et al., 2017), in a typical case of theropods taking advantage of a carcass. They have also been recovered in sites in palustrine environments, with little or no permanent water present, as is the case with the site of La Cantalera from the lower Barremian of Teruel (Alonso and Canudo, 2016). Other examples include sites in the Mirambel Fm. preserved in alluvial and lacustrine environments (Gasca et al., 2017). Likewise, the holotype of *Camarillasaurus* was found in alluvial plain facies and thus in an environment without permanent water bodies, as is the case with other spinosaurid remains found in the Camarillas Formation (e.g., Cabrera-Argudo et al., 2024). Thus, the presence of spinosaurids in clearly continental environments of the Iberian Lower Cretaceous is noteworthy. Recent papers have proposed the hypothesis that *Spinosaurus* and other spinosaurids might have had aquatic habits, with characters described that would have allowed them to adapt to a fully aquatic lifestyle and preferring estuarine and other nearshore environments (Ibrahim et al., 2014, 2020; Beevor et al., 2021; Fabbri et al., 2022; though see also Sereno et al., 2022; Myhrvold et al., 2024). Unfortunately, to date, there is no Iberian record of spinosaurid specimens as complete as *Spinosaurus* that would shed further light on their palaeoecology. Nevertheless, geological data suggest a significant presence of Iberian spinosaurs in terrestrial environments, at a considerable distance from deeper and permanent aquatic environments. These animals were thus probably predators in more terrestrial environments, specialized on rather smaller and elusive prey, as indicated by the functional implications of the skull morphology in spinosaurids (Schade et al., 2023). This does, of course, not exclude the possibility that these animals also frequented the probably rather shallow water bodies present to hunt fish, but a fully aquatic lifestyle seems rather unlikely. Thus, if the highly derived *Spinosaurus* had indeed fully aquatic habits, these might have been the exception in spinosaurs rather than the norm.

CONCLUSIONS

Camarillasaurus cirugedae is a valid taxon of medium to large-sized spinosaurine spinosaurid theropods from the Barremian of the Iberian Range (Spain). The newly found cranial and postcranial material and the re-study of the previously described material has provided interesting diagnostic data. Although it was initially assigned to Ceratosauria, it exhibits cranial and postcranial characters that situate it within the spinosaurid group, in the Spinosaurinae. Isolated spinosaur remains, especially isolated teeth, are abundant in the Barremian of Spain, showing high morphological diversity (see also Isasmendi et al., 2025). At least two taxa are represented in the Barremian of the Maestrazgo Basin: *Camarillasaurus* and *Vallibonavenatrix*, and in total four probably valid spinosaurid species have been described from deposits of similar age of the Iberian Peninsula, indicating a high taxonomic diversity of that clade during that time. In contrast to the roughly contemporaneous spinosaurids from the British Wealden, all of which represent baryonychines, most Iberian spinosaurids seem to belong to the spinosaurine branch within this clade. This might indicate closer biogeographic affinities of the Iberian Barremian spinosaurid fauna to the younger northern African fauna than to the coeval northern European one. Many of the remains of the Spanish Barremian spinosaurids, including *Camarillasaurus*, are found in continental facies, suggesting that these taxa would have had less aquatic affinities than those proposed for the spinosaurs of the end of the Lower Cretaceous and beginning of the Upper Cretaceous.

ACKNOWLEDGEMENTS

We especially thank D.P. Cirugeda, who discovered the site of Fuente Arnar and showed it to us. Moreover, his valuable field assistance is greatly appreciated. We thank the owner of the land on which the site is located, D.J. José Villarroya Ariño, for facilitating the excavation permit, and the Herrero Family, M.A. Herrero and A. Gargallo for granting access to the *Camarillasaurus* type material in the Museo Paleontológico de Galve José María Herrero. I. Pérez Urresti is thanked for her help with the figures. E. Cuesta helped with discussions and advice about TNT procedures. Critical reviews by E. Isasmendi and two anonymous reviewers greatly helped to improve this work. This study was funded by the Deutsche Forschungsgemeinschaft under grant RA 1012/25-1 and subsidized in part by Project CGL2017-85038-P of the Spanish Ministerio de Economía y Competitividad-ERDF, as well as by the Aragón Regional Government (Grupo de referencia E18-23R Aragosaurus: Recursos Geológicos y Paleoambientales). DC is supported by a postdoctoral fellowship of the Manuel López Programme,

funded by the Programa Propio de Política Científica of the Universidad de Zaragoza. DC has been also supported by the Beatriu de Pinós postdoctoral programme (BP2017-00195) of the Government of Catalonia's Secretariat for Universities and Research of the Ministry of Economy and Knowledge developed at Institut Català de Paleontologia Miquel Crusafont, and by Fundación Conjunto Paleontológico de Teruel-Dinópolis. The excavation of the Fuente Arnar site was carried out under permission 184/2018 and the recovered partial teeth are included in the prospection 068/23-2024. Both permits were issued by the Dirección General de Patrimonio Cultural of the Aragon Government.

REFERENCES

Allain, R. and Chure, D.J. 2002. *Poekilopleuron bucklandii,* the theropod dinosaur from the Middle Jurassic (Bathonian) of Normandy. Palaeontology, 45(6):1107–1121. https://doi.org/10.1111/1475-4983.00277

Allain, R., Xaisanavong, T., Richir, P., and Khenthavong, B. 2012. The first definitive Asian spinosaurid (Dinosauria: Theropoda) from the Early Cretaceous of Laos. Naturwissenschaften, 99:369–377. https://doi.org/10.1007/s00114-012-0911-7

Alonso, A. and Canudo, J.I. 2016. On the spinosaurid theropod teeth from the Early Barremian (Early Cretaceous) Blesa Formation (Spain). Historical Biology, 28(6):823–834. https://doi.org/10.1080/08912963.2015.1036751

Alonso, A., Canudo, J.I., Torcida Fernández Baldor, F., and Huerta, P. 2017. Isolated theropod teeth associated with sauropod remains from El Oterillo II (Early Cretaceous) site of Salas de los Infantes (Burgos, Spain). Journal of Iberian Geology, 43(2):193–215. https://doi.org/10.1007/s41513-017-0017-3

Aurell, M., Bádenas, B., Gasca, J.M., Canudo, J.I., Liesa, C., Soria, A.R., Moreno-Azanza, M., and Najes, L. 2016. Stratigraphy and evolution of the Galve sub-basin (Spain) in the middle Tithonian-early Barremian: implications for the setting and age of some dinosaur fossil sites. Cretaceous Research, 65:138–162. https://doi.org/10.1016/j.cretres.2016.04.020

Aurell, M., Bádenas, B., Canudo, J.I., Castanera, D., García-Penas, A., Gasca, J.M., Martín-Closas, C., Moliner, L., Moreno-Azanza, M., Rosales, I., Santas, L., Sequero, C., and Val, J. 2019. Kimmeridgian–Berriasian stratigraphy and sedimentary evolution of the central Iberian Rift System (NE Spain). Cretaceous Research, 103:104153. https://doi.org/10.1016/j.cretres.2019.05.011

Barker, C.T., Hone, D.W., Naish, D., Cau, A., Lockwood, J.A., Foster, B., Schneider, P., and Gostling, N.J. 2021. New spinosaurids from the Wessex Formation (Early Cretaceous, UK) and the European origins of Spinosauridae. Scientific Reports, 11(1):19340. https://doi.org/10.1038/s41598-021-97870-8

Barrón, E., Navarrete, R., Rodríguez-López, J.P., Soria, A.R., Lassaletta, L., and Liesa, C.L. 2025. Palynological trends and sedimentological framework of a Barremian estuarine and barrier-island system in the western Tethys (Camarillas Formation, eastern Spain). Journal of Iberian Geology, online first. https://doi.org/10.1007/s41513-025-00299-5

Beevor, T., Quigley, A., Smith, R.E., Smyth, R.S., Ibrahim, N., Zouhri, S., and Martill, D.M. 2021. Taphonomic evidence supports an aquatic lifestyle for *Spinosaurus*. Cretaceous Research, 117, 104627. https://doi.org/10.1016/j.cretres.2020.104627

Benson, R.B. 2010. A description of *Megalosaurus bucklandii* (Dinosauria: Theropoda) from the Bathonian of the UK and the relationships of Middle Jurassic theropods. Zoological Journal of the Linnean Society, 158(4):882–935. https://doi.org/10.1111/j.1096-3642.2009.00569.x

Bonaparte, J.F. 1986. Los dinosaures (Carnosaures, Allosauridés, Sauropodes, Cétiosauridés) du Jurassique moyen de Cerro Cóndor (Chubut, Argentina). Annales de Paléontologie, 72(3):325–386.

Bonaparte, J.F., Novas, F.E., and Coria, R.A. 1990. *Carnotaurus sastrei* Bonaparte, the horned, lightly built carnotaur from the middle Cretaceous of Patagonia. Contributions Science Natural History Museum of Los Angeles County, 416:1–42. https://doi.org/10.5962/p.226819

Britt, B.B. 1991. Theropods of the Dry Mesa Quarry (Morrison Formation, Late Jurassic), Colorado, with emphasis on the osteology of *Torvosaurus tanneri*. Brigham Young University Geology Studies, 37:1–72.

Brochu, C.A. 2003. Osteology of *Tyrannosaurus rex:* insights from a nearly complete skeleton and high-resolution computed tomographic analysis of the skull. Society of Vertebrate Paleontology, Memoir, 7:1–138. https://doi.org/10.1080/02724634.2003.10010947

Burch, S.H. and Carrano, M.T. 2012. An articulated pectoral girdle and forelimb of the abelisaurid theropod *Majungasaurus crenatissimus* from the Late Cretaceous of Madagascar. Journal of Vertebrate Paleontology, 32 (1):1–16. https://doi.org/10.1080/02724634.2012.622027

Cabrera-Argudo, P., García-Cobeña, J., and Cobos, A. 2024. Variability of spinosaurid teeth in the Barremian of the province of Teruel (eastern Spain). Journal of Iberian Geology, 1–20.

Canudo, J.I. 2018. The collection of type fossils of the Natural Science Museum of the University of Zaragoza (Spain). Geoheritage, 10: 385–392. https://doi.org/10.1007/s12371-017-0228-1

Canudo, J.I. and Ruiz-Omeñaca, J.I. 2003. Los restos directos de dinosaurios terópodos (Excluyendo Aves) en España, p. 347–373. In Pérez-Lorente, F. (ed.), Dinosaurios y otros reptiles mesozoicos de España. Instituto de Estudios Riojanos, 26, Logroño.

Canudo, J.I., Gasulla, J.M., Gómez-Fernández, D., Ortega, F., Sanz, J.L., and Yagüe, P. 2008. Primera evidencia de dientes aislados atribuidos a Spinosauridae (Theropoda) en el Aptiano inferior (Cretácico Inferior) de Europa: Formación Arcillas de Morella (España). Ameghiniana, 45(4):649–652.

Canudo, J.I., Gasca, J.M., Moreno, M., and Aurell, M. 2012. New information about the stratigraphic position and age of the sauropod *Aragosaurus ischiaticus* from the Early Cretaceous of the Iberian Peninsula. Geological Magazine, 149(2):252–263. https://doi.org/10.1017/S0016756811000732

Carrano, M.T. 2007. The appendicular skeleton of *Majungasaurus crenatissimus* (Theropoda: Abelisauridae) from the Late Cretaceous of Madagascar. Society of Vertebrate Paleontology, Memoir, 8:163–179. https://doi.org/10.1671/0272-4634(2007)27[163:TASOMC]2.0.CO;2

Carrano, M.T., Sampson, S.D., and Foster, C.A. 2002. The osteology of *Masiakasaurus knopfleri*, a small abelisauroid (Dinosauria: Theropoda) from the Late Cretaceous of Madagascar. Journal of Vertebrate Paleontology, 22(3):510–534. https://doi.org/10.1671/0272-4634(2002)022[0510:TOOMKA]2.0.CO;2

Carrano, M.T., Benson, R.B.J., and Sampson, S.D. 2012. The phylogeny of Tetanurae (Dinosauria: Theropoda). Journal of Systematic Palaeontology, 10(2): 211–300. https://doi.org/10.1080/14772019.2011.630927

Charig, A.J. and Milner, A.C. 1997. *Baryonyx walkeri*, a fish-eating dinosaur from the Wealden of Surrey. Bulletin of the Natural History Museum of London (Geology Series), 53, 1:11–70.

Cuesta, E., Vidal, D., Ortega, F., and Sanz, J.L. 2018a. The cranial osteology of *Concavenator corcovatus* (Theropoda; Carcharodontosauria) from the Lower Cretaceous of Spain. Cretaceous Research, 91:176–194. https://doi.org/10.1016/j.cretres.2018.06.007

Cuesta, E., Ortega, F., and Sanz, J.L. 2018b. Appendicular osteology of *Concavenator corcovatus* (Theropoda: Carcharodontosauridae) from the Lower Cretaceous of Spain. Journal of Vertebrate Paleontology, 38(4): 1–24. https://doi.org/10.1080/02724634.2018.1485153

Cuesta, E., Ortega, F., and Sanz, J.L. 2019. Axial osteology of *Concavenator corcovatus* (Theropoda; Carcharodontosauria) from the Lower Cretaceous of Spain. Cretaceous Research, 95: 106–120. https://doi.org/10.1016/j.cretres.2018.10.026

Cuesta, E., Vidal, D., Ortega, F., Shibata, M., and Sanz, J.L. 2022. *Pelecanimimus* (Theropoda: Ornithomimosauria) postcranial anatomy and the evolution of the specialized manus in ornithomimosaurs and sternum in maniraptoriforms. Zoological Journal of the Linnean

Society, 194(2), 553–591.
https://doi.org/10.1093/zoolinnean/zlab013
Currie, P.J. and Zhao, X.-J. 1993. A new carnosaur (Dinosauria, Theropoda) from the Jurassic of Xinjiang, People's Republic of China. Canadian Journal of Earth Sciences, 30:2037–2081.
https://doi.org/10.1139/e93-17
Currie, P.J. and Chen, P-j. 2001. Anatomy of *Sinosauropteryx prima* from Liaoning, northeastern China. Canadian Journal of Earth Sciences, 38:1705–1727.
https://doi.org/10.1139/e01-050
Dal Sasso, C., Maganuco, S., Buffetaut, E., and Mendez, M.A. 2005. New information on the skull of the enigmatic theropod *Spinosaurus*, with remarks on its size and affinities. Journal of Vertebrate Paleontology, 25, 4:888–896.
https://doi.org/10.1671/0272-4634(2005)025[0888:NIOTSO]2.0.CO;2
Dal Sasso, C., Maganuco, S., and Cau, A. 2018. The oldest ceratosaurian (Dinosauria: Theropoda), from the Lower Jurassic of Italy, sheds light on the evolution of the three-fingered hand of birds. PeerJ, 6:e5976.
https://doi.org/10.7717/peerj.5976
Estes, R. and Sanchiz, F. 1982. Early Cretaceous Lower Vertebrates from Galve (Teruel), Spain. Journal of Vertebrate Paleontology, 2:21–39.
https://doi.org/10.1080/02724634.1982.10011915
Evers, S.W., Rauhut, O.W.M., Milner, A.C., McFeeters, B., and Allain, R. 2015. A reappraisal of the morphology and systematic position of the theropod dinosaur *Sigilmassasaurus* from the “middle” Cretaceous of Morocco. Plos One, 3: e1323.
https://doi.org/10.7717/peerj.1323
Evers, S.W., Foth, C., and Rauhut, O.W.M. 2020. Notes on the cheek region of the Late Jurassic theropod dinosaur *Allosaurus*. PeerJ, 8:e8493.
https://doi.org/10.7717/peerj.8493
Fabbri, M., Navalón, G., Benson, R.B.J., Pol, D., O’Connor, J., Bhullar, B.A.S., Erickson, G., Norell, M.A., Orkney, A., Lamanna, M., Zouhri, S., Becker, J., Emke, A., Dal Sasso, C., Bindellini, G.M., Maganuco, S., Auditore, M., and Ibrahim, N. 2022. Subaqueous foraging among carnivorous dinosaurs. Nature, 603:852–857.
https://doi.org/10.1038/s41586-022-04528-0
Filippi, L.S., Mendez, A., Valieri, R., and Garrido, A. 2016. A new brachyrostran with hypertrophied axial structures reveals an unexpected radiation of latest Cretaceous abelisaurids. Cretaceous Research, 61:209–219.
Filippi, L.S., Méndez, A.H., Gianechini, F.A., Valieri, R.D.J., and Garrido, A.C. 2018. Osteology of *Viavenator exxoni* (Abelisauridae; Furileusauria) from the Bajo de la Carpa Formation, NW Patagonia, Argentina. Cretaceous Research, 83:95–119.
https://doi.org/10.1016/j.cretres.2017.07.019
Fitzinger, L. 1843. Systema Reptilium. Fasciculus Primus. Amblyglossae. Apud Braumüller and Seidel Bibliopolas, Vienna.
García-Cobeña, J., Castanera, D., Verdú, F.J., and Cobos, A. 2024. Diversity and discrimination of large ornithopods revealed through their tracks (Lower Cretaceous, Spain): A phenetic correlation approach. Palaeoworld.
https://doi.org/10.1016/j.palwor.2024.03.005
Gasca, J.M., Moreno-Azanza, M., and Canudo, J.I. 2008. Dientes de dinosaurios terópodos espinosáuridos de la Formación El Castellar (Cretácico Inferior, Teruel). Palaeontologica Nova. SEPAZ, 8:233–234.
Gasca, J.M., Moreno-Azanza, M., and Canudo, J.I. 2011. Dientes de dinosaurios en el Barremiense de Allepuz, Teruel, p. 145–155. In Pérez-García, A., Gascó, F., Gasulla, J.M., Escaso, F., and Narváez, I. (eds.), Viajando a Mundos Pretéritos. Ajuntament de Morella, Morella.
Gasca, J.M., Canudo, J.I., Ruiz-Omeñaca, J.I., and Moreno-Azanza, M. 2015. New material and phylogenetic position of the basal iguanodont dinosaur *Delapparentia turolensis* from the Barremian (Early Cretaceous) of Spain. Journal of Iberian Geology, 41(1):57–70.
https://doi.org/10.5209/rev_JIGE.2015.v41.n1.4
Gasca, J.M., Moreno-Azanza, M., Bádenas, B., Díaz-Martínez, I., Castanera, D., Canudo, J.I., and Aurell, M. 2017. Integrated overview of the vertebrate fossil record of the Ladruñán anticline (Spain): evidence of a Barremian alluvial-lacustrine system in NE Iberia frequented

by dinosaurs. Palaeogeography, Palaeoclimatology, Palaeoecology, 472:192–202. https://doi.org/10.1016/j.palaeo.2017.01.050

Gasca, J.M., Díaz-Martínez, I., Moreno-Azanza, M., Canudo, J.I., and Alonso, A. 2018. A hypertrophied ungual phalanx from the lower Barremian of Spain: Implications for the diversity and palaeoecology of Spinosauridae (Theropoda) in Iberia. Cretaceous Research, 84:141–152. https://doi.org/10.1016/j.cretres.2017.11.011

Gasulla, J.M., Ortega, F., Escaso, F., and Pérez-García, A. 2011. Los yacimientos de vertebrados de la Formación Arcillas de Morella (Aptiense inferior), p. 157–171. In Pérez-García, A., Gascó, F., Gasulla, J.M., Escaso, F., and Narváez, I. (eds.), Viajando a Mundos Pretéritos. Ajuntament de Morella, Morella.

Gauthier, J.A. 1986. Saurischian monophyly and the origin of birds, p. 1–55. In Padian, K. (ed.), The origin of Birds and the Evolution of Flight. Memoirs of the California Academy of Sciences, 8, San Francisco.

Goloboff, P.A. and Morales, M.E. 2023. TNT version 1.6, with a graphical interface for MacOS and Linux, including new routines in parallel. Cladistics, 39(2):144–153. https://doi.org/10.1111/cla.12524

Goloboff, P.A., Torres, A., and Arias, J.S. 2018. Weighted parsimony outperforms other methods of phylogenetic inference under models appropriate for morphology. Cladistics, 34(4):407–437. https://doi.org/10.1111/cla.12205

Grillo, O.N. and Delcourt, R. 2017. Allometry and body length of abelisauroid theropods: *Pycnonemosaurus nevesi* is the new king. Cretaceous Research, 69:71–89. https://doi.org/10.1016/j.cretres.2016.09.001

Hendrickx, C., Mateus, O., and Araújo, R. 2015. The dentition of megalosaurid theropods. Acta Palaeontologica Polonica, 60(3):627-642.

Ibrahim, N., Sereno, P.C., Dal Sasso, C., Maganuco, S., Fabbri, M., Martill, D.M., Zouhri, S., Myhrvold, N., and Lurino, D.A. 2014. Semiaquatic adaptations in a giant predatory dinosaur. Science, 345, 6204:1613–1616. https://doi.org/10.1126/science.1258750

Ibrahim, N., Maganuco, S., Dal Sasso, C., Fabbri, M., Auditore, M., Bindellini, G., Martill, D.M., Zhouri, S., Mattarelli, D.A., Unwin, D.M., Wiemann, J., Bonadonna, D., Amane, A., Jakubczak, J., Joger, U., Lauder, G.V., and Pierce, S.E. 2020. Tail-propelled aquatic locomotion in a theropod dinosaur. Nature, 581(7806), 67–70. https://doi.org/10.1038/s41586-020-2190-3

Isasmendi, E., Sáez-Benito, P., Torices, A., Navarro-Lorbés, P., and Pereda-Suberbiola, X. 2020. New insights about theropod palaeobiodiversity in the Iberian Peninsula and Europe: spinosaurid teeth (Theropoda, Megalosauroidea) from the Lower Cretaceous of La Rioja (Spain). Cretaceous Research, 116:104600. https://doi.org/10.1080/08912963.2022.2069019

Isasmendi, E., Navarro-Lorbés, P., Sáez-Benito, P., Viera, L.I., Torices, A., and Pereda-Suberbiola, X. 2023. New contributions to the skull anatomy of spinosaurid theropods: Baryonychinae maxilla from the Early Cretaceous of Igea (La Rioja, Spain). Historical Biology, 35 (6):909–923. https://doi.org/10.1080/08912963.2022.2069019

Isasmendi, E., Cuesta, E., Díaz-Martínez, I., Company, J., Sáez-Benito, P., Viera, L.I., Torices, A., and Pereda-Suberbiola, X. 2024. Increasing the theropod record of Europe: A new basal spinosaurid from the Enciso Group of the Cameros Basin (La Rioja, Spain). Evolutionary implications and palaeobiodiversity. Zoological Journal of the Linnean Society, 202:zlad193. https://doi.org/10.1093/zoolinnean/zlad193

Isasmendi, E., Cuesta, E., Páramo, A., and Pereda-Suberbiola, X. 2025. A giant spinosaurid from the Iberian Peninsula and new data on the Early Cretaceous Iberian non-avian theropod palaeodiversity. Cretaceous Research, 173:106134. https://doi.org/10.1016/j.cretres.2025.106134

Kellner, A.W.A. and Campos, D.A. 2002. On a theropod dinosaur (Abelisauria) from the continental Cretaceous of Brazil. Arquivos do Museu Nacional, Rio de Janeiro, 60, 3:163–170.

Lex, M. 2016. Morphology and systematic classification of an unusual caudal vertebra from the Cenomanian of Morocco. BSc thesis, Ludwig-Maximilians-Universität, Munich, Germany.

Liesa, C.L., Soria, A.R., Casas, A., Aurell, M., Meléndez, N., Bádenas, B., Fregenal-Martínez, M., Navarrete, R., Peropadre, C., and Rodríguez-López, J.P., 2019. The South Iberian, Central-Iberian and Maestrazgo basins, p. 214–228. In Quesada, C. and Oliveira, J.T. (eds.), The Geology of Iberia: A Geodynamic Approach, vol. 5. Springer Nature, Switzerland.

Liesa, C.L., Casas-Sainz, A.M., Aurell, M., Simón, J.L., and Soria, A.R. 2023. Salt tectonics vs. inversion tectonics: The anticlines of the western Maestrazgo revisited (eastern Iberian Chain, Spain). Basin Research, 35(1):295–335. https://doi.org/10.1111/bre.12713

Madsen, J. H. 1976. *Allosaurus fragilis*: a revised osteology. Utah Geological and Mineral Survey Bulletin, 109:1–163.

Madsen, J.H.J. and Welles, S.P. 2000. *Ceratosaurus* (Dinosauria, Theropoda). A revised osteology. Miscellaneous Publication, Utah Geological Survey, 00-2:1–80.

Malafaia, E., Gasulla, J.M., Escaso, F., Narváez, I., Sanz, J.L., and Ortega, F. 2018. New spinosaurid (Theropoda, Megalosauroidea) remains from the Arcillas de Morella Formation (upper Barremian) of Morella, Spain. Cretaceous Research, 92:174–183. https://doi.org/10.1016/j.cretres.2018.08.006

Malafaia, E., Gasulla, J.M., Escaso, F., Narvaéz, I., and Ortega, F. 2020a. An update of the spinosaurid (Dinosauria: Theropoda) fossil record from the Lower Cretaceous of the Iberian Peninsula: distribution, diversity, and evolutionary history. Journal of Iberian Geology, 46(4):431–444. https://doi.org/10.1007/s41513-020-00138-9

Malafaia, E., Gasulla, J.M., Escaso, F., Narváez, I., Sanz, J.L., and Ortega, F. 2020b. A new spinosaurid theropod (Dinosauria: Megalosauroidea) from the upper Barremian of Vallibona, Spain: Implications for spinosaurid diversity in the Early Cretaceous of the Iberian Peninsula. Cretaceous Research, 106:104221. https://doi.org/10.1016/j.cretres.2019.104221

Marsh, O.C. 1881. Principal characters of American Jurassic dinosaurs. Part V. American Journal of Science, series 3, 21:339–340.

Marsh, A.D. and Rowe, T. B. 2020. A comprehensive anatomical and phylogenetic evaluation of *Dilophosaurus wetherilli* (Dinosauria, Theropoda) with descriptions of new specimens from the Kayenta Formation of northern Arizona. Journal of Paleontology, 94(S78):1–103. https://doi.org/10.1017/jpa.2020.14

Martín-Closas, C. 1989. Els caròfits del Cretaci inferior de les conques perifèriques del Bloc de l'Ebre. PhD Thesis, University of Barcelona, Barcelona, Spain.

Mateus, O., Araujo, R., Natário, C., and Castanhinha, R. 2011. A new specimen of the theropod dinosaur *Baryonyx* from the Early Cretaceous of Portugal and taxonomic validity of *Suchosaurus*. Zootaxa, 2827(5). https://doi.org/10.5281/zenodo.205679

Mateus, O. and Estraviz-López, D. 2022. A new theropod dinosaur from the early cretaceous (Barremian) of Cabo Espichel, Portugal: Implications for spinosaurid evolution. PLoS One, 17(2):e0262614. https://doi.org/10.1371/journal.pone.0262614

Myhrvold, N.P., Baumgart, S.L., Vidal, D., Fish, F.E., Henderson, D.M., Saitta, E.T., and Sereno, P.C. 2024. Diving dinosaurs? Caveats on the use of bone compactness and pFDA for inferring lifestyle. Plos one, 19(3):e0298957. https://doi.org/10.1371/journal.pone.0298957

Navarrete, R., Rodríguez-López, J.P., Liesa, C.L., Soria, A.R., and Fernanda de Mesquita, L.V. 2013. Changing physiography of rift basins as a control on the evolution of mixed siliciclastic–carbonate back-barrier systems (Barremian Iberian Basin, Spain). Sedimentary Geology, 289: 40–61. https://doi.org/10.1016/j.sedgeo.2013.02.003

Navarrete, R., Liesa, C.L., Castanera, D., Soria, A.R., Rodríguez-López, J.P., and Canudo, J.I. 2014. A thick Tethyan multi-bed tsunami deposit preserving a dinosaur megatracksite within a coastal lagoon (Barremian, eastern Spain). Sedimentary Geology, 313:105–127. https://doi.org/10.1016/j.sedgeo.2014.09.007

Novas, F.E., Dalla Vecchia, F.M., and Pais, D.F. 2005. Theropod pedal unguals from the Late Cretaceous (Cenomanian) of Morocco, Africa. Revista del Museo Argentino de Ciencias Naturales, 7(2):167–175.

Ortega, F., Escaso, F., and Sanz, J.L. 2010. A bizarre, humped Carcharodontosauria (Theropoda) from the Lower Cretaceous of Spain. Nature, 467: 203–206. https://doi.org/10.1038/nature09181

Owen, R. 1857. Monograph on the fossil Reptilia of the Wealden Formations. Part III. *Megalosaurus bucklandi*. Monographs of the Palaeontographical Society, 9(34):1–26.

Pérez-Moreno, B., Sanz, J.L., Buscalioni, A.D., Moratalla, J.J., Ortega, F., and Rasskin-Gutman, D. 1994. A unique multitoothed ornithomimosaur dinosaur from the Lower Cretaceous of Spain. Nature, 370: 363–367. https://doi.org/10.1038/370363a0

Pol, D. and Escapa, I.H. 2009. Unstable taxa in cladistic analysis: identification and the assessment of relevant characters. Cladistics, 25(5):515–527. https://doi.org/10.1111/j.1096-0031.2009.00258.x

Rauhut, O.W.M. 2003. The interrelationships and evolution of basal theropod dinosaurs. Special Papers in Palaeontology 69:1–213.

Rauhut, O.W.M. 2011. Theropod dinosaurs from the Late Jurassic of Tendaguru (Tanzania). Special Papers in Palaeontology, 86:195–239. https://doi.org/10.1111/j.1475-4983.2011.01084.x

Rauhut, O.W.M. and Carrano, M.T. 2016. The theropod dinosaur *Elaphrosaurus bambergi*, from the Late Jurassic of Tendaguru, Tanzania. Zoological Journal of the Linnean Society, 178(3):546–610. https://doi.org/10.1111/zoj.12425

Rauhut, O.W.M., Hübner, T., and Lanser, K.P. 2016. A new megalosaurid theropod dinosaur from the late Middle Jurassic (Callovian) of north-western Germany: implications for theropod evolution and faunal turnover in the Jurassic. Palaeontologia electronica, 19.2.29A:1-65. https://doi.org/10.26879/654

Rauhut, O.W.M., Canudo, J.I., and Castanera, D. 2019. A reappraisal of the Early Cretaceous theropod dinosaur *Camarillasaurus* from Spain. Program and abstracts XVII Conference of the EAVP, 96.

Rauhut, O.W.M. and Pol, D. 2019. Probable basal allosauroid from the early Middle Jurassic Cañadón Asfalto Formation of Argentina highlights phylogenetic uncertainty in tetanuran theropod dinosaurs. Scientific Reports, 9(1):18826. https://doi.org/10.1038/s41598-019-53672-7

Rauhut, O.W.M. and Pol, D. 2021. New theropod remains from the Late Jurassic Cañadón Calcáreo Formation of Chubut, Argentina. Journal of South American Earth Sciences, 111:103434. https://doi.org/10.1016/j.jsames.2021.103434

Ruiz-Omeñaca, J.I., Canudo, J.I., Aurell, M., Bádenas, B., Barco, J.L., Cuenca-Bescós, G., and Ipas, J. 2004. Estado de las investigaciones sobre los vertebrados del Jurásico Superior y Cretácico Inferior de Galve (Teruel). Estudios geológicos, 60(3-6):179–202. https://doi.org/10.3989/egeol.04603-694

Samathi, A., Sander, P.M., and Chanthasit, P. 2021. A spinosaurid from Thailand (Sao Khua Formation, Early Cretaceous) and a reassessment of *Camarillasaurus cirugedae* from the Early Cretaceous of Spain. Historical Biology, 33(12):3480–3494. https://doi.org/10.1080/08912963.2021.1874372

Salas, R., Guimerà, J., Mas, R., Martín-Closas, C., Meléndez, A., and Alonso, A. 2001. Evolution of the Mesozoic central Iberian Rift System and its Cainozoic inversion (Iberian chain). Mémoires du Muséum National d'Histoire Naturelle, 186: 145–186.

Sánchez-Hernández, B., Benton, M.J., and Naish, D. 2007. Dinosaurs and other fossil vertebrates from the Late Jurassic and Early Cretaceous of the Galve area, NE Spain. Palaeogeography, Palaeoclimatology, Palaeoecology, 249(1-2): 180–215. https://doi.org/10.1016/j.palaeo.2007.01.009

Sánchez-Hernández, B. and Benton, M.J. 2014. Filling the ceratosaur gap: a new ceratosaurian theropod from the Early Cretaceous of Spain. Acta Palaeontologica Polonica, 59 (3):581–600. https://doi.org/10.4202/app.2011.0144

Santos-Cubedo, A., de Santisteban, C., Poza, B., and Meseguer, S. 2023. A new spinosaurid dinosaur species from the Early Cretaceous of Cinctorres (Spain). Scientific Reports, 13(1):6471. https://doi.org/10.1038/s41598-023-33418-2

Sauvage, H.E. 1897-1898. Vertébrés fossiles du Portugal. Contribution à l'étude des poissons et des reptiles du Jurassique et du Crétacique. Mémoires de la Direction de Travaux Géologiques du Portugal, 46p.

Schade, M., Rauhut, O.W.M., Foth, C., Moleman, O., and Evers, S.W. 2023. A reappraisal of the cranial and mandibular osteology of the spinosaurid *Irritator challengeri* (Dinosauria: Theropoda). Paleontologia Electronica, 26.2.a17 https://doi.org/10.26879/1242

Schudack, U. and Schudack, M. 2009. Ostracod biostratigraphy in the lower cretaceous of the Iberian chain (eastern Spain). Journal of Iberian Geology, 35(2):141–168.

Sereno, P.C., Beck, A.L., Dutheil, D.B., Gado, B., Larsson, H.C.E., Lyon, G.H., Marcot, J.D., Rauhut, O.W.M., Sadleir, R.W., Sidor, C.A., Varricchio, D.D., Wilson, G.P., and Wilson, J.A. 1998. A long-snouted predatory dinosaur from Africa and the evolution of spinosaurids. Science, 282(5392):1298-1302. https://doi.org/10.1126/science.282.5392.1298

Sereno, P.C., Myhrvold, N., Henderson, D.M., Fish, F.E., Vidal, D., Baumgart, S.L., Keillor, T.M., Formoso, K.K., and Conroy, L. L. 2022. *Spinosaurus* is not an aquatic dinosaur. Elife, 11, e80092. https://doi.org/10.7554/eLife.80092

Smyth, R.S., Ibrahim, N. and Martill, D.M. 2020. *Sigilmassasaurus* is *Spinosaurus*: a reappraisal of African spinosaurines. Cretaceous Research, 114: 104520. https://doi.org/10.1016/j.cretres.2020.104520

Soria, A.R., 1997. La sedimentación en las cuencas marginales del surco ibérico durante el Cretácico inferior y su control estructural. PhD Thesis. Universidad de Zaragoza, Zaragoza, Spain.

Soria, A.R., Liesa, C.L., Navarrete, R., and Rodríguez-López, J.P. 2023. Sedimentology and stratigraphic architecture of Barremian synrift barrier island–estuarine depositional systems from blended field and drone?derived data. Sedimentology, 70(6):1812–1855. https://doi.org/10.1111/sed.13097

Stromer, E. 1915. Ergebnisse der Forschungsreisen Prof. E. Stromers in den Wüsten Agyptens. II. Wirbeltier-Reste der Baharîje-Stufe (unterstes Cenoman). 3. Das Original des Theropoden *Spinosaurus aegyptiacus* nov. gen., nov. spec. Abhandlungen der Königlich Bayerischen Akademie der Wissenschaften. Mathematisch-physikalische Klasse Abhandlung 28, 1e31.

Stromer, E. 1934. Ergebnisse der Forschungsreisen Prof. E. Stromers in den Wüsten Ägyptens. II. Wirbeltierreste der Baharije-Stufe (unterstes Cenoman). 13. Dinosauria. Abhandlungen der Bayerischen Akademie der Wissenschaften, Mathematisch-naturwissenschaftliche Abteilung, Neue Folge, 22:1–79.

Suñer, M., Poza, B., Vila, B., and Santos-Cubedo, A. 2008. Síntesis del registro fósil de dinosaurios en el Este de la Península Ibérica. Palaeontologica Nova. SEPAZ, 2008, 8:397–420.

Tortosa, T., Buffetaut, E., Vialle, N., Dutour, Y., Turini, E., and Cheylan, G. 2014. A new abelisaurid dinosaur from the Late Cretaceous of southern France: Palaeobiogeographical implications. Annales de Paléontologie, 100 (1):63–86. https://doi.org/10.1016/j.annpal.2013.10.003

Verdú, F.J., Royo-Torres, R., Cobos, A., and Alcalá, L. 2015. Perinates of a new species of *Iguanodon* (Ornithischia: Ornithopoda) from the lower Barremian of Galve (Teruel, Spain). Cretaceous Research, 56:250–264. https://doi.org/10.1016/j.cretres.2015.05.010

Verdú, F.J., Royo-Torres, R., Cobos, A., and Alcalá, L. 2020. Systematics and paleobiology of a new articulated axial specimen referred to *Iguanodon* cf. *galvensis* (Ornithopoda, Iguanodontoidea). Journal of Vertebrate Paleontology, 40(6):e1878202. https://doi.org/10.1080/02724634.2021.1878202

Villanueva-Amadoz, U., Sender, L.M., Royo-Torres, R., Verdú, F.J., Pons, D., Alcalá, L., and Diez, J.B. 2015. Palaeobotanical remains associated with dinosaur fossils from the Camarillas Formation (Barremian) of Galve (Teruel, Spain). Historical Biology, 27(3-4):374–388. https://doi.org/10.1080/08912963.2014.931385

Wilkinson, M. 1995. Coping with abundant missing entries in phylogenetic inference using parsimony. Systematic biology, 44(4): 501–514. https://doi.org/10.1093/sysbio/44.4.501

Xu, X., Clark, J.M., Forster, C., Norell, M.A., Erickson, G.M., Eberth, D.A., Jia, C., and Zhao, Q. 2006. A basal tyrannosauroid dinosaur from the Late Jurassic of China. Nature, 439:715–718.
https://doi.org/10.1038/nature04511

APPENDIX.

Characters used in the phylogenetic analysis, modified from Schade et al. (2023)

1. Premaxilla, height/length ratio ventral to external naris (length measured along ventral border of bone): < 0.5 (0), 0.5-0.99 (1), 1-1.49 (2), 1.5 or higher (3) ordered

2. Premaxilla, shape of ventral margin in lateral view: straight to slightly convex (0); markedly concave (1)

3. Maxilla, participation in the ventral border of naris: absent, subnarial process of the premaxilla contacts the nasal (0), subnarial process of premaxilla reduced or absent, maxilla expressed on the ventral margin of the nares (1)

4. Premaxilla, posterior extent of nasal process relative to posterior tip of subnarial process: considerably more anterior (0); even (1); posterior (2). ordered

5. Premaxilla, form of premaxilla-nasal suture: V-shaped (0), W-shaped (1).

6. External nares: position of anterior end with respect to premaxillary body: over anterior half of ventral margin of premaxillary body (0); over the posterior half of the ventral margin of the premaxillary body (1); posterior to the ventral margin of the premaxillary body (2). ordered

7. Premaxilla, diastema adjacent to maxilla along dentigerous margin: absent (0), present, with alveolar margin being continuous between premaxilla and maxilla (1), present, with alveolar margin being discontinuous between premaxilla and maxilla ("subnarial gap") (2)

8. Premaxilla, mediolateral constriction of posterior portion: absent (0), present (1).

9. Premaxilla, development of subnarial (maxillary) process: well-developed, rod or plate-like (0), reduced to a short, stout triangle, as long as or shorter than its basal width (1).

10. Subnarial foramen on the premaxilla–maxilla suture: absent (0), present (1).

11. Premaxilla, articulation with maxilla: planar (0), interlocking (1).

12. Anterior ramus of the maxilla: absent, anterior margin of maxillary body confluent with anterior margin of the ascending process (0); present but very short (length/height ratio less than 1) (1); present moderately long (1-1.35) (2); present, long (1.35-1.7) (3); present, very long (more than 2) (4). ordered

13. Subnarial fossa on the maxilla: absent (0); present (1)

14. Maxilla, orientation of anteriormost alveolus: vertical (0), angled anteriorly (1).

15. Anterodorsal margin of the ascending process of the maxilla: straight or gently curved (0), with pronounced kink at about mid-length, with a more anteriorly facing margin ventral and a more dorsally facing margin dorsal to the kink (1).

16. Relative posterior length of the ascending process and jugal ramus of the maxilla: jugal ramus extends considerably further posteriorly than ascending process (0); subequal in length or ascending process longer (1)

17. Maxilla, morphology of palatal process: long, ridged or fluted prong (0), long and plate-shaped (1).

18. Maxilla, position of palatal process: ventral, immediately dorsal to paradental plates (0), dorsal, immediately ventral to dorsal surface of maxillary anterior ramus (1).

19. Maxilla, horizontal ridge (prominent 'lingual bar') between palatal process and antorbital fenestra: absent (0), present (1).

20. Maxilla, depth of paradental plates relative to anteroposterior width: low, < 1.8 (0); tall > 1.8 (1).

21. Maxilla, ventral extent of paradental plates relative to lateral wall: as far ventral (0); fall short (1).

22. Maxilla, arrangement of nutrient foramina on lateral surface: single row or no distinct pattern (0); a second, more dorsally placed row is present anteriorly and converges with the ventral row posteriorly (1); a second, dorsally placed row is present and extends posteriorly more or less parallel to the ventral row (2).

23. Maxilla, anteroventral border of antorbital fossa: graded or stepped (0), demarcated by raised ridge (1).

24. Maxilla, anterior margin of antorbital fossa: rounded (0); squared (1).

25. Maxilla, ventral extent of antorbital fossa (as measured from the rim of the antorbital fenestra to the highest point of the ridge marking its border) at the level of about the half length of the antorbital fenestra: small or absent, less than 1/3 the height of the maxillary body at this level (0); moderate, between 1/3 and half the height (1), dorsoventrally deep, more than half the height (2). ordered

26. Maxilla, position of anterior end of antorbital fossa: posterior to or level with posterior rim of external nares (0), ventral to external nares (1).

27. Medial wall of the anterior end of the maxillary antorbital fossa: lacking depressions or foramina (0); with a large depression without sharply defined margins (1); with a sharply rimmed maxillary fenestra (2).

28. Development of maxillary fenestra: opens medially into a small maxillary antrum with a robust medial wall (0); opens medially into a large maxillary antrum that is medially open or only covered by a very thin bony wall (1); opens anteriorly into a large antrum within the ascending process of the maxilla (2) This character is inapplicable in taxa that lack a maxillary fenestra.

29. Promaxillary foramen: absent (0), present and opens anteriorly into pneumatic recesses in the ascending process of the maxilla (1).

30. Size of the promaxillary foramen in relation to the maxillary fenestra: smaller (0); larger (1). This character is inapplicable in taxa that lack a maxillary fenestra.

31. Maxilla, development of pneumatic fossa (excavatio pneumatica) in ascending process: absent (0), present (1).

32. Maxilla, pneumatic region on medial side of maxilla posteroventral to maxillary fenestra: absent (0); present (1).

33. Shape of the alveolar border of the maxilla: straight (0); convex (1); sinusoidal (2)

34. Maxilla, posterior end of tooth row relative to orbit: beneath (0), anterior (1).

35. Posterior end of the jugal ramus of the maxilla: single (0); forked (1)

36. Posteriormost end of the jugal ramus of the maxilla: straight, in line with alveolar border (0); markedly downturned (1)

37. Maxilla and nasal, external surface texture: smooth (0), sculptured (1).

38. Nasal, inter-nasal contact in adults: separate (0), partly or fully fused (1).

39. Nasal, posterior narial margin: absent or weak fossa (0), large fossa (1), laterally splayed hood (2).

40. Posteriorly pointed, sharply rimmed depression on the lateral side of the nasal posterodorsal to the external nares: absent (0), present (1).

41. Nasal, participation in antorbital fossa: absent or at edge (0), present (1).

42. Nasal, antorbital fossa in lateral view: visible (0); occluded by ventrolaterally overhanging lamina (1).

43. Nasal, pneumatic foramina: absent (0), present (1).

44. Nasal, development of dorsolateral surfaces: none, nasals low and dorsally convex (0), pronounced dorsolateral rims, sometimes with lateral crests (1), tall, parasagittal crests (2) ordered

45. Midline crest on the nasals: absent (0); present (1)

46. Posterior end of nasal crest on the nasal: not expanded, crest stays of subequal width throughout length (0); transversely broadened into a notable tubercle (1)

47. Nasal, sculpturing: smooth or low rugosity (0), deeply rugose, bears large excresences (1)

48. Posterior end of the nasals: thin, plate-like (0); strongly thickened, robust (1)

49. Antorbital fossa and dorsal rim on the anterior process of the lacrimal: present, but fossa is largely hidden in lateral view by an overhanging lateral lamina and only exposed anteriorly (0); present, widely exposed laterally and confluent with the antorbital fossa of the dorsal part of the ventral process (1); dorsal rim absent, no differentiation between fossa and rim on the lateral surface of anterior process (2).

50. Lacrimal, morphology of lateral lamina of ventral process of lacrimal: forming a continuous sheet of bone between the ventral and anterior processes (0); invaginated dorsally and convex anteriorly, anteriormost point situated dorsal to midheight of ventral process (1); anteriormost point situated around midheight of ventral process (2).

51. Anteroposterior expansion of ventral process of the lacrimal: begins at two thirds of the height of the ventral process or lower (0); begins at the dorsal end of the ventral process (1)

52. Lacrimal, dorsal and ventral portions of antorbital fossa: separated by anterior projection of lateral lamina (0), continuous, lateral lamina does not project far anteriorly (1).

53. Lacrimal fenestra: absent (0); present (1).

54. Lacrimal, openings in lacrimal recess: single (0), multiple (1).

55. Lacrimal horn: absent (0); small dorsal rugosity (1); low, broad, rugose bar (2); large triangular horn (3). ordered

56. Lacrimal, suborbital process: absent (0), present (1).

57. Lacrimal, angle between anterior and ventral rami: ~90° (0), < 75° (1).

58. Lacrimal, length of anterior process relative to ventral process: more (0), or less than 80% (1).

59. Jugal, position of anterior end: excluded from internal antorbital fenestra (0), posterior to internal antorbital fenestra, but reaching its posterior rim (1), expressed at rim of internal antorbital fenestra, with distinct anterior process extending beneath it (2). Ordered

60. Jugal, pneumatisation: absent (0), internally hollowed and transversely inflated by foramen in posterior rim of antorbital fossa (1).

61. Jugal, antorbital fossa that is clearly offset from the lateral jugal surface by a raised rim: absent (0), present (1).

62. Anterior end of jugal: slender and not or only slightly expanded (0); strongly expanded, and expansion forms at least a small part of the anterior margin of the orbit (1).

63. Jugal, orientation of orbital margin on postorbital process: angled posterodorsally (0), vertical (1).

64. Horizontal ridge along the jugal body: absent (0); present (1)

65. Lateral ridge along the postorbital contact on the postorbital process of the jugal: absent (0); present (1)

66. Dorsoventral height of the posterior process of jugal: less than half the height of the suborbital part (0), more than half the height, but less than height of suborbital part (1), or subequal or more than dorsoventral height of suborbital part (2).

67. Postorbital, articulation with jugal: planar or with a shallow, V-shaped groove dorsally (0), with a deep, broad groove posteriorly, ventral process with U-shaped cross-section (1).

68. Postorbital, suborbital flange: absent (0), present (1).

69. Development of suborbital flange of postorbital: small, triangular eminence (0), dorsoventrally elongate, large rounded flange (1), jugal process curved anteroventrally and suborbital process developed as large, sharply angled, triangular flange (2) This character is not applicable to taxa that do not have a suborbital flange.

70. Postorbital, ventral extent relative to ventral margin of orbit: substantially above (0), approximately same level (1).

71. Dorsal margin of postorbital above jugal process in lateral view: convex (0); straight to slightly concave (1); with pointed, triangular cornual process that is anteriorly offset from a possible step at the beginning of the squamosal articulation (2)

72. Laterosphenoid facet on medial side of the postorbital: large and placed at the junction of the three postorbital processes (0), reduced in size and placed entirely on the anterior process (1)

73. Medial side of posterior process of the postorbital: straight or concave, dorsal margin forms a sharp rim (0); convex, medial margin curves into dorsal margin (supratemporal fossa extends onto process) (1).

74. Supratemporal fossa on the anterior process of the postorbital and posterior end of frontal: forms a large shelf on the dorsal surface of the process (0); reduced, restricted to the posteriormost part and faces more posterodorsally than dorsally (1).

75. Supraorbital brow: absent, anterior end of postorbital tapers (0); present as a dorsoventrally expanded, anteriorly rounded, rugose swelling over the posterior part of the orbit (1); large, strongly rugose supraorbital brow (possibly formed by a separate palpebral ossification fused to the postorbital) that connects the postorbital with the lacrimal present (2). ordered

76. Anterior process of the postorbital: straight (0); downturned anteriorly (1)

77. Posterior process of the postorbital: Pointed and transversely narrow (0); broadened transversely posteriorly and wider than high (1).

78. Parietal-postorbital contact at the anterior end of the supratemporal fenestra: absent, parietal and postorbital separated by posterior process of frontal that reaches the laterosphenoid (0); present, frontal excluded from laterosphenoid in dorsal view (1).

79. Prefrontal in adult individuals: Exposed on the anterodorsal margin of the orbit (0), reduced, not exposed at the anterior margin of the orbit, might only be visible at the dorsal margin of the orbit (1), absent as separate ossification (2).

80. Frontal-prefrontal contact: prefrontal contacts anterolateral margin of the frontal, placed mainly lateral to the frontal (0); prefrontal contacts anterior margin of the frontal, placed mainly anterior to frontal (1)

81. Frontal, exposure along orbital rim: broad, one third or more of the dorsal orbital margin (0), reduced, less than one third of the dorsal orbital margin (1).

82. Midline ridge on the frontal: absent (0); present (1)

83. Proportions of frontal (as exposed on the skull roof): longer than wide (0); wider than long (1)

84. Frontals in adult individuals: unfused (0); partially or completely fused (1)

85. Clearly offset lateral postorbital process of the frontal: absent (0); present (1)

86. Nasal-frontal suture: anterior end of articulated frontals medially tapering or rounded (0); anterior end of articulated frontals separated by a broad medial posterior process of the nasal (1)

87. Overlap of the parietal over the median supraoccipital ridge/thickening: absent (0), present (1).

88. Parietal, development of median skull table between supratemporal fossae: flat, but relatively narrow (less than 50% of width of supratemporal fenestrae) (0), separated by a triangular plate of bone anteriorly, but narrowing to a sagittal crest posteriorly (1), narrow with sharp sagittal crest (2),

very broad, widely separating upper temporal fenestrae, skull table at least 50% of width of supratemporal fenestra and fossa (3).

89. Parietal, size and elevation of nuchal wedge and alae: small to moderate, height of alae less than height of base of paroccipital process (0), expanded, height more than height of base of paroccipital process (1).

90. Supratemporal fossa, anteromedial corner: open dorsally (0); partially roofed over by a small shelf of the frontalparietal (1).

91. Squamosal, constriction of lower temporal fenestra: absent (0), present (1).

92. Squamosal, anterodorsal lamina: emarginated by upper temporal fenestra (0); continuous (1).

93. Strongly developed and sharply defined horizontal ridge extending from the ventral margin of the postorbital facet towards the quadrate articulation on the lateral side of the squamosal body: absent (0); present (1)

94. Posterior extent of postorbital facet on squamosal: ends anterior to or at the anterior border of the ventral process (0); extends posteriorly to at least the half-width of the ventral process (1)

95. Relative length of anterior and posterior processes of squamosal: anterior process considerably longer than posterior process (0); anterior process as long as or shorter than posterior process (1)

96. Squamosal, flange covering quadrate head laterally: absent (0), present, covers the posterior part of the head and separated from quadratojugal process of squamosal by a wide, U-shaped incision (1), present, covers most of quadrate head and separated from quadratojugal process only by a narrow, slit-like incision (2). ordered

97. Squamosal-quadratojugal contact: present (0); absent (1)

98. Squamosal, articulation with quadratojugal: at tip (0); broad (1)

99. Quadratojugal, anteriormost point of ventral process relative to lower temporal fenestra: ventral, no further than two thirds of the length of the fenestra from the posterior border (0), further anterior, subequal to the anterior border of the fenestra (1).

100. Large pneumatic foramen in quadrate: absent (0), present (1).

101. Position of the quadrate head in relation to the orbit: low, below two-thirds of the height of the orbit (0), at two-thirds of the height of the orbit or higher (1)

102. Angle between quadrate ridge and distal quadrate condyles in posterior view: more than 70° (0), less than 70° (1)

103. Medial side of quadrate ridge at mid-height in posterior view: straight or concave (0); convex (1)

104. Proportion of the length of the quadrate that is occupied by the pterygoid wing: less than 70% (0) or 70% or more (1).

105. Proximal part of the dorsal margin of the pterygoid wing of the quadrate: forms a sharp crest (0); notably thickened mediolaterally (1)

106. Ventral margin of pterygoid wing of the quadrate: Offset from mandibular condyles (0); confluent with expansion for mandibular condyles (1)

107. Ventral margin of the pterygoid wing of the quadrate: flexed medially to form a medial shelf or ridge (0); forms a sharp ventral edge; only the most proximal part flexes medially (1)

108. Quadrate foramen: present (0); absent (1).

109. Development of quadrate foramen in the quadratojugal flange of the quadrate: semioval notch, widely open laterally (0); with a ventrally flexed lateral spur at at least the dorsal margin (1), completely enclosed in the quadrate (2)

110. Orientation of the quadrate in lateral view: anteroventrally inclined, mandibular joint notably anterior to quadrate head (0), more or less vertical, mandibular joint approximately straight below quadrate head (1), posteroventrally inclined, mandibular joint notably posterior to quadrate head (2).

111. Quadrate, head shape in dorsal view: oval (0), subrectangular (1).

112. Mediolateral expansion of quadrate head in relation to quadrate shaft: absent (0); present (1)

113. Quadrate, medial foramina adjacent to condyles: absent (0), present (1).

114. Medial condyle of the quadrate: anteroposteriorly narrow and long axis of condyle mainly mediolaterally oriented (0); anteroposteriorly expanded and more anteroposteriorly oriented (1)

115. Ventral rim of the basis of the paroccipital processes: above or level with the dorsal border of the occipital condyle (0); situated at mid-height of occipital condyle or lower (1).

116. Paroccipital processes: directed laterally or slightly ventrolaterally (0); directed strongly ventrolaterally, with distal end entirely below the level of the foramen magnum (1).

117. Marked depression on the exoccipital lateral to the foramen magnum, above the paracondylar recess: present (0); absent (1)

118. Supraoccipital, anteroposterior depth of median ridge relative to occipital condyle length: less (0), greater (1).

119. Maximal width of dorsal expansion of supraoccipital ridge: less than or subequal to width of foramen magnum (0), notably greater than width of foramen magnum (1).

120. Posterior exit of mid-cerebral vein: on the posterior surface of the supraoccipital, without any associated marked depressions (0); placed within a notable, funnel-shaped depression (1); associated with a curved groove leading towards the posttemporal fenestra (2)

121. Supraoccipital, participation in foramen magnum: present, ventral margin of supraoccipital forms a more or less straight line above the foramen, forming most of its dorsal rim (0), narrow, formed by a small median ventral process of the supraoccipital separating the exoccipitals on the dorsal edge of foramen (1), absent, exoccipitals meet in the midline above the foramen magnum (2). ordered

122. Attachment for proatlas on dorsolateral rim of foramen magnum: inconspicuous (0); marked as paired raised lips (1)

123. Basioccipital, ventrolateral pair of pneumatic cavities invading neck of occipital condyle and joining medially: absent (0), present (1).

124. Morphology of posterior basioccipital surface below the condyle: with undivided longitudinal median groove (0), median groove divided dorsally by small median lamina (1), with large longitudinal ridge separating two large lateral depressions (2).

125. Basioccipital, fossa ventral to occipital condyle in basioccipital apron: narrow and groove-like, one half or less of the width of the occipital condyle (0), broad depression, approximately two thirds or more the width of the occipital condyle.

126. Notch on the basioccipital-basisphenoid suture separating a medial basioccipital portion of the basal tubera from a lateral basisphenoid portion: absent (0), present (1).

127. Width of basioccipital ventral to the occipital condyle: greater than width of occipital condyle (0), subequal to or less than the width of the occipital condyle (1).

128. Basisphenoid, location of basipterygoid processes relative to basal tubera: anterior or slightly anteroventral, basisphenoid recess opens ventrally (0), anteroventrally, basisphenoid recess opens posteroventrally (1), almost directly ventral, basisphenoid recess anteroposteriorly narrower than wide and opens more posteriorly than ventrally (2).

129. Basisphenoid, presence and depth of basisphenoid recess: absent (0), shallow, longer than deep (1), deep, deeper than long (2). ordered

130. Basisphenoid, shape of opening for basisphenoid recess: elongate oval (0), teardrop-shaped, narrowing posteriorly (1), subcircular (2), anteroposteriorly compressed, slit-like (3), trapezoidal, widening posteriorly (4).

131. Longitudinal lamina at least partially dividing the basisphenoid recess in its interior into left and right compartments: present (0); absent (1)

132. Subdivision of basisphenoid recess into anterior and posterior recesses: absent (0); present (1)

133. Posterior part of the ventral margin of the basisphenoid between the basal tubera and the basipterygoid processes: gently concave in lateral view (0), straight or slightly convex in lateral view (1).

134. Basipterygoid processes: on elongate stalks, with rather small articular surface (0), broad, enlarged articular surface facing anteroventrolaterally at lateral sides of the anterior end of the basisphenoid (1)

135. Exit of cranial nerves X and XI: laterally through the metotic foramen (0), posteriorly through a foramen in the paracondylar recess (1).

136. Subcondylar recess on the occiput: small, restricted to the occiput lateral to the occipital condyle (0), extended ventrally, developed as deep depression on the lateral sides of the ventral part of the occiput (1)

137. Orientation of the occipital condyle in respect to the skull table: posteriorly (0); posteroventrally (1)

138. Angle between the posterior end of the dorsal skull roof and the main body of the supraoccipital: approximately 90° (0), notably obtuse (1).

139. Braincase, morphology of trigeminal foramen: single (0), partly split (1), fully split (2). Ordered

140. Exit of the abducens nerve (cranial nerve VI): placed within the pituitary fossa or the depression surrounding it (0), placed lateral to the pituitary fossa and its surrounding depression (1).

141. Dorsal process on the parasphenoid rostrum anterior to the pituitary fossa: absent (0); present (1)

142. Well-developed anterior tympanic recess in the braincase: absent (0), present (1).

143. Braincase, ossification of interorbital region: weak or absent (0), extensive, ossified sphenethmoid and interorbital septum (1).

144. Length of the anterior, maxillary process of the palatine (as measured from the anterior end of the junction with the vomerine process to the anterior tip) in relation to length of jugal process (as measured from the posterior end of the junction with the pterygoid process to the posterior tip): less or subequal (0), longer (1).

145. Palatine, pneumatic recess on the dorsolateral side of the base of the vomerine process: absent (0), present (1)

146. Deep, posterodorsally opening recess at the confluence of the jugal, pterygoid and vomerine processes of the palatine: absent (0); present (1)

147. Pterygoid, pocket on ectopterygoid flange: absent (0), present (1).

148. Anteroventral expansion of jugal process of ectopterygoid: absent (0), present (1)

149. Ectopterygoid, ventral fossa: absent (0), present (1).

150. Ventral fossa of the ectopterygoid: simple depression (0), invaginates the lateral ectopterygoid body (1).

151. Size of external mandibular fenestra: Large, surangular above the fenestra accounts for less than half of the height of the mandible (0), reduced, surangular accounts for more than half the height of the mandible (1).

152. Mandible, position of anterior end of external mandibular fenestra relative to last dentary tooth: posterior (0), ventral (1).

153. Dorsal (alveolar) margin of anterior end of dentary: not expanded (0), slightly expanded (1), strongly dorsally expanded, expansion is 33% or more of the minimal height of the dentary posterior to the expansion (2) ordered (modified from Schade et al. 2023)

154. Ventral margin of anterior end of dentary: straight or slightly convex (0); bulges ventrally (1); curves anterodorsally (2) (new)

155. Shape of the anterior end of the dentary: rounded (dorsoventrally convex) (0), squared (dorsoventrally straight) (1).

156. Anteroventral flange or process at the anterior end of the dentary: absent (0), present (1).

157. Enlarged tooth or teeth in the anterior end of the dentary: absent (0), present, usually in the third and/or fourth dentary alveolus (1).

158. Dentary, shape in dorsal view: straight (0), curves anteromedially (1).

159. Dentary, longitudinal groove housing dorsally situated row of neurovascular foramina on lateral surface: absent or weak (0), present and well-defined (1).

160. Dentary, number of Meckelian foramina: one (0), two (1).

161. Posterior end of the dentary: with dorsal and ventral processes subequal in length or dorsal process slightly longer (0), sloping posteroventrally, ventral end extends considerably further posteriorly than dorsal end (1).

162. Morphology of posterior margin of dentary: forked (0), posteroventrally sloping margin with incision for mandibular fenestra (1).

163. Splenial, contour of posterior edge: straight (0), curved (1), notched (2).

164. Splenial, size of splenial ('mylohyoid') foramen: small (height less than 15 % of height of splenial at the level of the foramen) (0), intermediate (height between 15 % and 25 % (1), large (height 25% or more) (2). ordered

165. Splenial, foramen in ventral part: completely enclosed by bone (0), open anteroventrally (1).

166. Deep incision in the anteroventral part of the prearticular: absent (0); present (1)

167. Surangular, horizontal ridge on lateral surface below mandibular joint: weak or absent (0), strong (1).

168. Surangular, depressed lateral shelf for the attachment of the M. adductor mandibulae externus superficialis, bound medially by a dorsally facing ridge: absent, dorsal surface of the surangular mediolaterally convex anterior to the glenoid (0); present (1)

169. Shelf on surangular for the attachment of the M. adductor mandibulae externus superficialis: faces mainly dorsally (0); faces notably laterodorsally (1)

170. Surangular, number of posterior surangular foramina: one (0), two (1).

171. Surangular and articular: separate (0); fused (1) (new)

172. Articular: rectangular ventral projection below the foramen for the chorda tympani on the medial side at the posteromedial margin of the mandibular glenoid: absent, ventromedial margin of glenoid rounded (0), present (1).

173. Anterior rim of the mandibular glenoid in lateral view: confluent with the dorsal margin of the surangular (0), raised above the dorsal margin of the surangular (1).

174. Ossified antarticular in the mandible: absent (0), present (1)

175. Retroarticular process of the mandible: elongate, as long as or longer than anteroposterior length of mandibular glenoid (0), short, shorter than length of mandibular glenoid (1).

176. Retroarticular process, mediolateral width relative to posterior width of dentary: ≤ (0), > (1).

177. Retroarticular process, orientation of attachment surface: posterodorsal (0), posterior (1).

178. Attachment area for the M. depressor mandibulae: mediolaterally notably concave (0); flat to slightly convex (1)

179. Lateral margin of retroarticular process: more or less aligned with glenoid (0); strongly offset ventrally from glenoid (1)

180. Articular: semioval dorsal process posterior to lateral half of mandibular glenoid: absent (0); present, but low, considerably less in height than the length of the mandibular articular facet anterior to it (1); present and high, about as high as length of articular surface anterior to it or higher (2) ordered (new)

181. Paradental plates, continuity and replacement groove: separated, groove present (0), forming a continuous medial lamina ('fused'), groove absent (1).

182. Interdental plates, visibility in medial view: widely exposed, subpentagonal and moderate–tall (0), obscured by an expanded paradental lamina, triangular apices only may be visible (1).

183. Paradental plates, surface texture: smooth (0), vertically striated or ridged (1).

184. Lateral maxillary and dentary teeth: recurved, so that tip of the tooth is placed distal to distal carina, distal carina concave (0); straight or almost straight, tip of tooth placed mesial to distal carina, distal carina straight or convex (1).

185. Teeth, crown striations: absent (0), present on premaxillary and/or anterior dentary teeth only (1), present on all tooth crowns (2).

186. Teeth, enamel wrinkles: absent (0), pronounced marginal enamel wrinkles (1).

187. Lateral teeth, ratio between mesiodistal length and transverse width at the base: more than 1.5 (0), 1.5 or less (1).

188. Teeth, maxillary and dentary, serrations: present (0), absent (1).

189. Teeth, maxillary and dentary, extent of anterior carina: to base of crown (0), at mid-height of crown or more apically (1).

190. Premaxillary teeth, arrangement of carinae: nearly symmetrical, on opposite sides (0), more asymmetrical, both on lingual side (1).

191. Premaxillary teeth, serrations: present (0), absent (1).

192. Premaxillary teeth, number: three (0), four (1), five (2), more than five (3). ordered

193. Premaxillary teeth, spacing: even (0), paired and spaced (1).

194. Size of first premaxillary tooth (or alveoli): subequal to second premaxillary tooth (0), less than two thirds of the size of the second premaxillary tooth (1), less than half the size of the second premaxillary tooth (2). ordered

195. Maxillary teeth, number: > 17 (0), 11–17 (1), < 11 (2). ordered

196. Maxillary teeth, mid-tooth spacing: adjacent, closely spaced (0); more widely spaced in the mid-section (at least one-third of an alveolar width apart), but spacing decreases posteriorly again (1); more widely spaced, spacing increases posteriorly towards the end of the tooth row (2) ordered

197. Rapid increase in tooth size at the anterior end of the maxilla: absent (0); present (1)

198. Dentary teeth, size and number relative to maxillary teeth: approximately equal (0), smaller and approximately 1.5 times as numerous (1).

199. Cervical vertebrae, anterior articular facet: concave (0), flat (1), convex (2). ordered

200. Pneumatic feature posterior or posterodorsal to parapophysis (anterior pleurocoel) in cervical vertebrae: absent (0), large, blind depressions (1), large foramina (2).

201. Pneumatic feature on the posterior half of the vertebral centrum in cervical vertebrae: absent (0), large depression (1), foramen (2).

202. Presacral vertebrae, extent of anterior pleurocoel: anterior dorsals only (0), to sacrum (1).

203. Vertebrae, internal structure of pneumatic centra: absent (0), camerate (1), camellate (2).

204. Epipophysis of the atlantal neural arch in lateral view: slender, rod-like (0), expanded, triangular (1).

205. Axial neural spine: anteroposteriorly extensive, sheet-like, with convex or only gently ascending dorsal margin (0), anteroposteriorly reduced, rod-like, with steeply ascending dorsal margin (1).

206. Axis, orientation of intercentrum ventral surface: horizontal or slightly anteroventral (0), tilted anterodorsally (1).

207. Length of epipophyses of the axis: short, approximately level with posterior end of postzygapophyses (0), long, overhang postzygapophyses posteriorly for more than half the length of the postzygapophyseal articular facet (1).

208. Spinopostzygapophyseal laminae of the axis: Extensive, connecting the spine with the postzygapophyses in a large arch, resulting in a large, triangular to rhomboid fossa on the posterior side of the neural arch (0), reduced, strongly invaginated between spine and postzygapophyses, so that at least the distal part of the spine has parallel borders and the posterior fossa is reduced (1).

209. Development of parapophysis on axis: well-developed facet on the anteroventral side (0), indistinct, or only developed as a slightly roughened patch (1)

210. Development of diapophysis on axis: indistinct, probably absent (0), developed as distinct ventrolateral projection (1).

211. Axis, pleurocoels: absent (0), present (1).

212. Neural spine of third cervical vertebra: not significantly different from other postaxial cervical neural spines (0), slender and strongly backswept (1)

213. Cervical vertebrae, morphology of anterior pleurocoel: single opening (0), two openings oriented anteroventralposterodorsal or very plastic morphology (1).

214. Cervical vertebrae, middle, shape of anterior pleurocoel: round (0), anteroposteriorly elongate (1).

215. Cervical vertebrae, anterior, ventral keel: present (0), absent or weak ridge (1).

216. Cervical vertebrae, anterior, demarcation of dorsal surface of neural arch from diapophyseal surface: gently sloping (0), pronounced edge or ridge that offsets the dorsal from the lateral surface (1), elevated prezygoepipophyseal lamina, dorsal surface concave between neural spine and the lamina (2). ordered

217. Cervical vertebrae, articular surface of prezygapophyses: planar (0), flexed (1).

218. Cervical vertebrae, perimeter of anterior articular surface: not rimmed by a flattened peripheral band (0), flat, forming a distinct rim (1).

219. Cervical vertebrae, anterior, transverse distance between prezygapophyses relative to width of neural canal: < (0), >, prezygapophyses situated lateral to neural canal (1).

220. Cervical vertebrae, anterior, morphology of epipophyses: low, wider than high, posteriorly pointed (0), transversely narrow, high (1), high, robust (2).

221. Neural spine of mid-cervical vertebrae: anteroposteriorly longer than dorsoventrally high (0), higher than long (1).

222. Cervical vertebrae, longest post-axial elements: first five (0), last five (1).

223. Length/posterior height ratio of mid-cervical centra: less than 1.75 (0), 1.75-2.75 (1), more than 2.75 (2). ordered

224. Width/height ratio of anterior articular surface of posteriormost cervical and anteriormost dorsal vertebrae: less than 1.3 (0); more than 1.3 (1)

225. Height of anterior dorsal neural spines (as measured from the dorsal margin of the postzygapophysis): less (0) or more (1) than 1.25 times the height of the neural arch (as measured from the dorsal rim of the centrum to the dorsal margin of the postzygapophysis).

226. Ventral keel in posterior-most cervicals and anterior-most dorsals: ventrally concave, a rounded hypapophysis might be present anteriorly (0), forming a straight to slightly convex ventral margin, anterior end of keel protrudes ventrally from the anterior articular surface and is separated from the latter by a distinct step (1).

227. Dorsal vertebrae, pneumaticity/webbing at base of neural spines in middle to posterior dorsals: absent (0), present (1).

228. Mid-dorsal vertebrae (posterior to D4): platy- amphicoelous (0); opisthocoelous (1) (new)

229. Middle to posterior dorsal vertebrae, accessory centrodiapophyseal lamina: absent (0), present (1).

230. Dorsal vertebrae, anterior, ventral keel: absent or developed as a weak ridge (0), pronounced, around 1/3 the height of centrum and inset from lateral surfaces (1).

231. Dorsal vertebrae, anterior, size of pneumatic foramen in centrum: small (0); enlarged (1).

232. Dorsal vertebrae, elevation of parapophyses: slightly elevated from centrum (0), project far laterally, more than half the diapophyseal length (1).

233. Dorsal vertebrae, orientation of hyposphene laminae: diverge ventrolaterally (0), parallel and sheet-like (1).

234. Dorsal vertebrae, position of parapophyses in posteriormost elements: on the same level as transverse process (0); distinctly below transverse process (1).

235. Dorsal vertebrae, distinct step-like ridge lateral to hyposphene, running posterodorsally from dorsal border of neural canal to posterior edge of postzygapophyses: absent (0); present (1); ridge present and is developed into a prominent lamina that bisects the infrapostzygapophyseal fossa in posterior dorsal vertebrae (2). ordered

236. Posterior dorsal vertebrae, shape of ventral surface of vertebral centra: transversely rounded (0); flattened, sometimes with a shallow medial sulcus (1)

237. Dorsal vertebrae, morphology of neural spines: transversely compressed sheets (0), transversely broad anteriorly and posteriorly, central regions of lateral surface embayed by deep vertical troughs (1).

238. Dorsal vertebrae, posterior, inclination of neural spines: vertical or posterior (0), anterior (1).

239. Dorsal vertebrae, height of neural spines relative to centrum height: low, ≤ 1.3x (0), moderate, 1.4-1.8x (1); tall, ≥ 2.0x (2). ordered

240. Middle to posterior dorsal vertebrae, centrum length relative to height: centrum higher than long (0), centrum longer than high (1), centrum more than 1.5 times longer than high (2) ORDERED

241. Angulation of mid- to posterior dorsal prezygapophyses: low, less than 30° from the horizontal (0); high, more than 30° from the horizontal (1) (new)

242. Shape of posterior dorsal and sacral neural spines: rectangular (0); funnel-shaped, gradually expanding dorsally (1) (new)

243. Anteroposterior bulge at the base of the posterior dorsal neural spines: absent (0); present (1) (new)

244. Sacral vertebrae, centrum pneumaticity: absent (0), pleurocoelous fossae (1); pneumatic foramina (2).

245. Sacral vertebrae, number: 2 [primordial sacrals only] (0), 5 [1 dorsosacral, 2 caudosacrals] (1), 6 [2 dorsosacrals, 2 caudosacrals] (2). ordered

246. Sacral vertebrae, transverse dimensions of middle centra relative to other sacrals: equivalent (0), constricted (1).

247. Sacral vertebrae, orientation of ventral margin of middle centra: approximately horizontal (0), strongly arched (1).

248. Sacral vertebrae, dorsal edge of neural spines: as thin as remainder of spine (0), transversely thickened (1).

249. Sacral vertebrae, pneumaticity of neural arches: weak or absent (0), paired fossa ventral to diapophyses (1).

250. Caudal vertebrae, anterior, morphology of ventral surface: flat (0), groove (1), ridge (2).

251. Caudal vertebrae, L-shaped neural spines: absent (0), present (1).

252. Anterior to mid-caudal vertebrae, depressions or pneumatic foramina in centrum: absent (0), large, pronounced pleurocentral depressions on the dorsal part of the lateral side (1), pneumatic foramina (2).

253. Caudal vertebrae, anterior, centrodiapophyseal laminae on neural arch: weak or lacking (0), only anterior centrodiapophyseal lamina well developed, defining a deep prezygodiapophyseal fossa (1), as prominent as in dorsal vertebrae, defining deep infradiapophyseal fossa that penetrates neural arch (pneumatic) (2).

254. Spinodiapophyseal ridge or lamina in at least mid-caudal vertebrae: absent (0); present (1)

255. Caudal vertebrae, anterior, proportions of neural arch base relative to centrum proportions: < (0), ≥ (1).

256. Caudal vertebrae, posterior middle to distal, shape of articular surfaces: circular to oval (0); subrectangular (1) (new)

257. Caudal vertebrae, posterior middle to distal, position of postzygapophyses: directly below neural spine (0); projects posteriorly from base of neural spine (1) (new)

258. Caudal vertebrae, posterior middle to distal, morphology of neural spines: plate-like (longer anteroposteriorly than thick transversely) and posteriorly inclined (0); subrectangular and sheet-like (1); rod-like and vertical (2); rod-like (about as thick or thicker transversely as long anteroposteriorly) and posteriorly inclined (3). (modified from Schade et al. 2023)

259. Cervical ribs, length of anterior process: short (0), long (1).

260. Gastralia, posteriormost gastral segments: separate (0), united into single, boomerang-shaped elements (1).

261. Sacral ribs, articulations in adults: separate (0), fused together (1).

262. Sacral ribs, position of posterior attachment to ilium: ventral (0), posterodorsal (1).

263. Sacral ribs, depth relative to ilium height: < 85% (0), ≥ 90% (1).

264. Chevrons, morphology in middle caudal vertebrae: rodlike or only slightly expanded ventrally (0), L-shaped (1).

265. Chevrons, proximal articular surface: divided into anterior and posterior facets by distinct transverse ridge (0), no ridge, but low lateral mounds may be present, one on each side (1).

266. Chevrons, curvature: straight or gently curved (0), strongly curved (1).

267. Chevrons, anterior process: absent (0); present (1).

268. Chevrons, morphology of distal end in anterior and middle elements: expanded anteroposteriorly (0), unexpanded, tapers ventrally (1).

269. Scapula, angle between blade and acromion: gradual, oblique (0), abrupt, perpendicular (1).

270. Scapula, size of acromion process: moderate (0), marked (1).

271. Scapula, midshaft expansion of blade: absent (0), present (1).

272. Scapula, distal expansion of blade: marked (0), weak/absent (1).

273. Scapula, length:width ratio of blade: ≤ 7 (0), 7.5–9 (1), > 10 (2). ordered

274. Scapulocoracoid, shape of anterior margin: indented or notched between acromial process and coracoid suture (0), smoothly curved and uninterrupted across scapula–coracoid contact (1).

275. Scapulocoracoid, glenoid lip: moderate (0), marked (1).

276. Coracoid, development of posteroventral process: low, rounded posteroventral eminence (0), pronounced, posteroventrally tapering process (1).

277. Coracoid, development of biceps tubercle (= acrocoracoid process): absent or poorly developed (0), conspicuous and well developed as tuber (1), developed as a posteroventrally oriented ridge (2).

278. Coracoid, prominent fossa on ventral surface posteroventral to glenoid (subglenoid fossa): absent (0); present (1).

279. Humerus, shape of head: elongate (0), globular (1).

280. Humerus, longitudinal torsion of shaft: absent (0), present (1).

281. Humerus, size of trochanters relative to midshaft diameter: < (0), > 150% (1) > 250% (2). ordered

282. Humerus, development of internal tuberosity: low/rounded (0), hypertrophied (1).

283. Humerus, length of deltopectoral crest relative to total bone length: < 0.4 (0), 0.43–0.49 (1) > 0.52 (2). ordered

284. Humerus, development of deltopectoral crest: large rectangular crest (0), reduced to a low, rounded flange (1).

285. Humerus, orientation of deltopectoral crest apex: anteriorly (0), anterolaterally (1).

286. Humerus, relative orientation of proximal and distal condyles in anteroposterior view: parallel, humerus straight (0), distal canted (1).

287. Humerus, anterior surface of bone adjacent to ulnar condyle: smooth or gently depressed (0), bears well-defined fossa (1).

288. Humerus, shape of distal condyles: rounded (0), flattened (1).

289. Radius and ulna, development of radial external tuberosity and ulnar internal tuberosity: low, rounded (0), hypertrophied distal ends of radius and ulna broadened (1).

290. Radius, shaft: straight (0); curves laterally (1).

291. Radius, development of medial biceps tubercle: small or indistinct (0), hypertrophied (1).

292. Ulna, olecranon process: absent (0), present (1).

293. Ulna, morphology of olecranon process: transversely robust (0); transversely compressed and 'blade-like' (1).

294. Ulna, crest extending distally along posterior surface from olecranon process: absent (0), present (1).

295. Ulna, hypertrophied medial and lateral processes on proximal end: absent (0), present (1).

296. Ulna, length relative to minimum circumference: stout, < 2.3 (0); gracile > 2.6 (1).

297. Carpus, morphology and articulations of distal carpals: separate dc1 and dc2 over separate metacarpals, flattened proximodistally (0), fused dc1 and dc2, dc1 overlaps metacarpals I and II, flattened proximodistally (1), fused dc1 and dc2, dc1 overlaps metacarpals I and II, strongly arched proximodistally (2).

298. Manus, length of digit II relative to length of humerus: < (0), > (1)

299. Manus, composition: digit IV and V present (0), digit IV present, digit V absent (1), MC IV present, IV phalanges and digit V absent (2), digits IV and V absent (3). ordered

300. Manual digits, lengths: III longest (0), II longest (1).

301. Metacarpals, transverse width of proximal articular ends relative to minimum transverse shaft width: < (0), ≥ 2x (1).

302. Metacarpal I, length to minimum width ratio: 1.4–1.9 (0), ≥ 2.4 (1).

303. Metacarpal I, length relative to length of metacarpal II: > 57% (0), < 57% (1).

304. Metacarpal I, extent of contact with metacarpal II relative to shaft length: < 1/3 (0), 1/2 (1).

305. Metacarpal I, angle between facet for metacarpal II and proximal articular facet: perpendicular (0), obtuse (1).

306. Metacarpal III, position of base relative to those of other metacarpals: at same level (0), on palmar surface (1).

307. Metacarpal III, shape of proximal end: rectangular (0), triangular (1).

308. Metacarpal III, width relative to width of metacarpal II: > 50% (0), < 50% (1).

309. Manual ungual I, length:height ratio: < 2.5x (0), > 2.5x (1).

310. Manual unguals, proximal height:width ratio: transversely broad, < 2.0 (0), transversely narrow, > 2.4 (1).

311. Pelvic elements, articulations in adults: separate (0), fused (1).

312. Ilium, large external pneumatic foramina and internal spaces: absent (0), present (1).

313. Ilium, vertical ridge on lateral surface of blade dorsal to acetabulum: absent (0), low swollen ridge (1), low double ridge (2).

314. Ilium, posterior width of brevis fossa: subequal to anterior width, fossa margins subparallel (0), twice anterior width, fossa widens posteriorly (1).

315. Ilium, height of lateral wall of brevis fossa relative to medial wall: taller along whole length (0), shorter anteriorly, exposing medial wall in lateral view (1).

316. Ilium, morphology between supraacetabular crest and brevis shelf on lateral surface: gap (0), continuous ridge (1).

317. Ilium, ventrolateral development of supraacetabular crest: large/pendant ‘hood’ (0), reduced shelf (1).

318. Ilium, orientation of pubic peduncle: mostly ventral (0), mostly anterior or ‘kinked’ double facet with anterior and ventral components (1).

319. Ilium, shape of acetabular margin of pubic peduncle: transversely convex or flat (0); transversely concave (1).

320. Ilium, relative sizes of pubic and ischial articulations: subequal (0), pubic articulation ≥ 130% of iliac articulation (1).

321. Ilium, morphology of ischial peduncle: rounded (0), acuminate (1).

322. Ilium, pubic peduncle length to width ratio: ≤ 1 (0), 1.3–1.75 (1), > 2 (2). ordered

323. Ilium, ridge on medial surface adjacent to preacetabular notch: absent (0), present (1), strongly developed, forming a shelf (2). ordered

324. Ilium, preacetabulum length relative to anterior edge of pubic peduncle: reaches anteriorly to same point as (‘brachyiliac’) (0), or well past (‘dolichoiliac’) (1).

325. Ilium, depth of preacetabular process: shallow (0), deep (1).

326. Ilium, anteroventral lobe of preacetabular process: absent (0), present (1).

327. Ilium, shape of dorsal margin: convex (0), straight (1).

328. Ilium, postacetabulum length relative to ischial peduncle length: ≤ (0), > (1).

329. Ilium, depth of postacetabular process: shallow (0), deep (1).

330. Shape of posterior margin of postacetabular process of ilium: rounded, dorsal margin curves gradually into posterior margin (0), only slightly convex or straight, dorsal margin offset from posterior margin by marked posterodorsal angle (1), concave (2), tapering (3).

331. Posterior process on the dorsal end of the posterior margin of the postacetabular blade, formed by a posterior expansion of the medial brevis shelf: absent (0), present (1).

332. Obturator foramen in pubis: completely enclosed in bone (0), ventrally open notch (1), absent (2) ordered

333. Pubic fenestra below obturator foramen: absent (0); present (1)

334. Obturator plate of ischium: largely continuous with pubic articulation (0), with large notch below the pubic peduncle, obturator process offset from pubic articulation (1)

335. Foramen in obturator plate of ischium: absent (0); present (1)

336. Pubis, shaft orientation: anterodorsally curved (0); straight (1), posteroventrally curved (2).

337. Pubis, articulation between apices in adults: unfused (0); fused (1).

338. Pubis, contact between distal portions: separate distally (0), contacting (1), contacting with slit-like opening proximal to distal expansion (interpubic fenestra) (2).

339. Pubis, angle between long axes of shaft and boot: 75–90° (0), < 60° (1).

340. Pubis, morphology of symphysis: marginal (0), broad (1).

341. Pubis, morphology of obturator foramen: small and subcircular (0), large and oval (1).

342. Pubis, anterior expansion of distal end: absent (0), present (1).

343. Pubis, boot length relative to shaft length: < (0), > 30% (1), > 60% (2). ordered

344. Pubis, shape of boot in ventral view: broadly triangular (0), narrow, with subparallel margins (1).

345. Pubis, articulation with ilium: planoconcave (0), peg-and-socket (1).

346. Ischium, length relative to pubis length: 75–80% (0), ≤ 70% (1), > 80% (2).

347. Ischium, shaft orientation: straight (0), ventrally curved (1).

348. Ischium, articulation with ilium: planoconcave (0), peg-and-socket (1).

349. Ischium, morphology of antitrochanter: large and notched (0), reduced (1).

350. Ischium, notch ventral to obturator process: absent (0), present (1).

351. Ischium, morphology of symphysis: unexpanded (0), expanded as apron (1).

352. Ischium, cross-sectional shape of paired midshafts: oval (0), heart-shaped, medial portions of shafts extend posteriorly as midline flange (1).

353. Ischium, morphology of distal end: rounded (0), expanded, triangular (1).

354. Ischium, articulation at distal end in adults: separate (0), fused (1).

355. Femur, head orientation: 45° anteromedial (0), 10–30° anteromedial (1), medial (2). ordered

356. Femur, head angle: ventromedial (0), horizontal (medial) (1), dorsomedial (2). ordered

357. Femur, groove on proximal surface of head oriented oblique to long axis of head ('articular groove'): absent (0), present (1).

358. Femur, oblique ligament groove on posterior surface of head: shallow, groove bounding lip does not extend past posterior surface of head (0), deep, bound medially by well-developed posterior lip (1).

359. Femur, placement of lesser trochanter relative to femoral head: does not reach ventral margin (0), rises past ventral margin (1), rises to proximal surface (2). ordered

360. Femur, morphology of anterolateral muscle attachments at proximal end: continuous trochanteric shelf (0), distinct lesser trochanter and attachment bulge (1).

361. Femur, development of fourth trochanter: prominent semioval flange (0), very weak or absent (1).

362. Femur, distinctly projecting accessory trochanter (derived from lesser trochanter): weak, forms slightly thickened margin of lesser trochanter (0), present as triangular flange (1).

363. Femur, *M. femorotibialis externus* origin medially on anterodistal surface: faint, small rugose patch (0), pronounced rugose depression that extends to distal femur (1).

364. Femur, development of medial epicondyle: rounded (0), ridge (1).

365. Femur, distal extensor groove: absent (0), present (1).

366. Femur, morphology and orientation of *crista tibiofibularis:* broad (0), narrow, longitudinal (1), lobular, oblique (2).

367. Femur, infrapopliteal ridge connecting medial distal condyle and crista tibiofibularis: absent (0), present (1).

368. Femur, orientation of long axis of medial condyle in distal view: anteroposterior (0), posteromedial (1).

369. Femur, projection of lateral and medial distal condyles: approximately equal (0), lateral projects distinctly further than medial, distal surface of medial is gently flattened (1).

370. Femur, morphology of distal end: central depression connected to *crista tibiofibularis* by a narrow groove (0), anteroposteriorly oriented shallow trough separating medial and lateral convexities (1).

371. Tibia, lateral malleolus: backs astragalus (0), overlaps calcaneum (1).

372. Tibia, shape of edge of lateral malleolus: smoothly curved (0), tabular notch (1).

373. Tibia, morphology of distal cnemial process: rounded (0), expanded proximodistally (1).

374. Tibia, posterior extent of lateral (fibular) condyle: as far as medial condyle or only ends only slightly more anteriorly (0), considerably offset anteriorly from posterior end of medial condyle (1) (modified from Rauhut and Pol 2019)

375. Tibia, anterolateral process of lateral condyle: absent or horizontal projection (0), prominent, curves ventrally (1).

376. Tibia, anteromedial buttress for astragalus: absent (0), ventral (1), marked oblique step-like ridge (2), reduced oblique ridge (3), bluntly rounded vertical ridge on medial side (4).

377. Tibia, morphology of fibular crest: narrow (0), bulbous (1).

378. Tibia, development of fibular crest: extends to proximal end of tibia as high crest (0), extends to proximal end of tibia as low ridge (1), does not extend to proximal end of tibia (2). ordered

379. Groove or depression on the medial side of the proximal end of the fibula: absent or only shallow concavity present (0), deep groove on the posterior half of the medial side of the proximal end, offset from anterior margin and opening at least partially posteromedially (1), large, deep depression that opens medially and is offset from the anterior margin only by a thin ridge or lip (2)

380. Ridge on the medial side of the proximal end of the fibula that extends anterodistally from the posteroproximal part: absent (0), present (1).

381. Fibula, size of iliofibularis tubercle: faint scar (0), large (1), anterolaterally curving flange (2).

382. Fibula, size of proximal end relative to width of proximal tibia: < 75% (0), ≥ 75% (1).

383. Astragalus, articulation between ascending process and fibula in adults: separate (0), fused (1).

384. Astragalus, orientation of distal condyles: ventral (0), 30-45° anterior (1).

385. Astragalus, ascending process morphology: blocky (0), laminar (1).

386. Astragalus, ascending process height relative to depth of astragalar body: less (0), subequal (1), > 1.6 times (2).

387. Astragalus, prominent proximolateral extension: absent (0); present (1).

388. Astragalus, round fossa at base of ascending process: absent (0), small (1), large (2). ordered

389. Astragalus, development of articular surface for distal end of fibula: large, dorsal (0), reduced, lateral (1).

390. Astragalus, posterolateral crest: absent (0), present (1).

391. Astragalus, posteromedial crest: absent (0), present (1).

392. Astragalus, articulation with calcaneum in adults: separate (0), fused (1).

393. Metatarsal I, length relative to length of metatarsal II: ≥ 50% (0), < 50% (1).

394. Metatarsal III, shape of proximal end: rectangular (0), shallow notch (1), deep notch (2). ordered

395. Metatarsal III, midshaft cross-sectional shape: rectangular (0), wedge-shaped, plantar surface pinched (1).

396. Metatarsal III, relative proportions of shaft: short and thick, length:transverse width ratio < 12.0 (0), long and gracile, ratio > 12.5 (1).

397. Metatarsal IV, proportions of distal end: broader than tall (0), taller than broad (1).

398. Metatarsal V, morphology of distal end: articular (0), non-articular (1).

399. Metatarsal V, length relative to length of metatarsal IV: > 50% (0), < 50% (1).

400. Antarctometatarsus: absent (0), present (1).

401. Pedal unguals, morphology of lateral and medial grooves: single (0), double (1).

402. Pedal unguals, digits III and IV, cross-sectional shape: triangular (0), elliptical (0).

403. Pedal unguals, digit II, mediolateral symmetry: symmetrical (0), asymmetrical (1).

404. Pedal digit phalanges, length of I-1 + I-2 relative to III-1: greater (0), less than or equal

SUPPLEMENTARY MATERIAL

SUPPLEMENTARY FIGURE 1. Strict consensus tree of more than 100.000 equally parsimonious trees resulting from a phylogenetic analysis using equal weights.

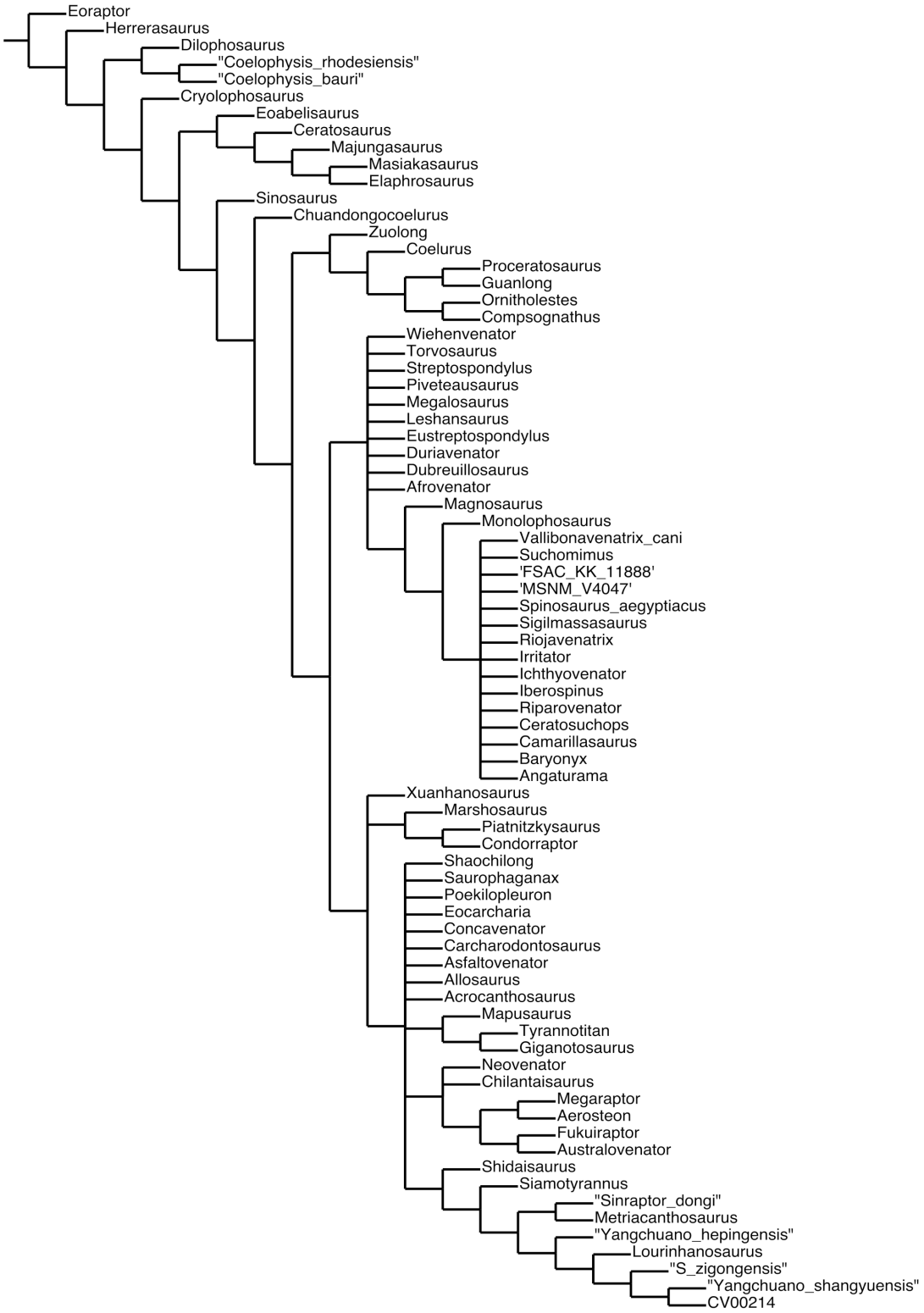

SUPPLEMENTARY FIGURE 2. Complete reduced consensus tree resulting from the phylogenetic analysis using equal weights.

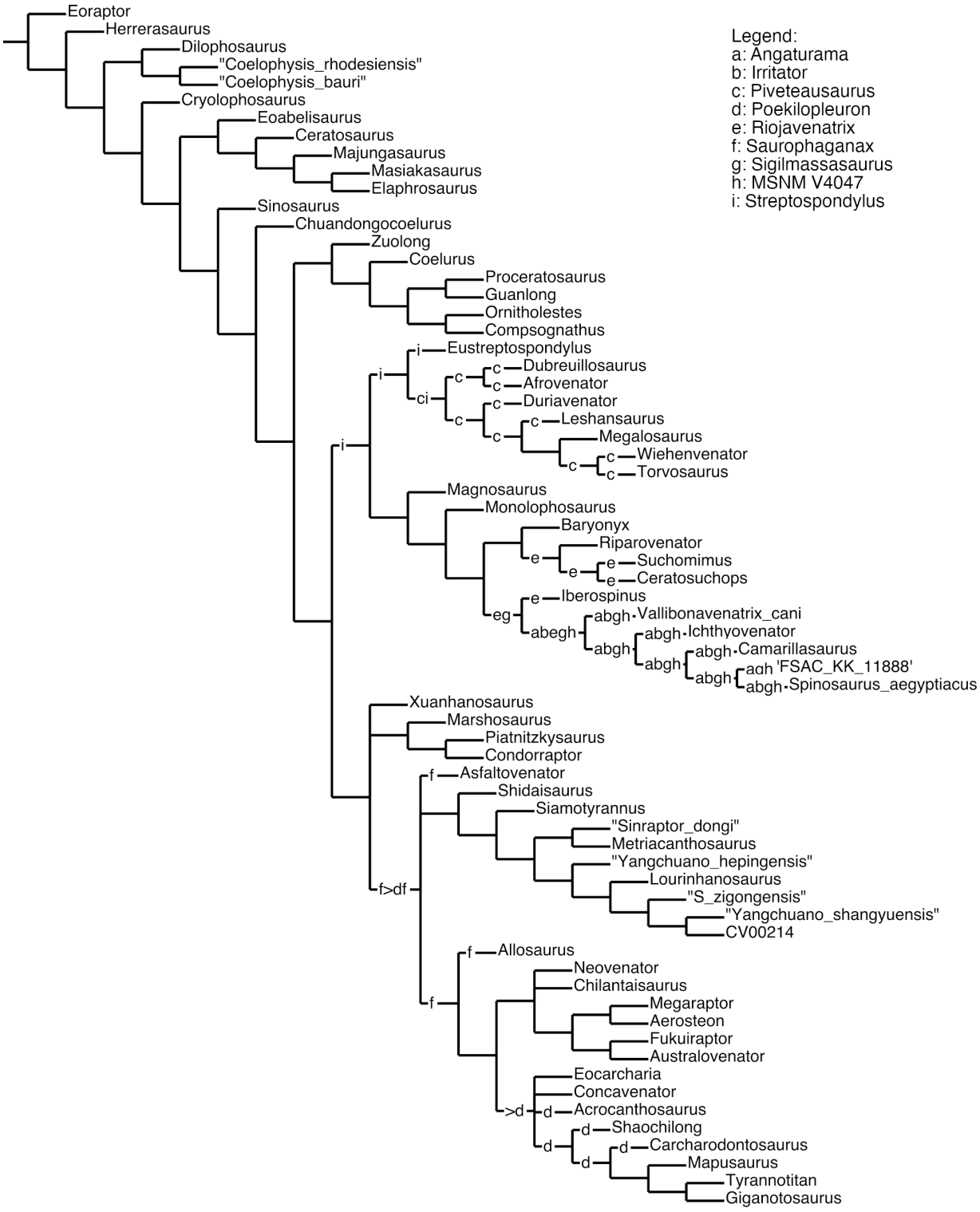

SUPPLEMENTARY FIGURE 3. Strict consensus tree resulting from the phylogenetic analysis using implied weights (k=12).

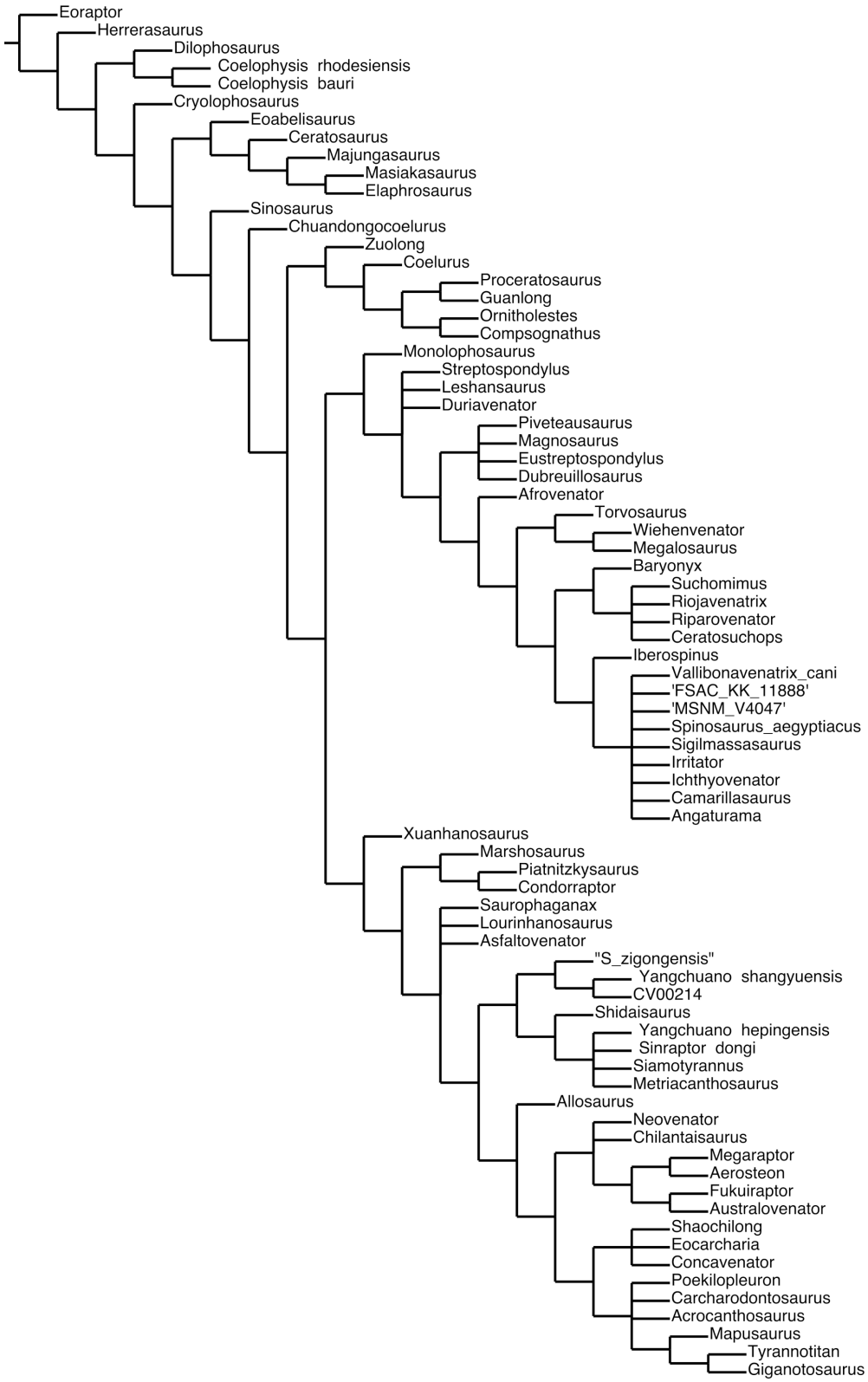

SUPPLEMENTARY FIGURE 4. Complete reduced consensus tree resulting from the phylogenetic analysis using implied weights.

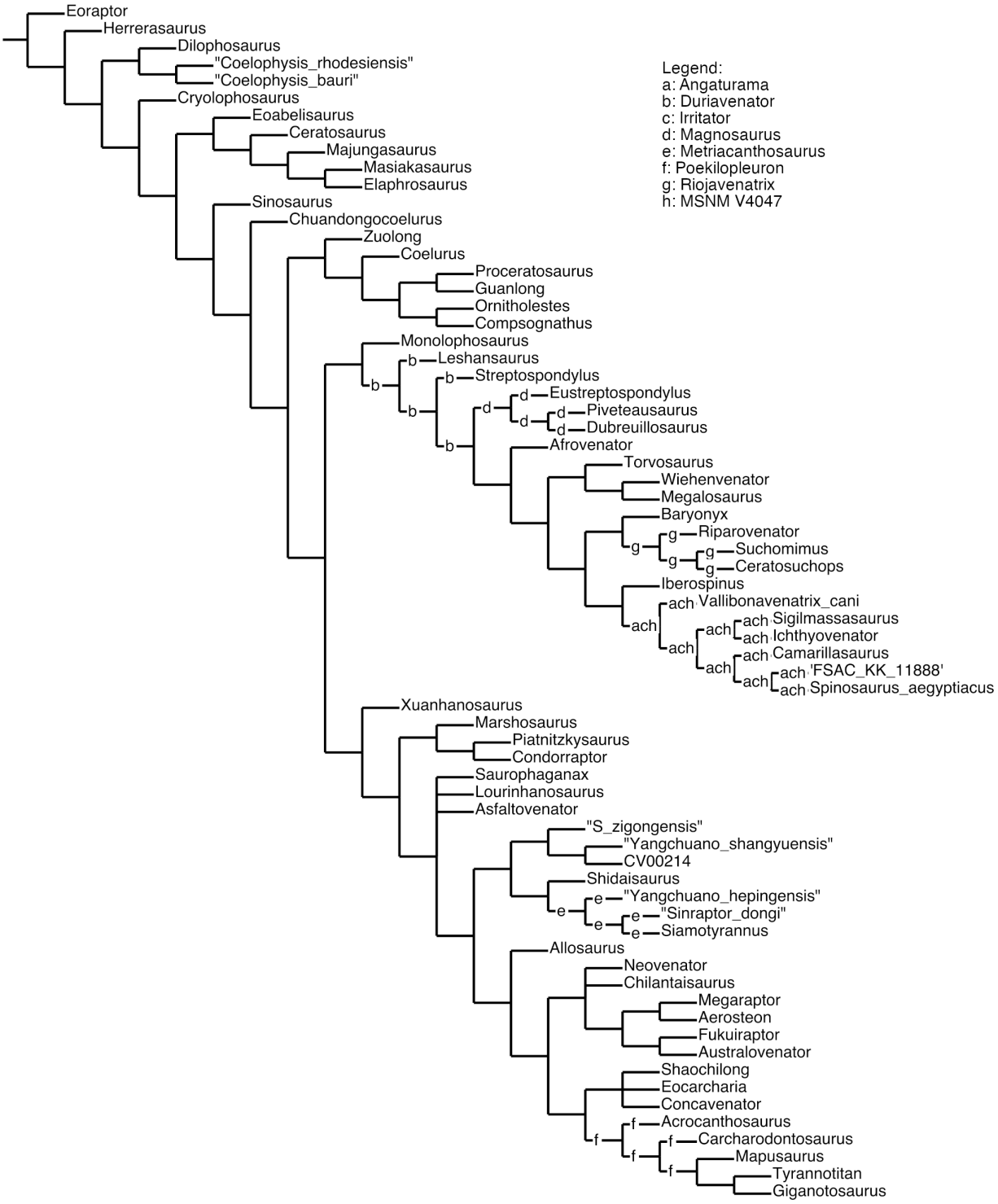

SUPPLEMENTARY DATA FILE. *Camarillasaurus* matrix.nex. Data matrix used for the phylogenetic analysis. This file is available for download at:
https://palaeo-electronica.org/content/2025/5627-revision-of-early-cretaceous-theropod-dinosaur